Technische Universität München
Lehrstuhl für Steuerungs- und Regelungstechnik

Sliding Mode Control of Electromechanical Systems

Heide Brandtstädter

Vollständiger Abdruck der von der Fakultät für Elektrotechnik und Informationstechnik der Technischen Universität München zur Erlangung des akademischen Grades eines

Doktor-Ingenieurs (Dr.-Ing.)

genehmigten Dissertation.

Vorsitzender: Univ.-Prof. Dr.-Ing. Wolfgang Utschick

Prüfer der Dissertation:

1. Univ.-Prof. Dr.-Ing./Univ. Tokio Martin Buss

2. Prof. Dr. Vadim I. Utkin,
Ohio State University/ USA

Die Dissertation wurde am 1.10.2008 bei der Technischen Universität München eingereicht und durch die Fakultät für Elektrotechnik und Informationstechnik am 16.3.2009 angenommen.

Abstract

Sliding mode control provides insensitivity to parameter variations and disturbances. These robustness properties make this discontinuous control strategy very attractive. However, its implementation in the presence of unmodeled dynamics leads to high-frequency oscillations termed chattering. This effect degrades the control performance and might damage the system. Many current implementations suffer from this drawback.

In this thesis, a novel sliding mode control strategy for mechanical systems with electric motors as actuators is proposed. The chattering problem is tackled by including actuator dynamics, which has so far been ignored, in the control unit design. The switching control law incorporates the dynamics of the electrical and the mechanical subsystem. The pulse width modulation (PWM) used in most present day implementations is eliminated and the controller directly drives the power switches. Hence, the discontinuous control inputs are the switched voltages applied to the motor.

In addition, a comprehensive methodology to realize the proposed control scheme is developed. It allows the systematic design of sliding mode controllers for complex electromechanical systems. Compared to the existing design procedures, it is applicable to a wider class of systems. It can handle nonlinear systems governed by a set of coupled differential equations of arbitrary order in canonical form, as well as infinite dimensional systems. This thesis identifies and solves implementation issues of the generalized block control principle. Presented are necessary observers and a method to reject disturbances with known structure.

The complete design procedure is illustrated by controlling an inverted pendulum system driven by a DC and a synchronous motor, as well as an induction machine. Simulations and experiments demonstrate the high performance and the robustness of the proposed control architecture. An essential contribution of this thesis is the position control of an induction machine that lays a foundation for building more robust and inexpensive robotic systems.

Zusammenfassung

Sliding Mode Regelungen zeichnen sich durch hohe Robustheit gegenüber Parameterunsicherheiten und Störungen aus. Jedoch kann die Implementierung dieser schaltenden Regelung zu hochfrequenten Schwingungen im Regelkreis führen, wenn Dynamiken der Regelstrecke beim Entwurf nicht berücksichtigt wurden. Dieses sogenannte *Chattering* verschlechtert die Regelgüte und kann das System beschädigen. Viele gegenwärtige Implementierungen weisen diesen Nachteil auf.

Die vorliegende Dissertation behandelt ein neuartiges Konzept zur *Sliding Mode* Regelung mechanischer Systeme, die von Elektromotoren angesteuert werden. Es bezieht Aktordynamiken, die in herkömmlichen *Sliding Mode* Regelungen vernachlässigt wurden, in den Reglerentwurf ein und kann so *Chattering*-Effekte stark reduzieren. Die Regelung berücksichtigt sowohl Dynamiken des elektrischen als auch des mechanischen Systems. Die in den meisten bestehenden Implementierungen verwendete Pulsweitenmodulation (PWM) entfällt und der Regler steuert direkt die Leistungsschalter an. Die diskontinuierlichen Stellgrößen des Systems sind somit die geschalteten Versorgungsspannungen des Motors.

In dieser Arbeit wird in geschlossener Form eine Methodik zur systematischen *Sliding Mode* Reglersynthese für komplexe elektromechanische Systeme entwickelt. Sie erlaubt die einfache Umsetzung des vorgeschlagenen Konzeptes. Die Entwurfsmethode ist für nichtlineare Systeme, die mit gekoppelten Differentialgleichungen beliebiger Ordnung in kanonischer Form beschrieben werden, und für unendlich dimensionale Systeme geeignet. Damit ist sie auf eine größere Systemklasse als bestehende Methoden anwendbar. Als Lösungen für Anwendungsprobleme des *Generalized Block Control Principle* werden sowohl Entwurfsmethoden für Beobachter als auch eine Methode zur Unterdrückung von Störungen bekannter Dynamik präsentiert.

Die vorgestellte Designmethode wird für die Positionsregelung eines von einem Gleichstrom-, Synchron- und Asynchronmotor angesteuerten invertierten Pendels angewandt. Die Ergebnisse der Simulationen und Experimente zeigen die Robustheit und die hohe Regelperformanz des vorgeschlagenen Konzeptes. Eine besondere Innovation stellt die entwickelte Positionsregelung einer Asynchronmaschine dar, die den Weg für robustere und kostengünstigere Robotiksysteme weist.

Contents

Notation

Within the scope of this thesis lowercase letters represent scalars, bold lowercase letters represent vectors and bold uppercase letters represent matrices.

Abbreviations

PWM	pulse width modulation
BCP	Block Control Principle
BCF	Block Control Form
GBCP	Generalized Block Control Principle
GBCF	Generalized Block Control Form
PD-Controller	controller with proportional and differential component
PT2-function	proportional, time-delayed function of 2nd order
$\forall$	for all

Mathematical Conventions

x	a scalar
$\boldsymbol{x}$	a vector
$x(.)$	a scalar function
$\boldsymbol{x}(.)$	a vector function
$\lvert\boldsymbol{x}\rvert$	modulus of vector $\boldsymbol{x}$
$\dot{\boldsymbol{x}}\,,\ddot{\boldsymbol{x}}$	first and second time derivative of $\boldsymbol{x}$: $\frac{\mathrm{d}t}{\mathrm{d}t}\boldsymbol{x}\,,\frac{\mathrm{d}^2}{\mathrm{d}t^2}\boldsymbol{x}$
$\overset{(i)}{\boldsymbol{x}}$	ith time derivative of $\boldsymbol{x}$: $\frac{\mathrm{d}^i}{\mathrm{d}t^i}\boldsymbol{x}$
$\mathbf{X}^T$	transpose of matrix $\mathbf{X}$
$\mathbf{X}^{-1}$	inverse of matrix $\mathbf{X}$
$\mathbf{X}^+$	pseudo inverse of matrix $\mathbf{X}$
$\mathrm{rank}(\mathbf{M})$	rank of matrix $\mathbf{M}$
$\det(\mathbf{M})$	determinant of matrix $\mathbf{M}$
λ	eigenvalue
$\dim(\boldsymbol{x})$	dimension of vector $\boldsymbol{x}$
$\sinh(x)$	hyperbolic sine function, $\sinh(x)=\frac{e^x-e^{-x}}{2}$
$\cosh(x)$	hyperbolic cosine function, $\cosh(x)\frac{e^x+e^{-x}}{2}$
$\mathrm{sign}(x)$	sign function, $\mathrm{sign}(x)=\begin{cases} 1 & \text{for } x>0 \\ -1 & \text{for } x<0 \end{cases}$

$\mathrm{sat}(x)$	saturation function, $\mathrm{sat}(x) = \begin{cases} 1 & \text{for } x \geq 1 \\ x & \text{for } -1 < x < 1 \\ -1 & \text{for } x \leq -1 \end{cases}$
∇	vector differential operator, $\nabla = [\frac{\partial}{\partial x_1} \frac{\partial}{\partial x_2} \dots \frac{\partial}{\partial x_n}]$ for $\boldsymbol{x} = [x_1\, x_2 \dots x_n]^T \in \mathbb{R}^n$
$\boldsymbol{\mathcal{L}_f g}$	Lie derivative, $\boldsymbol{\mathcal{L}_f g} = \nabla \boldsymbol{g}\ \boldsymbol{f}$
$\mathbb{N}$	set of natural numbers
$\mathbb{R}$	set of real numbers
$\mathbb{R}^+$	set of positive real numbers
V	Lyapunov function candidate
ε	constant value , $\varepsilon \in \mathbb{R}^+$
$\Re$	real part of a complex number
$\Im$	imaginary part of a complex number
p	Laplace operator
$X(p)$	Transformation of variable x into Laplace domain
j	complex number $j^2 = -1$
σ	real part of a complex variable
υ	imaginary part of a complex variable
ω	frequency of a sinusoidal function

Sub- and Superscripts

x^*	desired value of x
x_{nom}	nominal value of x
x_0	initial value of x
x_T	target value of x
$\overline{x}$	error value: $\overline{x} = \hat{x} - x$
$\bar{x}$	constant value
$\hat{\boldsymbol{x}}$	observer state
x_{TA}	control parameter of the twisting algorithm
x_{STA}	control parameter of the super twisting algorithm
$\boldsymbol{x}_{abc}$	signals in stator coordinates (a, b, c)
$\boldsymbol{x}_{\alpha\beta}$	signals in rotating stator coordinates (α, β)
$\boldsymbol{x}_{dq}$	signals in rotating rotor coordinates (d, q)

Symbols

System

$\boldsymbol{x}$	state vector
n	order of the system

$\boldsymbol{f}(\boldsymbol{x})$	system function
$\mathbf{G}(\boldsymbol{x})$	system input matrix
$\boldsymbol{g}_i(\boldsymbol{x})$	ith column of the system input matrix
$\boldsymbol{u}$	system control input
m	order of control input $\boldsymbol{u}$
$\boldsymbol{z}(\boldsymbol{x})$	unknown parameter uncertainties and external disturbances of the system
t	time
$\sigma(p)$	step function

Sliding Mode Control

$\boldsymbol{s}(\boldsymbol{x})$	switching function
$\boldsymbol{u}^+(\boldsymbol{x}), \boldsymbol{u}^-(\boldsymbol{x})$	switched feedback signal
$\boldsymbol{f}^-(\boldsymbol{x}), \boldsymbol{f}^+(\boldsymbol{x})$	two possible limits of the state velocity vectors of a system in the neighborhood of a point of discontinuity
$\boldsymbol{u}_{eq}$	equivalent control input

Chattering Reduction Concepts

$\boldsymbol{u}_{lin}(\boldsymbol{x})$	continuous feedback signal (component-wise control law, hybrid control algorithm)
$\bar{\mathbf{U}}(\boldsymbol{x})$	diagonal matrix, rank$\bar{\mathbf{U}}(\boldsymbol{x}) = m$, $\bar{\mathbf{U}}(\boldsymbol{x})$ possesses the elements $u_i(\boldsymbol{x}), i = 1 \ldots m$ (component-wise control law)
λ_{min}	control design parameter, smallest eigenvalue of the matrix (component-wise control law) $\frac{1}{2}\left(\nabla \boldsymbol{s}\mathbf{G}\bar{\mathbf{U}} + (\nabla \boldsymbol{s}\mathbf{G}\bar{\mathbf{U}})^T\right)$
$\phi(\boldsymbol{x})$	scalar function for control design (unit control law)
M, ε, δ	control design parameters (boundary layer solution, state-dependent, gain modification, twisting algorithm)
$B(\varepsilon)$	boundary layer around a manifold, $\boldsymbol{s}(\boldsymbol{x}) = \mathbf{0}$, $B(\varepsilon) = \{\boldsymbol{x} \mid \lvert\boldsymbol{s}(\boldsymbol{x})\rvert < \varepsilon\}$
σ	switching ratio (switching ratio-dependent gain)
$\boldsymbol{u}_{dis}$	discontinuous control signal (hybrid control algorithm)
$\tilde{\boldsymbol{f}}(\boldsymbol{x})$	feedback function (observer-based solution)
R, c	control design parameter (second order sliding mode, twisting algorithm)
F, G_m, G_M	system parameters (twisting and super-twisting algorithm)
V_M, V_m	control design parameters (twisting and super-twisting algorithm)
$\rho_{STA}, \varepsilon_{STA}$	control design parameters (super-twisting algorithm)

Generalized Block Control Principle

$\boldsymbol{x}_i$	state of the $i$the subsystem of system
r	number of the considered subsystems
$\boldsymbol{\phi}$	system transformation, $\boldsymbol{\phi} : \mathbb{R}^n \mapsto \mathbb{R}^n$

$\tilde{\boldsymbol{f}}$	system function
$\boldsymbol{\Lambda}, \mathbf{M}, c, \lambda_i$	control design parameters
v, w	system state
c_i	control design parameters
J_0, θ, K, m, g, l	model parameters (rotational inverted pendulum system)

Flexible Shaft System

q	degree of rotation of the torsion bar in time domain
x	position along the torsion bar
e	basic rotation of the shaft without flexibility
f	rotation caused by the flexibility of the bar
M	torque attacking at the left side of the shaft
$a = \sqrt{\frac{G}{\rho}}$	velocity of propagation in the shaft
G	modulus of rigidity
I_p	geometrical moment of inertia of the shaft
r	radius of the torsion bar
J	mass moment of inertia of the load
m_L	mass of the load
r_L	radius of the load
$A_t\{p\}, \tilde{A}_t\{p\},$ $B_t\{p\}, \tilde{B}_t\{p\}$	operators with respect to time
$A_x\{p\}$	operator with respect to location
$g_1(p), g_2(p)$	algebraic functions
$\tau = \frac{l}{a}$	time delay
s_1, s_2, s_3, s_4	state variables of the flexible shaft system in GBCF, $(s_1 = q, s_2 = \dot{q})$
V_1, V_2	parameters of the sliding mode observer for the flexible shaft system
T_L	disturbance attacking at the load
$\tilde{T}_L$	amplitude, slope or peak value of a disturbance

Electromechanics

$\boldsymbol{x}_{mech}$	state of the mechanical subsystem
$\boldsymbol{x}_{el}$	state of the electrical subsystem
$\boldsymbol{x}_{mag}$	state of the magnetical subsystem
τ	torque
$\boldsymbol{u}_a$	supply voltages for the electric motor

θ	angular position
ω	angular velocity
τ_L	load torque
J_m	mass of inertia of the machine
J	mass of inertia of the system
m	pendulum mass
g	gravitation constant
l	pendulum length
μ	coefficient of friction

DC Motor

i	armature current
u_a	supplied voltage
R_a	armature resistance
L	armature inductance
K_n	induction constant
K_m	torque constant
w	control parameter (observer)
D, ω_0	linear control parameters (damping and frequency of the closed control loop)

Synchronous Motor

i_i	current components
u_i	voltages components
R	resistance
L	inductance
p	number of permanent magnet pole pairs
k	motor constant
u_a	supplied voltage
r	internal resistance of the switching devices
$\boldsymbol{g}$	switch commands vector
$\boldsymbol{u}_{dq}$	vector of rotor voltages
$\boldsymbol{i}_{dq}$	vector of rotor currents
Π	dissipative power loss of the synchronous machine
H	Hamilton function
Q	abbreviation, $Q = \sqrt{\frac{f^2}{J^2} + \frac{2fk^2}{3(R+r)J^2}}$
S	abbreviation, $S = \sinh(qT)$
K	abbreviation, $K = \frac{S(\theta_T - \theta_0)}{2D - qTS}$
D	abbreviation, $D = \cosh(qT) - 1$
$\breve{u}$	abbreviation, $\breve{u} := u_q - \frac{2}{3}k\omega$
$\mathbf{A}$	system matrix of a linear system

Induction Machine

λ_r	rotor flux components
i_i	stator current components
u_i	stator voltage components
L_r	rotor inductance
L_s	stator inductance
L_h	mutual inductance
R_r	rotor resistance
R_s	stator resistance
ω_e	electrical machine velocity
η	abbreviation: $\eta = \frac{R_r}{L_r}$
σ	abbreviation: $\sigma = 1 - \frac{{L_h}^2}{L_s L_r}$
β	abbreviation: $\beta = \frac{L_h}{\sigma L_s L_r}$
γ	abbreviation: $\gamma = \frac{1}{\sigma L_s}(R_s + \frac{{L_h}^2}{{L_r}^2} R_r)$
N_r	number of pole pairs
U_0	supply voltage
$\boldsymbol{g}$	switch command vector
$\mathbf{G}$	transformation matrix
$\mathbf{A}_{\alpha,\beta}^{a,b,c}$, $\mathbf{A}_{\alpha,\beta}^{d,q}$	transformation matrices
$\mathbf{C}$	flux dependent transformation matrix
$\boldsymbol{e}$	state dependent vector
ε_M , κ_M , U_m	control parameters (multiphase inverter algorithms)
d_1, d_2	abbreviations: $d_1 = \frac{3 L_h N_r}{2(L_r L_s - L_h^2)}$, $d_2 = \frac{L_h R_r}{L_r L_s - L_h^2}$
$\boldsymbol{q}_1$, $\boldsymbol{q}_2$	stator voltages vectors for lookup table
a_1, a_2	coordinates in stator voltages for lookup table

Implementation/ Simulation Issues

T_{on}	"'on"' time of a pulse width modulation signal
T_{off}	"'off"' time of a pulse width modulation signal
α	duty cycle of a pulse width modulation
t_s	simulation time
T	sampling time
T_{min}	minimum delay time

List of Figures

List of Tables

1 Introduction

Forcing a mechanical structure to follow a desired trajectory is a fundamental task for various applications and products in e.g. aerospace, automotive industry, manufacturing, and robotics. To achieve this, algorithms have to be found that generate adequate forces and/or torques. For these systems the demands on precision and fast response time rise steadily. In most applications the mechanical systems are governed by a set of nonlinear and strongly coupled differential equations. These properties pose a challenge when designing control algorithms that meet the requirements stated above.

The performance of linear controllers becomes poor or unstable when the required operating range is large. If there are significant deviations from the linearization point nonlinearities cannot be properly compensated. Moreover, nonlinearities such as Coulomb friction or saturation are not linearizable as required by linear control tools. The gain scheduling approach [62] is also based on linear controllers, but it can cover the complete operation range by selecting more than one operating point and designing linear controllers around each point. Between the operation points, the controller parameters are interpolated. This design method is conceptually simple, but stability cannot always be guaranteed.

Among the nonlinear methods the design approaches based on Lyapunov's direct method or the phase plane methods offer analysis tools that guide the construction of nonlinear controllers. Since they are not systematic, their application to complex systems often fails.

The trajectory control problem for mechanical systems can be solved by decoupling and compensation approaches. A common solution for robotic systems is the computed torque control [88]. It cancels effects like gravity, friction, manipulator inertia, as well as Coriolis and centrifugal forces. The original system model is transformed to an equivalent but simpler system model. However, when the dynamic model of the mechanical system cannot be assigned precisely, the decoupling and compensation in the control structure is not accurate, which may result in insufficient control performance. Sources for these errors in the dynamic model are parameter variations, e.g. unknown loads or inaccuracies of the actuator parameters that even exist in a well structured system, as well as unmodeled dynamics, which result e.g. from imprecise friction models, or neglected actuator and sensor dynamics. This is the major drawback of all feedback linearization approaches, including the backstepping approach [40] and the control unit design based on flatness [28, 29]: They do not guarantee robustness in the presence of parameter uncertainties or unmodeled dynamics.

Adaptive control [2, 52] handles systems with known dynamic structure and unknown constant or slowly-varying parameters. However, they do not solve the problem of robustness in general, especially when the parameters change quickly.

The trajectory control of mechanical systems requires control schemes that take nonlinearities of the system, modeling uncertainties as well as disturbances into account. Sliding mode control theory [74, 75] provides means to overcome these problems. Sliding mode

control algorithms ensure that the desired system dynamics is insensitive against parameter variations and external perturbations. As long as the upper and lower bounds of the model parameters and the disturbances are known, sliding mode controllers with high accuracy within finite transient time can be designed. The otherwise complex design procedure for nonlinear systems is inherently simplified because it is broken down into two simpler subproblems.

Table 1.1 summarizes challenges that arise when controlling mechanical systems, as well as solutions provided by the sliding mode control theory. This comparison shows that sliding mode control strategies present an efficient way to control mechanical systems. The theory offers simple tools for the design process and tackles the problem of robustness.

Challenges in Controlling Mechanical Systems	Solutions offered by Sliding Mode Control Strategies
- Mechanical systems are governed by a set of nonlinear and strongly coupled differential equations	- Decoupling and order reduction
- Unknown system parameters (e.g. unknown friction coefficients, unknown loads)	- Robustness against unknown disturbances and parameter uncertainties

Table 1.1: Challenges in controlling mechanical systems and solutions offered by sliding mode control strategies.

Most of the applications of sliding mode control theory to mechanical systems show the undesired effect known as chattering. These are finite-amplitude high-frequency oscillations of the controlled structure. Chattering can cause audible noise, low control accuracy, high wear of moving mechanical parts, and high heat losses in power circuits.

Sliding mode control has successfully been applied in different trajectory tracking applications of mechanical structures: [82] presents a wide range of automotive applications. In [68, 69] a linear approximation of the discontinuous control input is used in order to reduce chattering. [14, 38] use an integrator to smooth the switching function. [3] and [57] propose sliding mode control designs based on Lyapunov functions in order to simplify the design. Many works combine continuous nonlinear control approaches with sliding mode control in order to improve robustness, e.g. [25] combines flatness properties, [30] combines adaptive control methods with sliding mode control theory. Recent works merge fuzzy or neural networks with sliding mode control theory [32, 54]. The results show that sliding mode successfully addresses the problem of nonlinearities and eliminates disturbances. Simulations and experiments prove accuracy in the presence of modeling errors. However, in all the approaches mentioned above the objectives of high robustness and low chattering are competing with each other.

This thesis investigates sliding mode control designs of mechanical systems with a focus on means to overcome chattering while maintaining control accuracy and robustness. The analysis considers only mechanical systems that use electric motors as actuators due to the following reasons: Firstly, electric motors are widely spread actuators. They are extremely versatile, offer high energy efficiency and may be controlled in a comparatively simple way. Secondly, these actuators usually are driven by power elements which inherently include

switching devices. Therefore it is straightforward to apply the discontinuous control law of the sliding mode control theory to them.

1.1 Challenges

The main challenges when implementing sliding mode controllers are chattering and complexity of the design procedure. Both problems will be addressed in this thesis.

Design Issues

A systematic approach for sliding mode control design is the block control principle (BCP) [21, 22, 45, 47]. By transforming the system into the regular form [48] it is broken down into a set of subsystems. The control law can be designed independently for each of these subsystems. The subsystems are of lower dimension than the original system. As the dimensions of the control input and the system state are equal for each subsystem, the control design becomes elementary. The idea is to use the system state of each subsystem as a virtual control input for the preceding subsystem. On the one hand, designing a control law for the subproblem is simpler, but on the other hand, the BCP approach may lead to a very large number of nonlinear transformations needed for the decomposition. Finding the right nonlinear system transformation into the regular form can be difficult for some systems and is non-existent in some cases.

A challenge addressed in this thesis is the research for a design method that does not need a consequent decomposition of the system into the afore mentioned subproblems. A limited decomposition of the electromechanical system into electrical and mechanical subsystems may shorten the design procedure.

Chattering Issue

The causes of chattering are limited- and consequently finite- switching frequencies and fast dynamics that have been neglected in the plant model. These reasons may be assigned to different components of the electromechanical system, as illustrated in Figure 1.1.

Sliding mode theory is based on the assumption that the discontinuous control input can be switched infinitely fast. However, in practice digital as well as analog implementations give rise to finite time delays that lead to limited switching frequencies. Digital implementations are inherently time-discrete. They depend on finite sampling rates of the analog to digital and digital to analog converters and on a finite clock rate of the processor calculating the control output. The time delays are subject to the complexity of the calculations involved. Greater complexity results in lower switching frequencies. The finite switching times of the components in the power converter or inverter driving the electric actuator limit the switching frequencies as well. Because there is a constant energy loss per switching operation, the energy losses increase linearly with the switching frequency. Furthermore, the resulting finite switching frequencies cause discretization chatter because the control is constant within the sampling intervals allowing the state of the system to drift away from the desired trajectory during this period.

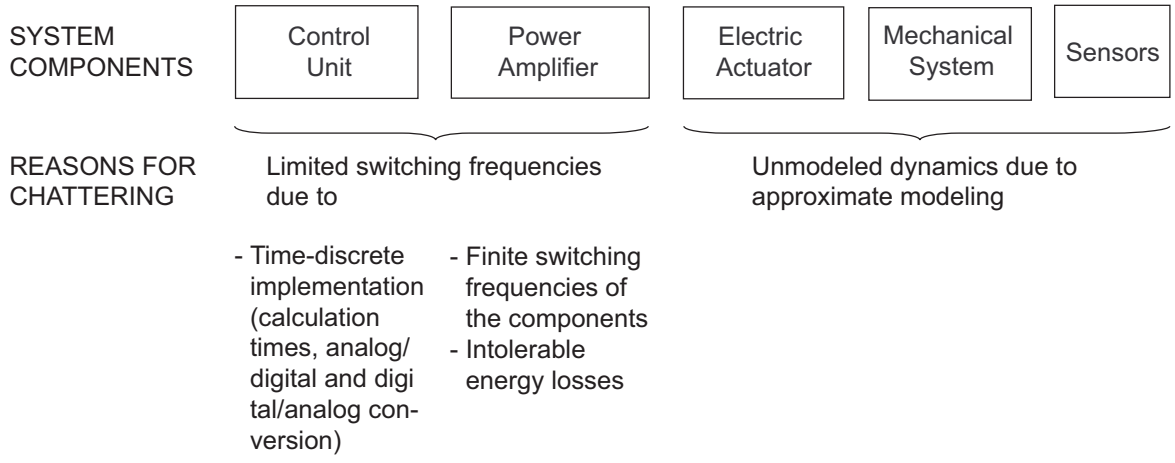

Figure 1.1: Reasons for chattering in sliding mode controlled electromechanical systems.

Assuming that the control unit can switch ideally, chattering may also be caused by unmodeled dynamics in the plant. Sliding mode controllers are discontinuous controllers. Due to the fast switching, the control input contains high-frequency components. These excite high-frequency dynamics in the plant, which are usually neglected in plant models, as proposed by singular perturbation theory. Actuator or sensor dynamics in electromechanical systems are typical examples of such neglected high-frequency dynamics. As mentioned above there usually is a trade-off between chattering reduction and robustness. Chattering can be reduced without sacrificing robustness when actuator dynamics is not neglected but considered in the control unit design. The cost of this approach is the increased complexity of the plant model resulting in an increased number of nonlinear transformations needed to decompose the system into subsystems.

This thesis targets the goal conflict explained above. It focuses on finding a control concept for electromechanical systems that leads to chattering reduction while maintaining robustness properties. A main challenge faced is the development of an appropriate methodology that keeps the control unit design process simple.

1.2 Main Contributions of this Thesis

This work proposes sliding mode control concepts for mechanical systems driven by different types of electric motors. The main motivation is to overcome chattering while preserving robustness and keeping the design procedure manageable. A core contribution is the development of a control unit design concept for mechanical systems that takes actuator dynamics into account. A comprehensive methodology that simplifies the application of the proposed control principle to arbitrary electromechanical systems is developed. As a practical illustration, the design of a position controller of a mechanical system driven by an induction machine is discussed in detail.

Methodology to Overcome Control Unit Design Difficulties

In this thesis, a novel comprehensive control unit design methodology for electromechanical systems, composed of subsystems in canonical form, the Generalized Block Control Principle (GBCP) is proposed. It is an extension of the design procedure presented in [78], which is formulated for nonlinear mechanical systems governed by a set of interconnected second-order equations. The design method waives the requirement of the BCP that the control input and the state of the subsystem must have equal dimension. The decomposition into subsystems can thereby be simplified. The complexity of the control unit design process is reduced and the range of dynamic systems to which the principle can be applied is enlarged. The GBCP allows to handle the control unit design process for complex system models that include the actuator dynamics.

Control Concept that Solves the Chattering Problem

This thesis investigates and develops a control concept for mechanical systems that takes actuator dynamics into account. The electric actuators considered are different types of electric motors. The control law incorporates the dynamics of the electrical and mechanical subsystem. In this case, the voltages applied to the actuator are the actual discontinuous control input vector instead of the torques and/or the forces. Thereby, chattering due to unmodeled actuator dynamics is avoided while retaining robustness and disturbance rejection, the main benefits of sliding mode control. The discontinuous output signal of the switching controller directly drives the power switches and the pulse width modulation (PWM) used in most present day controllers, which converts the continuous output of the control algorithm into a variable duty cycle, is eliminated. The implementation of the control law is simple, since the control signals are discontinuous and digital to analog converters are not required. Chattering due to finite switching frequencies is also reduced because the inductance of the motor coil forms a low pass filter for the motor current.

Present-day semiconductor technologies offer high-speed low-loss solid state switches that allow high switching frequencies. They constitute the technological basis for the implementation of the proposed sliding mode control concept.

Position Control of an Induction Machine

Induction machines have a number of desirable features: They are inexpensive, robust, compact, highly efficient and have a small mass inertia. However, the control of induction machines is far from trivial, because even very simplified models are high-dimensional and nonlinear. Additionally, most existing control algorithms require knowledge of all state variables and/or machine parameters, which are not always measurable.

The GBCP as well as the sliding mode control theory simplify the control unit design for complex systems. With the help of these two tools, two position control algorithms for a mechanical system driven by an induction machine are developed in this thesis. The proposed control schemes include actuator dynamics into the control design and the voltages impressed on the actuator are the actual discontinuous control input vector. The control strategies benefit from the strong robustness and fast dynamics of the sliding mode control scheme. At the same time chattering effects due to unmodeled actuator dynamics are decreased.

1.3 Outline of this Thesis

Chapter 2 summarizes the sliding mode control theory and surveys the state of the art of applied sliding mode control algorithms. In Chapter 3, the GBCP is introduced. The design principle is formulated for systems composed of interconnected subsystems in canonical form. Chapter 4 illustrates the benefits of the novel control concept for electromechanical systems when the voltages impressed on the actuator are the actual discontinuous control input vector. Chapter 5 focuses on the application of the GBCP to control the position of an induction machine. Again, discontinuous signals are used as control input vector. Moreover, in Chapter 5 multilevel control strategies are discussed as methods to reduce chattering in the control loop. Finally, chapter 6 concludes this thesis and discusses future research directions. An overview of the state of the art in the considered research fields is given at the beginning of each chapter.

2 Sliding Mode Control Theory: Fundamentals and State of the Art

Based on the sliding mode control theory robust controllers for high-order nonlinear plants operating under various uncertainty conditions can be designed. However, their implementation may lead to oscillations of finite amplitude and frequency in the control loop. These chattering effects often result in poor control accuracy, high wear of moving mechanical parts or even break down of the controlled structure. Several methods to reduce chattering have been developed. But these solutions usually either suffer from decreased robustness or increased implementation complexity.

This chapter gives an overview of the sliding mode control theory and introduces the design tools that are used later in this thesis. It contributes a comprehensive report of existing chattering reduction methods. The final evaluation and comparison of the methods provides a basis for decisions on implementations of sliding mode controllers.

Section 2.1 presents the fundamental mathematical concepts of the sliding mode control theory. It introduces the system class considered in this thesis and illustrates the principle of sliding mode. Furthermore, it explains shortly the features of sliding mode control theory, the system motion in sliding mode; the existence conditions, and the sliding mode control design. The state-of-the-art techniques for solving the problem of chattering are presented and discussed in Section 2.2.

2.1 Fundamentals of Sliding Mode Control Theory

Detailed explanations of the issues dealt with in this section can be found in the books [81, 11] and the pioneering article [80].

2.1.1 System Class

The class of nonlinear time-invariant systems, which are linear with respect to control,

$$\begin{aligned}\dot{\boldsymbol{x}} &= \boldsymbol{f}(\boldsymbol{x}) + \mathbf{G}(\boldsymbol{x})\boldsymbol{u} + \boldsymbol{z}(\boldsymbol{x}) \\ &= \boldsymbol{f}(\boldsymbol{x}) + \sum_{i=1}^{m} \boldsymbol{g}_i(\boldsymbol{x})u_i + \boldsymbol{z}(\boldsymbol{x}) \quad \text{with } \boldsymbol{x}(t_0) = \boldsymbol{x}_0\,,\end{aligned} \tag{2.1}$$

where $\boldsymbol{x} \in \mathbb{R}^n$ is the system state and $\boldsymbol{u} \in \mathbb{R}^m$ represents the control input, is considered. The vector functions $\boldsymbol{f}, \boldsymbol{g} : \mathbb{R}^n \mapsto \mathbb{R}^n$ and the matrix $\mathbf{G}(\boldsymbol{x}) = (\boldsymbol{g}_1\, \boldsymbol{g}_2\, \ldots\, \boldsymbol{g}_m)$ are assumed to be continuously differentiable. The vector function $\boldsymbol{z} : \mathbb{R}^n \mapsto \mathbb{R}^n$ summarizes the unknown parameter uncertainties and external disturbances.

The sliding mode control theory deals with state feedback control schemes that use switching control actions. Therefore, the control input $\boldsymbol{u}(\boldsymbol{x})$ is chosen as a discontinuous function of the system state

$$\boldsymbol{u}(\boldsymbol{x}) = \begin{cases} \boldsymbol{u}^+(\boldsymbol{x}) & \text{for} \quad \boldsymbol{s}(\boldsymbol{x}) > 0 \\ \boldsymbol{u}^-(\boldsymbol{x}) & \text{for} \quad \boldsymbol{s}(\boldsymbol{x}) < 0 \end{cases} \tag{2.2}$$

where $\boldsymbol{s} : \mathbb{R}^n \mapsto \mathbb{R}^m$ is a continuously differentiable function. The feedback signal $\boldsymbol{u}(\boldsymbol{x})$ exhibits a point of discontinuity at $\boldsymbol{s}(\boldsymbol{x}) = \boldsymbol{0}$;

$$\lim_{\boldsymbol{s}(\boldsymbol{x})\to\boldsymbol{0}} \boldsymbol{u}^+(\boldsymbol{x}) \neq \lim_{\boldsymbol{s}(\boldsymbol{x})\to\boldsymbol{0}} \boldsymbol{u}^-(\boldsymbol{x})$$

and is not a continuous function of time.

2.1.2 Principle of Sliding Mode

To answer the question *What is sliding mode?* a simple 2-dimensional system is considered at first.

Example 2.1 (Sliding Mode Control of a 2-dimensional System with Scalar Control Input) Let $\boldsymbol{x} = (x_1, x_2)^T$ be the system state. If a scalar control input u is regarded, then the function $s(\boldsymbol{x})$ is scalar as well and its points of discontinuity, $S = \{\boldsymbol{x} \in \mathbb{R}^n |\ s(\boldsymbol{x}) = 0\}$ are a line in the state space. When a control algorithm is designed based on (2.2), the control input $u(\boldsymbol{x})$ is chosen in such a way that the tangent vectors of the state trajectory are oriented toward the manifold S. After reaching the manifold S, the state is forced back onto the manifold whenever a deviation occurs. Assuming infinitely fast switching the system will move along the manifold after finite time. This motion is called sliding mode. This is the ideal movement of the system. In all practical applications the system trajectory deviates from the manifold because chattering occurs. Figure 2.1 shows an example of an actual movement of the system state in the state plane.

The idea, demonstrated for the scalar control case, can easily be extended to the vector case. For systems with m-dimensional control input, the components of the vector $\boldsymbol{s}$ are chosen with $\boldsymbol{s}(\boldsymbol{x}) = \boldsymbol{0}$ defining m manifolds such that their intersection is of the dimension $(n - m)$. Now, sliding modes may be enforced individually on the manifolds or directly on their intersections.

The principle of sliding mode is to constrain the system state to stay on a manifold on which the system will exhibit desirable features. A sliding mode control scheme forces the system state to reach the manifold $\boldsymbol{s}(\boldsymbol{x}) = \boldsymbol{0}$ from any initial condition. Having reached $\boldsymbol{s} = \boldsymbol{0}$, it ensures that the control action is capable of maintaining the system state on the manifold $\boldsymbol{s}(\boldsymbol{x}) = \boldsymbol{0}$.

2.1.3 Features of Sliding Mode Control Strategies

The sliding mode control theory offers several advantages when compared to continuous controls schemes, such as low sensitivity to plant parameter variations and disturbances, which relaxes the necessity of exact modeling. Moreover, the original control problem decomposes into two subproblems of lower dimensions in the design process.

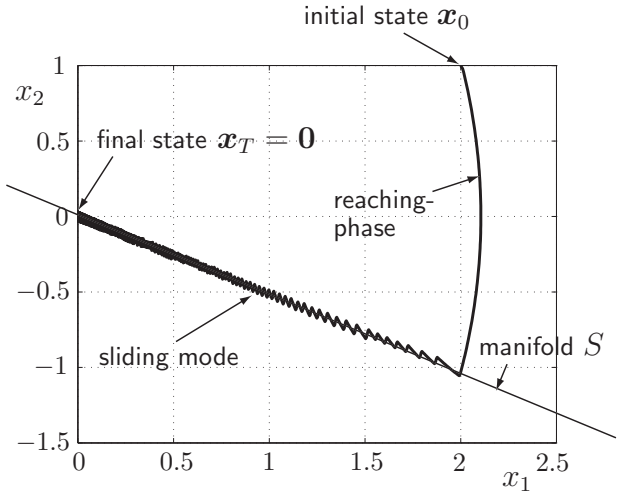

Figure 2.1: Phase portrait of a 2-dimensional system with scalar control input: Example of an actual movement of the system state if a sliding mode control algorithm is applied. The movement is divided into the reaching phase and sliding mode. Finite switching is considered for better illustration.

Order Reduction and Decoupled Design Process

In the sliding mode theory the system trajectory is located in a space of lower dimension than that of the original system. The order of the differential equations describing the sliding motion is reduced to $(n-m)$. As a result the control unit design can be decoupled into two simpler subproblems. These are:

- selecting a suitable sliding manifold of dimension $(n-m)$ in order to assign the desired dynamics and
- designing a discontinuous control function in the subspace of dimension m that enforces sliding mode on the sliding manifold.

This decomposition into subproblems is of particular interest in the control of high-dimensional plants as it decreases the complexity of the problem .

Robustness

Continuous controllers, whether linear or nonlinear, set the commands for the actuators in continuous dependence of the output error. The performance limits of the actuators are only reached in the presence of large control errors. For smaller errors, the actuators operate below their potential. Discontinuous controllers in contrast are very sensitive to small deviations and provide infinitely high gains to correct the smallest error. This is why the capacity of discontinuous controllers to suppress disturbances is superior compared to continuous controllers.

Sliding mode for the system (2.1) is invariant with respect to disturbances $\boldsymbol{z}(\boldsymbol{x})$, if an upper limit for the system uncertainties and disturbances $\bar{z}$

$$|\boldsymbol{z}(\boldsymbol{x})| \leq \overline{z}\,, \quad \bar{z} = \text{ constant} \tag{2.3}$$

exists and is known and there exists a vector $\boldsymbol{\gamma} \in \mathbb{R}^m$ such that the matching condition

$$\boldsymbol{z}(\boldsymbol{x}) = \mathbf{G}(\boldsymbol{x})\,\boldsymbol{\gamma}(\boldsymbol{x}) \tag{2.4}$$

is satisfied. [24]

This condition depends neither on the selected sliding manifold nor on the sliding mode controller, it rather provides a design rule for the selection and the placement of the system actuators. In the case that this condition is not satisfied and the disturbances are significant, the position of the actuators in the system should be changed or an additional actuator should be used to provide better controllability with respect to the disturbance.

Chattering

Sliding mode controllers according to (2.2) do exhibit the chattering, finite-amplitude high-frequency oscillations of the controlled structure. Chattering can cause low control accuracy, high wear of moving mechanical parts, or might even damage the system being controlled. Chattering is the main obstacle in implementing sliding mode controllers. The unwanted effect has two causes: First, high bandwidth dynamics are often neglected in the open-loop plant model used for control design. In sliding mode control implementations this dynamics is excited by the switched control input. Furthermore, the infinitely high switching frequencies assumed in sliding mode theory cannot be realized in practice. Methods to reduce chattering will be discussed in the second part of this chapter.

2.1.4 System Motion in Sliding Mode

To describe the dynamics of systems with discontinuous control inputs, special mathematical methods are required. In the case of closed loop operation of system (2.1) with the feedback (2.2) and assuming $\boldsymbol{z} = \mathbf{0}$, the system dynamics are

$$\dot{\boldsymbol{x}} = \begin{cases} \boldsymbol{f}(\boldsymbol{x}) + \mathbf{G}(\boldsymbol{x})\boldsymbol{u}^+(\boldsymbol{x}) & = \boldsymbol{f}^+(\boldsymbol{x}) \quad \text{for} \quad \boldsymbol{s}(\boldsymbol{x}) > 0 \\ \boldsymbol{f}(\boldsymbol{x}) + \mathbf{G}(\boldsymbol{x})\boldsymbol{u}^-(\boldsymbol{x}) & = \boldsymbol{f}^-(\boldsymbol{x}) \quad \text{for} \quad \boldsymbol{s}(\boldsymbol{x}) < 0\,. \end{cases} \tag{2.5}$$

Sliding mode is the solution of these system equations together for $\boldsymbol{s}(\boldsymbol{x}) = \mathbf{0}$. The differential equations have a point of discontinuity at $\boldsymbol{s}(\boldsymbol{x}) = \mathbf{0}$, the system thus is not Lipschitz-continuous at $\boldsymbol{s}(\boldsymbol{x}) = \mathbf{0}$ and conventional approaches to get a unique solution for the differential equation (2.5) cannot be applied.

Different mathematical methods have been developed to find a solution for (2.5) at the points of discontinuity. The solutions replace the discontinuity in different ways. What they have in common is that they define a velocity vector, which is tangential to the sliding manifold. The length as well as the direction of the velocity vector may vary with the method used. Depending on the application on hand, one solution may describe the real sliding mode motion of the system better then the other does.

Approaches to describe the discontinuities of sliding mode are e.g. Filippov's method [26] or the equivalent control method [74, 75, 81]. For systems which are linear with respect to the control input, these two methods lead to the same solution. However, for arbitrary systems

$$\dot{\boldsymbol{x}} = \boldsymbol{f}(\boldsymbol{x}\,, \boldsymbol{u}\,, \boldsymbol{z}) \quad \text{with } \boldsymbol{x}(t_0) = \boldsymbol{x}_0\,, \tag{2.6}$$

the solutions may differ. Due to this reason, the systems being treated in this thesis are all linear with respect to the control input. (See Section 2.1.1, (2.1))

Example 2.2 (Equivalent Control Method [74, 75, 81])
In order to describe the system dynamics in sliding mode this technique introduces a continuous control input $\boldsymbol{u_{eq}}$ so that a conventional solution to the differential equation (2.1) exists. Assume, that $\boldsymbol{x}(t=0)$ of system (2.1) lies on the manifold $\boldsymbol{s}=\boldsymbol{0}$ and sliding mode is enforced. Hence, for all future times $\boldsymbol{s}=\boldsymbol{0}$ will holds and

$$\dot{\boldsymbol{s}}(\boldsymbol{x}) = \boldsymbol{0} \tag{2.7}$$

will be true. Since the continuous equivalent control input $\boldsymbol{u_{eq}}$ is meant for describing sliding mode dynamics, it can be calculated using the condition (2.7). The approach

$$\begin{aligned} \dot{\boldsymbol{s}}(\boldsymbol{x}) &= \nabla \boldsymbol{s}(\boldsymbol{x})\, \dot{\boldsymbol{x}} && (2.8)\\ &= \nabla \boldsymbol{s}(\boldsymbol{x})\, \boldsymbol{f}(\boldsymbol{x}) + \nabla \boldsymbol{s}\, \boldsymbol{g}(\boldsymbol{x}) \boldsymbol{u_{eq}} && (2.9)\\ &= \mathcal{L}_{\boldsymbol{f}} \boldsymbol{s}(\boldsymbol{x}) + \mathcal{L}_{\boldsymbol{g}} \boldsymbol{s}(\boldsymbol{x}) \boldsymbol{u_{eq}} = \boldsymbol{0} && (2.10) \end{aligned}$$

leads to

$$\boldsymbol{u_{eq}} = -\frac{\mathcal{L}_{\boldsymbol{f}} \boldsymbol{s}(\boldsymbol{x})}{\mathcal{L}_{\boldsymbol{g}} \boldsymbol{s}(\boldsymbol{x})}. \tag{2.11}$$

Hence, the closed-loop dynamics- the sliding mode dynamics- is given by

$$\dot{\boldsymbol{x}} = \boldsymbol{f}(\boldsymbol{x}) + \boldsymbol{g}(\boldsymbol{x})\, \boldsymbol{u_{eq}}(\boldsymbol{x})\,. \tag{2.12}$$

2.1.5 Existence Conditions and Control Design

To ensure that the system state stays in sliding mode after reaching it, the existence conditions

$$\lim_{\boldsymbol{s}(\boldsymbol{x}) \to \boldsymbol{0}^+} \dot{\boldsymbol{s}}(\boldsymbol{x}) < \boldsymbol{0} \quad \text{and} \quad \lim_{\boldsymbol{s}(\boldsymbol{x}) \to \boldsymbol{0}^-} \dot{\boldsymbol{s}}(\boldsymbol{x}) > \boldsymbol{0} \tag{2.13}$$

have to be fulfilled. [79]

To ensure that the manifold is reached after a finite period of time and independent of the initial conditions of the system, in addition to (2.13) the sufficient reaching condition

$$\boldsymbol{s}\dot{\boldsymbol{s}} < 0,\ \forall \boldsymbol{s} \neq 0 \tag{2.14}$$

has to be fulfilled.

In terms of Lyapunov's theory the existence and reaching conditions for sliding mode can be summarized as follows: if there exists a Lyapunov function

$$V(\boldsymbol{s}) \in \mathbb{R}^+ : \begin{cases} V(\boldsymbol{s}) = 0 & \text{for} \quad \boldsymbol{s} = \boldsymbol{0} \\ V(\boldsymbol{s}) > 0 & \text{for} \quad \boldsymbol{s} \neq \boldsymbol{0} \end{cases} \tag{2.15}$$

and a constant $\varepsilon > 0$ satisfying the condition

$$\dot{V}(\boldsymbol{s}) \leq -\varepsilon \sqrt{V} \tag{2.16}$$

sliding mode exists on the manifold $\boldsymbol{s} = \mathbf{0}$ and is reached within finite time after starting from any initial state. Condition (2.16) guarantees finite transient time. If only $\dot{V}(\boldsymbol{s}) < 0$ were fulfilled for all $\boldsymbol{s} \neq \mathbf{0}$ but $\lim \dot{V}(\boldsymbol{s})_{\boldsymbol{s}\to\mathbf{0}} = 0$, points of attraction defined by $\boldsymbol{s} = \mathbf{0}$ would only be asymptotically stable and would not be reached in finite periods of time. This situation is common for differential equations with a right-hand side satisfying the Lipschitz condition.

Domains of attraction for sliding mode controllers may be found based on nonlinear control theory.

The reaching condition provides a design rule for sliding mode controller. Two possible sliding mode control unit design approaches for systems with vector control input will be explained next, the component-wise control and the unit control approach.

Component-Wise Control Law

The components of the control input $u_1, \ldots, u_m$ are chosen to undergo discontinuities on the corresponding surfaces $s_1(\boldsymbol{x}) = 0\,, \ldots\,,\ s_m(\boldsymbol{x}) = 0$,

$$u_i(\boldsymbol{x}) = \begin{cases} {u_i}^+(\boldsymbol{x}) & \text{for} \quad s_i(\boldsymbol{x}) > 0 \\ {u_i}^-(\boldsymbol{x}) & \text{for} \quad s_i(\boldsymbol{x}) < 0 \end{cases} \qquad i = 1 \ \ldots \ m\,. \tag{2.17}$$

Example 2.3 (Component-Wise Control Law)
The control input

$$\boldsymbol{u}(\boldsymbol{x}) = \boldsymbol{u}_{nom}(\boldsymbol{x}) + \bar{\mathbf{U}}(\boldsymbol{x}) \operatorname{sign} \boldsymbol{s} \tag{2.18}$$

with the continuous function $\boldsymbol{u}_{nom}(\boldsymbol{x})$, the diagonal matrix $\bar{\mathbf{U}}(\boldsymbol{x})$ possessing the non-zero elements $\bar{u}_i(\boldsymbol{x})$ with $i = 1 \ldots m$, and $\operatorname{sign} \boldsymbol{s} = (\operatorname{sign} s_1\,, \operatorname{sign} s_2\,, \ldots\,, \operatorname{sign} s_m)^T$, represents an example of a component-wise control law. In order to assign its parameters, the reaching condition (2.16) has to be evaluated for the Lyapunov function candidate

$$V = (\operatorname{sign} \boldsymbol{s})^T \boldsymbol{s}\,. \tag{2.19}$$

These considerations, which can be found in detail in [83], Section 2.5, especially page 33, yield the sufficient condition

$$\nabla \boldsymbol{s} \mathbf{G} \bar{\mathbf{U}} + (\nabla \boldsymbol{s} \mathbf{G} \bar{\mathbf{U}})^T > \mathbf{0} \quad \text{and} \tag{2.20}$$

$$\lambda_{min} \geq \sqrt{m} \left| \nabla \boldsymbol{s} (\boldsymbol{f} + \mathbf{G} \bar{\mathbf{U}} + \boldsymbol{z}) \right| + \varepsilon, \quad \varepsilon > 0 \tag{2.21}$$

where parameter λ_{min} denotes the smallest eigenvalue of the matrix

$$\frac{1}{2} \left(\nabla \boldsymbol{s} \mathbf{G} \bar{\mathbf{U}} + (\nabla \boldsymbol{s} \mathbf{G} \bar{\mathbf{U}})^T \right)\,. \tag{2.22}$$

Concerning condition (2.21), the design of the component-wise controller (2.18) requires the estimation of the upper limits of the disturbances. Finding a function $\bar{\mathbf{U}}(\boldsymbol{x})$ such that (2.21) is fulfilled is challenging, since eigenvalues for symbolic matrices are hard to calculate.

Unit Control Law

Sliding mode can be enforced even if not all components of $\boldsymbol{u}$ are designed individually as discontinuous state functions.

Example 2.4 (Unit Control Law)
An example of an unit control law is given in [19, 63]:

$$\boldsymbol{u} = -\phi(\boldsymbol{x}) \frac{(\nabla \boldsymbol{s}\ \mathbf{G})^T \boldsymbol{s}}{|(\nabla \boldsymbol{s}\ \mathbf{G})^T \boldsymbol{s}|} \qquad \text{rank}\,(\nabla \boldsymbol{s}\ \mathbf{G}) = m\,. \tag{2.23}$$

With a scalar function

$$\phi(\boldsymbol{x}) > \left|(\nabla \boldsymbol{s}\ \mathbf{G})^{-1} \nabla \boldsymbol{s}\ (\boldsymbol{f}(\boldsymbol{x}) + \boldsymbol{z}(\boldsymbol{x}))\right|. \tag{2.24}$$

it enforces sliding mode in the intersection $\boldsymbol{s}(\boldsymbol{x}) = \mathbf{0}$ of m. This existence condition for sliding mode can be derived on a Lyapunov function candidate

$$V = \frac{1}{2} \boldsymbol{s}^T \boldsymbol{s}\,. \tag{2.25}$$

Compared to the component-wise control law design this is a more straight forward approach. Nevertheless, it requires the full rank of matrix $\nabla \boldsymbol{s}\ \mathbf{G}$. To be able to calculate the function $\phi(\boldsymbol{x})$, the limits of the disturbances have to be estimated. The complete derivation of this control law can be found in [83], Section 3.5, especially page 45.

The component-wise control undergoes discontinuities as soon as any of the components of the vector $\boldsymbol{s}$ changes its sign, whereas the unit control undergoes discontinuities only if the manifold $\boldsymbol{s}(\boldsymbol{x}) = \mathbf{0}$ is reached.

2.1.6 Conclusion

This section summarizes the sliding mode control theory, introduces the design tools that are used in this thesis, and highlights the main characteristics of sliding mode control strategies. The theory presented presumes that

- the model of the controlled system is known exactly and
- the switching frequency of the control input is infinite.

Both assumptions do not hold for real-life applications. As a result, real-life applications of sliding mode control schemes often show chattering effects and insufficient performance.

In order to provide a basis for further investigations into implementation issues of sliding mode controllers, the next section summarizes the state-of-the-art solutions to the chattering problem.

2.2 Chattering Reduction Concepts

The most attractive feature of sliding mode control is robustness against parameter variations and disturbances. However, sliding mode comes along with the undesirable phenomenon of chattering.

Many different concepts exist that try to reduce the effect of chattering. They can be categorized as methods that modify the hardware or the control structure as illustrated in Figure 2.2. Schemes that change the control structure can be classified in gain modification algorithms and structural methods. Some methods offer a trade-off between chattering reduction and robustness, while others are quite effective but hard to implement. The following sections provide an overview of theses techniques, which are mainly given in the overview papers [89] and [84].

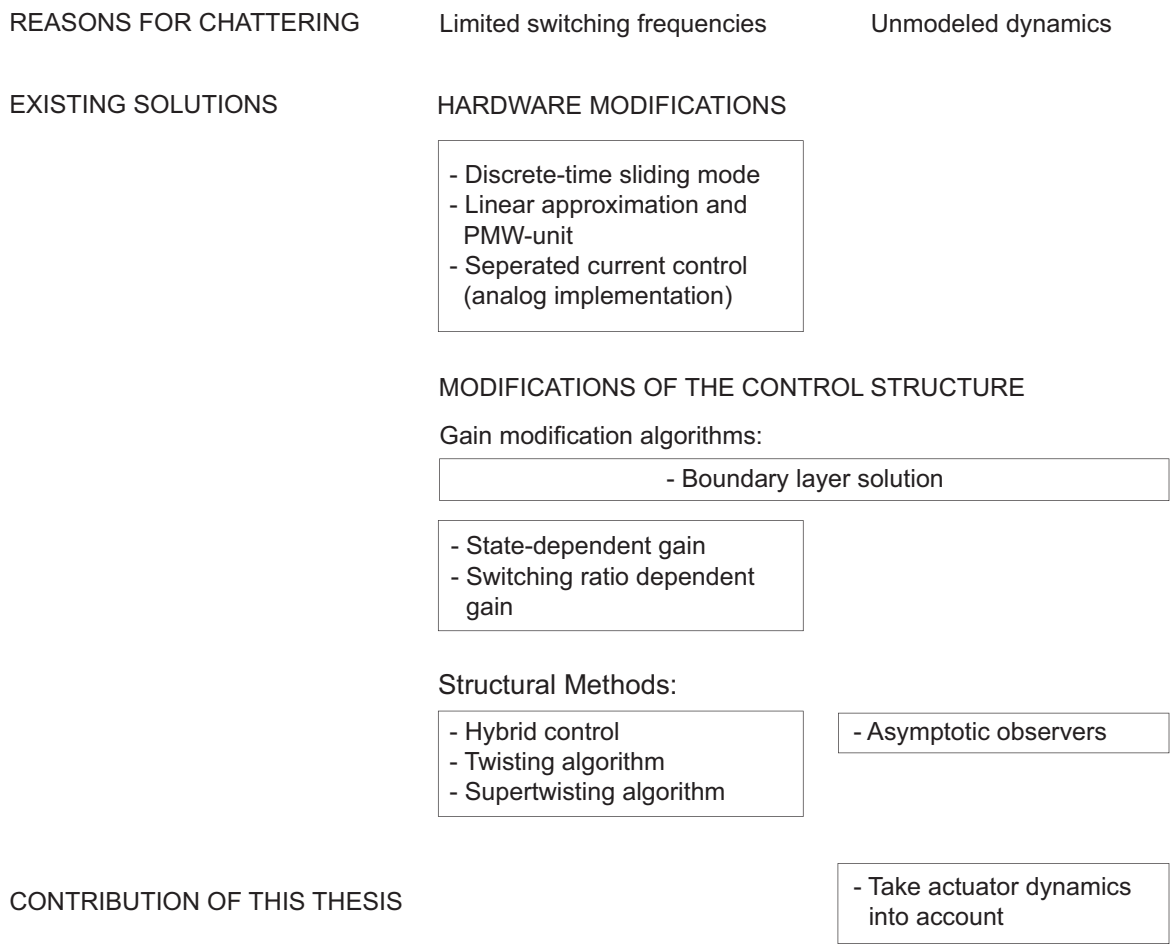

Figure 2.2: Chattering reduction methods.

2.2.1 Hardware Modifications

The problem of chattering caused by limited switching frequencies can be solved by the implementation of discrete-time sliding mode [23, 76]. Chattering may also be suppressed by a linear approximation of the switching control and implementation via pulse width modulated signals. An advantage of this control architecture is determined sampling times. In contrast to floating switching frequencies, constant switching frequencies are more convenient for filtering. Additionally, PWM-units can be optimized for low energy losses. If the control of the electrical variables, namely current, is separated from the control of the mechanical variables and implemented by analog devices, chattering due to finite switching frequencies may be decreased as well.

2.2.2 Gain Modification Algorithms

The algorithms presented in this subsection reduce chattering by modifying the gain of the discontinuous control function $\boldsymbol{u}(\boldsymbol{x})$ in a neighborhood of the sliding manifold.

Boundary Layer Solution

This technique replaces the discontinuous control law with a continuous approximation such that unmodeled dynamics is not excited [69, 68]. Chattering can be reduced if the approximation decreases the control gain. Inside a boundary layer defined around the manifold $B(\varepsilon) = \{\boldsymbol{x} \mid |\boldsymbol{s}(\boldsymbol{x})| < \varepsilon\}$ with $B \subset \mathbb{R}^n$, the discontinuous control function is approximated by a smooth or piecewise linear function. For example the scalar control function

$$u = -\operatorname{sign}(s) \tag{2.26}$$

can be approximated by the linear function

$$u = -M \operatorname{sat}(\frac{s}{\varepsilon}) \quad M, \varepsilon \in \mathbb{R}^+ \tag{2.27}$$

or the continuous nonlinear approximation

$$u = -M \frac{s}{|s| + \varepsilon} \quad M, \varepsilon \in \mathbb{R}^+ , \tag{2.28}$$

as shown in Figure 2.3. Outside of B, a control law, as before, guarantees that the state reaches the boundary layer B after a finite period of time and then stays there.

The singular perturbation theory [39] can be used to analyze the stability properties of the closed loop with the approximated control law. Using appropriate Lyapunov functions, it can be shown that the motion of systems disregarding unmodeled dynamics is unstable in a finite vicinity of the discontinuity surface, while the trajectories converge to this surface for larger deviations. A precondition is that the unmodeled dynamics have to be stable and faster than the system dynamics themselves. Thus, the bandwidth of the closed loop system and the gain of the linear feedback are limited. This in turn limits the robustness of the system.

With the boundary layer solution approach, the sliding manifold is tracked with a guaranteed imprecision ε. If the width ε of the boundary layer is chosen to be large, the linear gain within the ε-vicinity of the sliding manifold gets smaller and robustness is reduced. In order to reject unknown disturbances, sufficiently high gains are needed. If ε is too small, chattering is not completely eliminated. Usually neglected high-frequency dynamics must be considered when designing the approximation in order to avoid instability inside the boundary layer.

State Dependent Gain Modification

This approach follows the original variable structure control methodology [84]. The loop gain does not depend on $\boldsymbol{s}(\boldsymbol{x})$ but only on one state variable x of the system. For the control law (2.26) this means

$$u = -M(\frac{|x|}{\varepsilon} + \delta) \operatorname{sign}(s) \quad M, \varepsilon, \delta \in \mathbb{R}^+ . \tag{2.29}$$

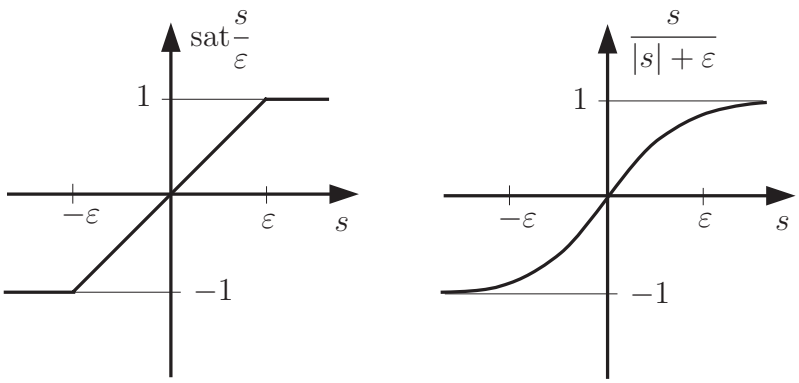

Figure 2.3: Linear and nonlinear continuous approximation of a scalar discontinuous control function.

The major advantage of this method is its ease of implementation: the required rate of change of the gain M is determined by the dynamics of $x(t)$, whereas in the continuous approximation method, the gain needs to change with the sampling rate.

Switching Ratio Dependent Gain

A single input system with $u \in \{+M; -M\}$ is considered. Chattering is reduced by decreasing the gain of the discontinuous control function related to a reference switching ratio [84]

$$\sigma = \frac{T_{on} - T_{off}}{T_{on} + T_{off}}\,, \tag{2.30}$$

where T_{on} represents the time when control input $u = +M$ and T_{off} represents the time when the control input $u = -M$. The switching ratio is the average of the function $\text{sign}(s)$, which can in practice be implement using a low-pass filter. Based on the switching ratio, the control is chosen to be

$$u = -M(|\sigma - \sigma^*| + \delta)\,\text{sign}(s) \quad M, \varepsilon, \delta \in \mathbb{R}^+\,. \tag{2.31}$$

where σ and σ^* represent actual and reference switching ratios.

A problem with this method is to find an appropriate reference switching ratio σ^* as it depends on system parameters and disturbances.

2.2.3 Structural Methods

The algorithms presented in this section modify not only the gain but the whole structure of the control system. The objective is to go beyond the limits of the previous algorithms and to try to suppress both sources of chattering while improving convergence behavior.

Observer-Based Solution

As a solution to reduce the chattering effect, an asymptotic observer to the system as shown in Figure 2.4 can be introduced [20].

$$\dot{\hat{\boldsymbol{x}}} = \hat{\boldsymbol{f}}(\hat{\boldsymbol{x}}) + \hat{\mathbf{G}}(\hat{\boldsymbol{x}})\boldsymbol{u} + \tilde{\boldsymbol{f}}(\hat{\boldsymbol{x}} - \boldsymbol{x}) \quad \hat{\boldsymbol{x}} \in \mathbb{R}^n \tag{2.32}$$

where $\hat{\boldsymbol{x}}$ represents the observer state, functions $\hat{\boldsymbol{f}}$ and $\hat{\mathbf{G}}$ describe modeled system dynamics, and the feedback function $\tilde{\boldsymbol{f}}$ corrects the difference between real and observed state, $\overline{\boldsymbol{x}} = \hat{\boldsymbol{x}} - \boldsymbol{x}$, to zero.

Unmodeled dynamics does not appear in the observer dynamics, hence chattering is suppressed. Moreover, since the control action is calculated based on the observer state $\hat{\boldsymbol{x}}$, chattering is suppressed in the control loop as well.

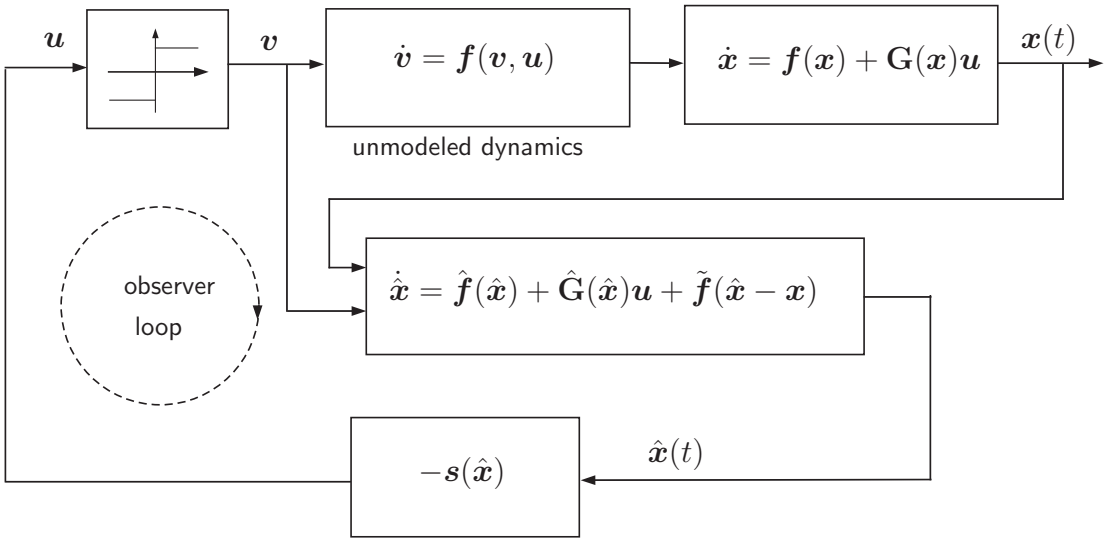

Figure 2.4: Observer-based solution.

However, this approach assumes that an asymptotic observer can be designed such that the observation error converges to zero asymptotically. Disturbances may effect the convergence of asymptotic observers and therefore methods which estimate both the state and the disturbances have to be applied. The method only removes the chattering caused by unmodeled dynamics while the chattering caused by finite switching frequencies is not reduced. This chattering can be reduced as well when the observer approach is combined with any of the gain modification algorithms. The observer-based solution requires some effort in the control unit design and is sensitive to sensor noise.

Hybrid Control Method

The control signal is divided into a continuous control signal $\boldsymbol{u}_{lin}$ and a discontinuous control signal $\boldsymbol{u}_{dis}$,

$$\boldsymbol{u} = \boldsymbol{u}_{lin} + \boldsymbol{u}_{dis}\,. \tag{2.33}$$

The control component $\boldsymbol{u}_{lin}$ assures ideal performance under the assumption that the system model is well known [11]. When disturbances or parameter uncertainties appear, the discontinuous control component $\boldsymbol{u}_{dis}$ is required to preserve robustness, as was shown before. Using this control method the major part of the control task is realized by the linear control making the non linear control negligible. Therefore robustness degrades.

Second Order Sliding Mode

While one of the main features of standard sliding mode control is finite time convergence, the convergence behavior of the standard second order sliding mode control [5] is asymptotic. The standard sliding mode control is of first order, e.g. $\dot{\boldsymbol{s}}$ is discontinuous. In second order sliding mode, $\ddot{\boldsymbol{s}}$ is discontinuous and $\dot{\boldsymbol{s}}$ is continuous. The order of state of the plant is artificially increased by introducing another state variable x_{n+1}. E.g. for a single input system, the discontinuous control signal u

$$\dot{u} = -R \operatorname{sign}(x_{n+1} + cs) \quad R, c \in \mathbb{R}^+ \tag{2.34}$$

is chosen to be the derivative of the control signal. Since the discontinuous control signal passes an integrator, the control signal u fed to the plant is continuous. Chattering can only be reduced by finding a trade-off with disturbance rejection capability. Second order sliding mode converges only $\dot{\boldsymbol{s}} = \boldsymbol{0}$ within finite time. Depending on implementation, the basic algorithm may require an observer.

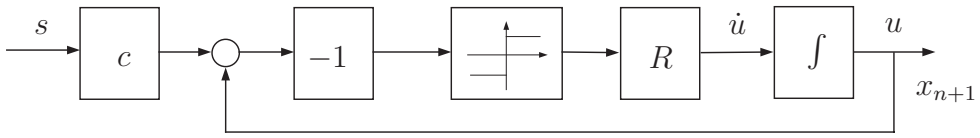

Figure 2.5: Second-order sliding mode algorithm.

Twisting Algorithm

The twisting algorithm [42] is a special form of second order sliding mode that provides finite time convergence. It is applicable only to single input systems. The sliding mode control problem is formulated as a finite time stabilization problem for uncertain second order systems

$$\ddot{s} = f(\boldsymbol{x}) + g(\boldsymbol{x})\dot{u} \tag{2.35}$$

with $|f(\boldsymbol{x})| \leq F$,$G_m \leq g \leq G_M$, $F, G_m, G_M \in \mathbb{R}^+$.

The algorithm features a bounded control input continuously depending on time with discontinuities in the control input time-derivative, which is given by

$$\dot{u} = R_{TA} \cdot \begin{cases} -u & \text{for} \quad |u| > M_{TA} \\ -V_{M_{TA}} \operatorname{sign}(s) & \text{for} \quad s\,\dot{s} > 0 \quad \text{and } |u| \leq M_{TA} \\ -V_{m_{TA}} \operatorname{sign}(s) & \text{for} \quad s\,\dot{s} \leq 0 \quad \text{and } |u| \leq M_{TA} \end{cases} \tag{2.36}$$

$$R_{TA}\,, V_{m_{TA}}\,, V_{M_{TA}} \in \mathbb{R}^+\,. \tag{2.37}$$

If the sufficient conditions

$$V_{M_{TA}} > V_{m_{TA}} \tag{2.38}$$

$$V_{m_{TA}} > \frac{4G_M}{M_{TA}} \tag{2.39}$$

$$V_{m_{TA}} > \frac{F}{G_M} \tag{2.40}$$

$$G_m V_{M_{TA}} - F > G_M V_{m_{TA}} + F \tag{2.41}$$

are fulfilled, the system converges in finite time to $s = \dot{s} = 0$. The algorithm can be implemented following Figure 2.6 where parameters are chosen as $c_{1_{TA}} = \frac{V_{M_{TA}} + V_{m_{TA}}}{2}$ and $c_{2_{TA}} = \frac{V_{M_{TA}} - V_{m_{TA}}}{2}$, $c_{1_{TA}} > c_{2_{TA}} > 0$. The sign of the time derivative of s can only be approximated by

$$\operatorname{sign}(\dot{s}(t)) \approx \operatorname{sign}(s(t) - s(t - \Delta T)) \,. \tag{2.42}$$

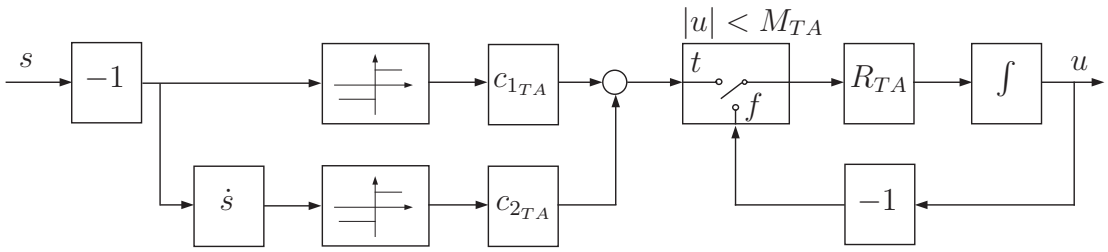

Figure 2.6: Twisting algorithm.

Super-Twisting Algorithm

This derivative from the twisting algorithm does not need any information about the time derivative of s. For single input systems it is given by [9]

$$u = -c_{1_{STA}} \int \operatorname{sign}(s) \mathrm{d}t - c_{2_{STA}} \begin{cases} |s|^{\rho_{STA}} \operatorname{sign}(s) & \text{if } |s| \leq \varepsilon_{STA} \\ |\varepsilon_{STA}|^{\rho_{STA}} \operatorname{sign}(s) & \text{if } |s| > \varepsilon_{STA} \end{cases} \tag{2.43}$$

$$c_{1_{STA}} \,, c_{2_{STA}} \,, \rho_{STA} \,, \varepsilon_{STA} \in \mathbb{R}^+ \,. \tag{2.44}$$

Sufficient conditions for the system's finite convergence to $\dot{s} = s = 0$ are

$$c_{1_{STA}} > \frac{F}{G_m} \tag{2.45}$$

$$c_{2_{STA}}{}^2 \geq \frac{4F}{G^2{}_m} \frac{G_M(c_{1_{STA}} + F)}{G_m(c_{1_{STA}} - F)} \tag{2.46}$$

$$0 < \rho_{STA} \leq 0.5 \,. \tag{2.47}$$

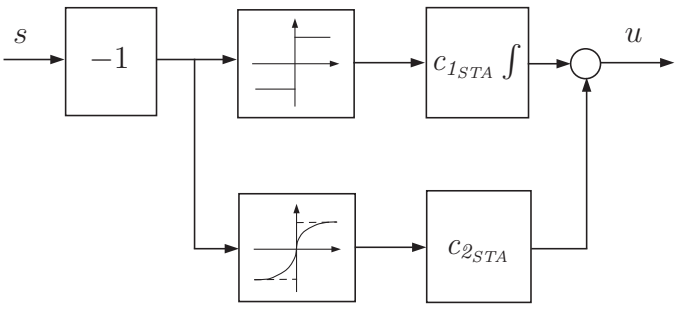

Figure 2.7: Super-twisting algorithm.

2.2.4 Discussion

In practical applications of sliding mode control, chattering due to unmodeled dynamics and limited switching frequencies may pose a problem. Present attempts to reduce or eliminate chattering included hardware changes as well as modifications of the control algorithm.

The proposed solutions based on hardware modification require considerable changes of the control unit. By decreasing the loop gain, the gain modification algorithms reduce chattering significantly but the ability to reject disturbances deteriorates. An efficient way to reduce chattering due to unmodeled dynamics is the use of asymptotic observers. But this method as well as other structural methods substantially increase the complexity of the implementation compared to conventional sliding mode control. The twisting and the super twisting algorithm represent very efficient chattering reduction methods. However, up to now their application is restricted to single input systems.

Table 2.1 summarizes the features of the pure sliding mode control algorithm and chattering reduction concepts that can be found in the current literature. The comparison shows that none of the existing chattering reduction methods is able to preserve both main advantages of sliding mode control which are simple implementation and robustness.

Method	Chattering reduction	Robustness	Design complexity
Pure sliding mode control algorithm	+	+++	+++
Discrete-time sliding mode	+++	+	++
Linear approximation or PMW-unit	++	++	+
Separated current control	++	+	+
Boundary layer solution	+++	++	+
State-dependent gain modification	++	++	+++
Switching ratio dependent gain	++	++	++
Observer based solution	+++	+++	+
Hybrid control	++	+	++
Second order sliding mode	++	+	+
Twisting algorithm	+++	++	+
Supertwisting algorithm	+++	++	++

Table 2.1: Evaluation of existing chattering reduction concepts. The summary is a result of numerical simulations, in which an electromechanical system of third order was exposed to both sources of chattering, unmodeled dynamics and limited switching frequencies. The denotation of the symbols in column one and two is adequate (+), moderate (++), and excellent (+++). The denotation in column three is high (+), moderate (++), and low (+++). The design complexity criterion regards the hardware as well as the calculation capacities that are required for the implementation of the control algorithm.

2.3 Conclusion

This chapter illustrates the theory and implementation issues of sliding mode controllers. It is shown that all implementations are a trade-off between chattering, robustness and implementation complexity. For this purpose an evaluation and comparison of the existing chattering reduction methods is given that provides a basis for control design decisions.

Nevertheless, with present-day technologies the more complex implementations become competitive. Since the computing power of the control units increases continuously, more complex solutions, e.g. adding an observer, no longer add significantly to the cost of implementation. In recent years, semiconductor technologies have rapidly improved. Today solid state switches that allow high switching frequencies together with minor energy losses are available. These modern devices make pure sliding mode control algorithms a viable option.

Based on the summary of the state of the art given in this chapter, this thesis investigates sliding mode control schemes that take advantage of state-of-the-art technological developments. For electromechanical systems a novel control concept is developed that provides excellent chattering reduction and robustness while accepting high implementation efforts. The proposed control scheme needs a control unit that provides very high switching frequencies and is based on a high-order system model. The control design process therefore becomes costlier. Both requirements can be met: As explained in the last paragraph, the latest technologies provide the necessary hardware. In Chapter 3 a control design methodologies is formulated that simplifies the design problem.

3 The Generalized Block Control Principle

On the one hand, if fast system dynamics is not neglected and more accurate system models are used for the sliding mode control design, chattering can be reduced. On the other hand, the control design for more accurate systems becomes more complicated. The block control principle (BCP) [21, 22, 45, 47] represents a method that simplifies the control unit design for complex systems. It is based on a system transformation into the block control form (BCF). This is a decomposition of the original system into independent subsystems of lower dimension for which the control is designed simpler than for the initial system. However, not every nonlinear system can be transformed into the BCF and finding the right nonlinear system transformation into the BCF can be difficult. Even if these transformations exist, the BCP-approach may lead to a very large number of nonlinear transformations needed for decomposing. When investigating chattering reduction by taking unmodeled dynamics into account, a main challenge is to find a design method that can handle the more accurate system models without disproportionate effort.

This chapter proposes a design technique that does not require a consequent decomposition of the system in the afore mentioned BCF, thus allowing to handle more accurate system models. The derived generalized block control principle (GBCP) is based on the idea that in the majority of cases electromechanical systems consist of subsystems in canonical form. Because the control design may easily be performed for these subsystems in canonical form, the strict transformation of the system into the BCF is not reasonable. A limited system decomposition may shorten the design procedure. The GBCP extends an existing generalized design procedure, which is introduced in [78]. Compared to this method the GBCP handles interconnected systems of arbitrary order in canonical form as well as systems with infinite dimension.

The innovation presented in this chapter is a closed methodology for the systematic control unit design for electromechanical systems. For the first time, solutions to implementation problems of sliding mode control based on the BCP are given. The main contribution is a new method for disturbance rejection.

In this chapter, Section 3.1 explains the BCP as the state-of-the-art design method. Section 3.2 states the limitations of the BCP and introduces as a solution to the problem the approach given in [78]. Section 3.3 extends the existing design procedures to nonlinear systems with subsystems in canonical form, which are common for mechanical and electromechanical plants, and introduces the GBCP. Section 3.4 illustrates the existing sliding mode control of a flexible shaft as a successful application of the GBCP to an infinite dimensional system. Practical issues of the proposed GBCP are discussed in Section 3.5. Necessary observers as well as a method to reject disturbances with known structure are presented. This chapter concludes with a summary in Section 3.6.

3.1 State of the Art: The Block Control Principle

The BCP is a control unit design principle that simplifies the design process for complex systems. Using a system transformation into BCF the control design problem is broken down into a set of design problems of lower dimensions. In [21, 22] the BCP is developed for linear systems and linked to the design of discontinuous control. In [45, 47] extensions to nonlinear systems are done. This section introduces the BCP.

The BCP is based on the BCF, which is a generalization of the regular form [48].

Definition 3.1: *Regular Form.*

A nonlinear system (2.1) in regular form is given as

$$\begin{aligned} \dot{\boldsymbol{x}}_1 &= \boldsymbol{f}_1(\boldsymbol{x}_1, \boldsymbol{x}_2) \\ \dot{\boldsymbol{x}}_2 &= \boldsymbol{f}_2(\boldsymbol{x}_1, \boldsymbol{x}_2) + \mathbf{G}_2(\boldsymbol{x}_1, \boldsymbol{x}_2)\boldsymbol{u} \end{aligned} \tag{3.1}$$

where $\boldsymbol{x}_1 \in \mathbb{R}^{n-m},\ \boldsymbol{x}_2 \in \mathbb{R}^m$, and $\det(\mathbf{G}_2) \neq 0$ ■

The necessary and sufficient conditions for the system transformation of system (2.1) into the regular form,

$$\boldsymbol{x} \overset{\phi}{\mapsto} \begin{pmatrix} \boldsymbol{x}_1 \\ \boldsymbol{x}_2 \end{pmatrix} \qquad \boldsymbol{\phi} : \mathbb{R}^n \mapsto \mathbb{R}^n\,;\ \boldsymbol{x}_1 \in \mathbb{R}^{(n-m)}\,, \boldsymbol{x}_2 \in \mathbb{R}^{(m)}\,, \tag{3.2}$$

are based on tools from differential geometry. They are found in [48] and are not discussed in detail in this thesis.

The control unit design for system (3.1) can be performed easily by decomposing it into two subsystems of lower dimension: The sub-vector $\boldsymbol{x}_2$ is handled as a virtual control input and selected as a function of the sub-vector $\boldsymbol{x}_1$ to provide desired dynamics in the first subsystem. This is a design problem in the system of $(n-m)$th order with m-dimensional control input. The control of the second subsystem is chosen to set the error between the real and the desired value of $\boldsymbol{x}_2$ asymptotically stable. This control problem for a m-dimensional system is rather simple since the dimension of the state $\boldsymbol{x}_2$ and the control input $\boldsymbol{u}$ coincide.

The design problem for system (3.1) can be simplified again by partitioning the first equation of the system (3.1) into two independent subproblems of lower order:

$$\boldsymbol{x}_1 \overset{\phi_1}{\mapsto} \begin{pmatrix} \boldsymbol{x}_{11} \\ \boldsymbol{x}_{12} \end{pmatrix} \qquad \boldsymbol{\phi}_1 : \mathbb{R}^{(n-m)} \mapsto \mathbb{R}^{(n-m)}\,;\ \boldsymbol{x}_{11} \in \mathbb{R}^{(n-2m)}\,, \boldsymbol{x}_{12} \in \mathbb{R}^{(m)}\,. \tag{3.3}$$

If required, further simplification of the design procedure is achieved by further partitioning of the first equation of the resulting systems. This decomposition of the original design

problem into a set of trivial ones with equal dimension of control input and state is called BCF.

Definition 3.2: *Block Control Form.*
A nonlinear system (2.1) in Block Control Form is given as

$$\begin{aligned} \dot{\boldsymbol{x}}_i &= \boldsymbol{f}_i(\boldsymbol{x}_r, \ldots, \boldsymbol{x}_i) &&+ \mathbf{G}_i(\boldsymbol{x}_r, \ldots, \boldsymbol{x}_i)\boldsymbol{x}_{i-1} && \text{for } i = 2 \ldots r \\ \dot{\boldsymbol{x}}_1 &= \boldsymbol{f}_1(\boldsymbol{x}_r, \ldots \boldsymbol{x}_1) &&+ \mathbf{G}_1(\boldsymbol{x}_r, \ldots, \boldsymbol{x}_1)\boldsymbol{u} && \text{for } i = 1\,. \end{aligned} \tag{3.4}$$

where $\dim(\boldsymbol{x}_i) = m$ and $\dim(\boldsymbol{x}_r) \leq m$ for $i = 1 \ldots (r-1)$. Subsystems with the state $\boldsymbol{x}_i$ $(i = 1 \ldots r)$ are called blocks. ■

The procedure of transformation of the nonlinear system (2.1) into the BCF (3.4) consists of $(r-1)$ steps. In each step a transformation of a subsystem into the regular form is done. Therefore, a system transformation into the BCF exists, if in each step the necessary and sufficient conditions for the transformation of the considered subsystem into the regular form, which are given in [48], are fulfilled. In [44, 45] the existence conditions of the BCF (3.4) for nonlinear systems are given. They also hold for systems with a control matrix of incomplete rank, meaning $\operatorname{rank}(\mathbf{G}) < m$.

To realize the control objective $\lim_{t\to\inf} \boldsymbol{x}_r^*(t) = \mathbf{0}$ for system (3.4), following the BCP, the control unit design is done as follows: The state of the second block $\boldsymbol{x}_{r-1}$ is handled as virtual control input for the first block in order to assign a desired dynamics $\dot{\boldsymbol{x}}_r^* = \boldsymbol{f}_r^*(\boldsymbol{x}_r^*)$, e.g. $\dot{\boldsymbol{x}}_r^* = \boldsymbol{\Lambda}\boldsymbol{x}_r^*$ with matrix $\boldsymbol{\Lambda}$ satisfying the Hurwitz condition. To realize these desired dynamics $\dot{\boldsymbol{x}}_r{}^*$, derived from (3.4) the virtual control input

$$\boldsymbol{x}_{r-1}^* = \mathbf{G}_r^+\big(\boldsymbol{f}_r^*(\boldsymbol{x}_r^*) - \boldsymbol{f}_r(\boldsymbol{x}_r^*)\big) = \tilde{\boldsymbol{f}}_{r-1}(\boldsymbol{x}_r^*) \tag{3.5}$$

is required. For the following block, the dynamics of the error between the desired and real value of the virtual control input is assigned to be asymptotically stable. Following (3.4), the dynamics of the error

$$\boldsymbol{s}_{r-1} = \boldsymbol{x}_{r-1} - \boldsymbol{x}_{r-1}^* \tag{3.6}$$

results in

$$\dot{\boldsymbol{s}}_{r-1} = \dot{\boldsymbol{x}}_{r-1} - \tilde{\boldsymbol{f}}_{r-1}(\boldsymbol{x}_r^*) \tag{3.7}$$

$$= \boldsymbol{f}_{r-1}(\boldsymbol{x}_r\,, \boldsymbol{x}_{r-1}) + \mathbf{G}_{r-1}(\boldsymbol{x}_r\,, \boldsymbol{x}_{r-1})\boldsymbol{x}_{r-2} - \tilde{\boldsymbol{f}}_{r-1}(\boldsymbol{x}_r^*)\,. \tag{3.8}$$

Based on (3.8), a desired behavior $\dot{\boldsymbol{s}}_{r-1}^* = \boldsymbol{f}_r^*(\boldsymbol{s}_{r-1}^*)$ can be realized by choosing the virtual control input

$$\begin{aligned} \boldsymbol{x}_{r-2}^* &= \mathbf{G}_{r-1}^+(\boldsymbol{x}_r^*\,, \boldsymbol{x}_{r-1}^*)\big(\dot{\boldsymbol{s}}_{r-1}^* - \boldsymbol{f}_{r-1}(\boldsymbol{x}_r^*\,, \boldsymbol{x}_{r-1}^*) + \tilde{\boldsymbol{f}}_{r-1}(\boldsymbol{x}_r^*)\big) \\ &= \tilde{\boldsymbol{f}}_{r-2}(\boldsymbol{x}_r^*\,, \boldsymbol{x}_{r-1}^*)\,. \end{aligned}$$

This procedure is repeated for each block $(i = (r-2) \ldots 2)$. The desired dynamics for

$$\dot{\boldsymbol{s}}_i = \dot{\boldsymbol{x}}_i - \tilde{\boldsymbol{f}}_i(\boldsymbol{x}_r^*\,, \ldots\,, \boldsymbol{x}_{i+1}^*) \tag{3.9}$$

$$= \boldsymbol{f}_i(\boldsymbol{x}_r\,, \ldots\,, \boldsymbol{x}_i) + \mathbf{G}_i(\boldsymbol{x}_r\,, \ldots\,, \boldsymbol{x}_i)\boldsymbol{x}_{i-1} - \tilde{\boldsymbol{f}}_i(\boldsymbol{x}_r^*\,, \ldots\,, \boldsymbol{x}_{i+1}^*) \tag{3.10}$$

is realized by the virtual control input

$$\begin{aligned}\boldsymbol{x}_{i-1}^* &= \mathbf{G}_i^+(\boldsymbol{x}_r^*, \dots, \boldsymbol{x}_i^*)\big(\dot{\boldsymbol{s}}_i^* - \tilde{\boldsymbol{f}}_i(\boldsymbol{x}_r^*, \dots, \boldsymbol{x}_i^*) + \boldsymbol{f}_i(\boldsymbol{x}_r, \dots, \boldsymbol{x}_{i+1})\big) \\ &= \tilde{\boldsymbol{f}}_{i-1}(\boldsymbol{x}_r^*, \dots, \boldsymbol{x}_i^*)\,.\end{aligned}$$

Finally, the desired dynamics for the last block is calculated with

$$\begin{aligned}\boldsymbol{x}_1^* &= \mathbf{G}_2^+(\boldsymbol{x}_r^* \dots, \boldsymbol{x}_2^*)\big(\dot{\boldsymbol{s}}_2^* - \boldsymbol{f}_2(\boldsymbol{x}_r^*, \dots, \boldsymbol{x}_1^*) + \tilde{\boldsymbol{f}}_2(\boldsymbol{x}_r^*, \dots, \boldsymbol{x}_3^*)\big) \\ &= \tilde{\boldsymbol{f}}_1(\boldsymbol{x}_r^*, \dots, \boldsymbol{x}_2^*)\end{aligned}$$

and the feedback control $\boldsymbol{u}(\boldsymbol{x})$ has to be chosen such that

$$\boldsymbol{s}_1 = \boldsymbol{x}_1 - \boldsymbol{x}_1^* = \mathbf{0} \tag{3.11}$$

is fulfilled. Regarding (3.4), follows

$$\dot{\boldsymbol{s}}_1 = \dot{\boldsymbol{x}}_1 - \tilde{\boldsymbol{f}}_1(\boldsymbol{x}_r^*, \dots, \boldsymbol{x}_2^*) \tag{3.12}$$

$$= \boldsymbol{f}_1(\boldsymbol{x}_r, \dots, \boldsymbol{x}_1) + \mathbf{G}_1(\boldsymbol{x}_r, \dots, \boldsymbol{x}_1)\boldsymbol{u} - \tilde{\boldsymbol{f}}_1(\boldsymbol{x}_r^*, \dots, \boldsymbol{x}_2^*)\,. \tag{3.13}$$

A linear feedback to establish $\lim_{t\to\infty} \boldsymbol{s}_1 = \mathbf{0}$ could be

$$\boldsymbol{u} = \mathbf{G}_1^+(\boldsymbol{x}_r \dots, \boldsymbol{x}_1)\big(\boldsymbol{\Lambda}_1\boldsymbol{s}_1 - \boldsymbol{f}_1(\boldsymbol{x}_r, \dots, \boldsymbol{x}_1) + \tilde{\boldsymbol{f}}_1(\boldsymbol{x}, \dots, \boldsymbol{x}_2)\big)\,, \tag{3.14}$$

where matrix $\boldsymbol{\Lambda}_1$ has to fulfill the Hurwitz condition in order to guarantee asymptotic stability. A discontinuous control could be

$$\boldsymbol{u} = -\mathbf{M}\,\mathrm{sign}(\boldsymbol{s}_1)\,, \quad \mathbf{M} \in \mathbb{R}^{m\times m} \tag{3.15}$$

by selecting $\mathbf{M}$ based on the design methodology of sliding mode control. Then sliding mode is enforced on the surface $\boldsymbol{s}_1 = \mathbf{0}$ and leads to

$$\boldsymbol{s}_1 = \mathbf{0} \tag{3.16}$$

after a finite time.

If the error $\boldsymbol{s}_1$ gets zero in finite or infinite time all other desired dynamics is realized and

$$\dot{\boldsymbol{x}}_i^* = \tilde{\boldsymbol{f}}_i^*(\boldsymbol{x}_r^*, \dots, \boldsymbol{x}_{i+1}^*)\,, \quad i = 2 \dots r\,. \tag{3.17}$$

The resulting motion of the system is described by pre-selected desired dynamics. Using the BCP the initial design problem is reduced to r simple subproblems. Control laws have to be found only for subsystems of low order with equal dimensions of the control input and the state.

3.2 Problem Statement

The BCP simplifies the design procedure. However, for high-order systems, the principle may complicate the control unit design. A problem arises from the potentially high number of subproblems necessary to be solved. It can be very large and correspondingly, a very large number of coordinate transformations is needed to get the system into the BCF, a system description the BCP can be applied to. In addition, for nonlinear systems, these coordinate transformations may not always exist [48]. Therefore, in this chapter a new control algorithm is developed. It is applicable to systems in generalized block control form (GBCF). Compared to the BCP the GBCP requires less system transformations during the design procedure and it preserves the design simplicity of subsystems in canonical form.

The GBCP is applicable to systems in GBCF. As systems in BCF, systems in GBCF consist of r subsystems and the state of each subsystem can be seen as intermediate control input for the preceding subsystem. But in contrast to the BCF, the subsystems are given in canonical form. This means that the dimension of the intermediate control $\boldsymbol{x}_{i-1}$ may be less than the dimension of the state $\boldsymbol{x}_i$ for $i = 2 \dots r$. The system dynamics of a block does not have to be linearly dependent on the state of the preceding block.

Definition 3.3: *Generalized Block Control Form.*
A nonlinear system (2.1) in Generalized Block Control Form (GBCF) is given as

$$\begin{aligned} &\overset{(n_i)}{x}_{i,1} = \overset{(n_i-1)}{x}_{i,2} = \dots = \dot{x}_{i,n_i} = f_i(\boldsymbol{x}_r, \dots, \boldsymbol{x}_i, \boldsymbol{x}_{i-1}) && \text{for } i = 2 \dots r \\ &\overset{(n_1)}{x}_{1,1} = \overset{(n_1-1)}{x}_{1,2} = \dots = \dot{x}_{1,n_1} = f_1(\boldsymbol{x}_r, \dots, \boldsymbol{x}_1) + \boldsymbol{g}_1^T(\boldsymbol{x}_r, \dots, \boldsymbol{x}_1)\boldsymbol{u} && \text{for } i = 1 \end{aligned} \tag{3.18}$$

where subsystems with the state $\boldsymbol{x}_i$ $(i = 1 \dots r)$, $\boldsymbol{x}_i^T = [x_{i,1} \dots x_{i,n_i}] \in \mathbb{R}^{n_i}$ are called blocks. ■

The system transformation into the GBCF follows the methods from the BCF. But the system decomposition into independent subsystems is stopped as soon as subsystems in canonical form appear. This way, additional blocks and system transformations are avoided. It is not efficient to decompose all subsystems, because for systems in canonical form the control input may be found easily in terms of the original blocks even if the control dimension is less than that of the system.

Example 3.5 (Illustration of the Inefficiency of the BCP)
The system

$$\begin{aligned} \ddot{x}_2 &= f_2(x_1, x_2, \dot{x}_1, \dot{x}_2) \\ \ddot{x}_1 &= f_1(x_1, x_2, \dot{x}_1, \dot{x}_2) + g_2(x_1, x_2, \dot{x}_1, \dot{x}_2)u\,, \end{aligned} \tag{3.19}$$

is given in GBCF (3.18) and not in BCF (3.4) since for both blocks the dimension of the control input is one and therefore lower than the dimension of the blocks themselves, which is two. To assign desired right-hand sides for each block of the system (3.19), for example

$$\ddot{x}_1^* = -c_1 x_1^* - c_2 \dot{x}_1^* \tag{3.20}$$

with the control parameters c_1 and c_2 satisfying the Hurwitz conditions, a simple algebraic equations has to be solved with respect to control. The desired dynamics (3.20) holds, if

$$-c_1 x_1 - c_2 \dot{x}_1 \overset{!}{=} f_1(x_1, x_2, \dot{x}_1, \dot{x}_2) + g_2(x_1, x_2, \dot{x}_1, \dot{x}_2)u^* \tag{3.21}$$

$$\leftrightarrow \quad u^* = \frac{-c_1 x_1 - c_2 \dot{x}_1 - f_1(x_1, x_2, \dot{x}_1, \dot{x}_2)}{g_2(x_1, x_2, \dot{x}_1, \dot{x}_2)}\,, \quad g_2 \neq 0\,. \tag{3.22}$$

Application of the BCP would be much more complicated. It would require two system transformations and lead to four equations for which desired dynamics has to be assigned.

Nevertheless, the direct application of the BCP to systems in GBCF is not always possible, as it may lead to unstable internal dynamics. Therefore new methods have to be developed. The new design method is referred to as the GBCP.

Remark 3.1 (The Hidden Problem of Unstable Internal Dynamics) In [78] the problem of unstable internal dynamics is illustrated. As an example, a rotational inverted pendulum system is regarded, that is actuated by a DC motor (Figure 3.1).

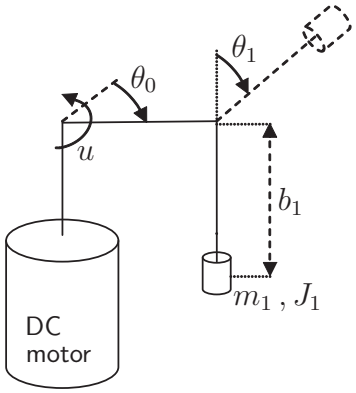

Figure 3.1: Rotational inverted pendulum system.

The system dynamics is of fourth order, dynamics of the rotational angle of the dc motor $\ddot{\theta}_0$ are influenced by friction and torque input u, dynamics of the inverted pendulum $\ddot{\theta}_1$ are characterized by friction, gravity and torque caused by base rotation:

$$\begin{aligned} J_0\ddot{\theta}_0 &= K_1\dot{\theta}_0 + u \\ J_1\ddot{\theta}_1 &= -K_2\dot{\theta}_1 + \frac{mgl}{\sin}\theta_1 - \frac{K_1K_3}{J_0}\dot{\theta}_0 + \frac{K_3}{J_0}u\,. \end{aligned} \tag{3.23}$$

In these equations $J_0\,, J_1\,, l\,, m\,, g\,, K_1\,, K_2\,, K_3 \in \mathbb{R}^+$ represent model parameters. The state transformation

$$(\theta_0\,, \theta_1) \mapsto (v = \theta_0 - \frac{J_1}{K_3}\theta_1,\ \theta_1) \tag{3.24}$$

yields new system equations

$$\begin{aligned} \ddot{v} &= \frac{K_2}{K_3}\dot{\theta}_1 - \frac{mgl}{K_3}\sin\theta_1 \\ \ddot{\theta}_1 &= -\frac{K_3K_1}{J_0J_1}\dot{v} - (\frac{K_2}{J_1} + \frac{K_1}{J_0})\dot{\theta}_1 + \frac{mgl}{J_1}\sin\theta_1 + \frac{K_3}{J_0J_1}u \end{aligned} \tag{3.25}$$

in the GBCF (3.18), but in contrast to (3.4), $\dim(\boldsymbol{x}_i) > \dim(\boldsymbol{u})$ holds ($\dim(\boldsymbol{x}_1) = \dim(\boldsymbol{x}_2) = 2; \dim(\boldsymbol{u}) = 1$). The decomposition into two subsystems is illustrated in Figure 3.2. The electromechanical system (3.25) and respectively system (3.23) are underactuated systems. They have fewer control inputs than degrees of freedom.

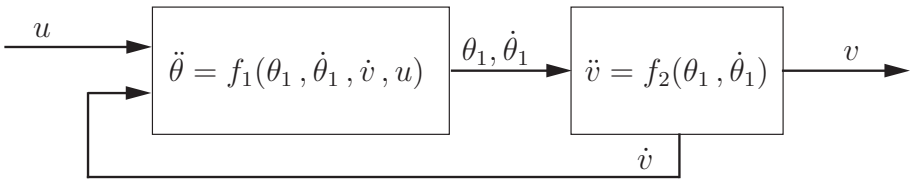

Figure 3.2: Subsystems of the rotational inverted pendulum system in the GBCF, see (3.25).

Now, following the GBCP, the state of the second block $(\theta_1, \dot{\theta}_1)$ is handled as fictitious control for the first block in such a way that

$$\ddot{v}^* = \frac{K_2}{K_3}\dot{\theta}_1^* - \frac{mgl}{K_3}\sin\theta_1^* = -c_1 v^* - c_2 \dot{v}^* \qquad (c_{1,2} \in \mathbb{R}) \tag{3.26}$$

is the desired equation for v. Assuming θ_1^* is realized by appropriate feedback control, resulting dynamics is

$$s = \frac{K_2}{K_3}\dot{\theta}_1^* - \frac{mgl}{K_3}\sin\theta_1^* + c_1 v + c_2 \dot{v} = 0\,. \tag{3.27}$$

Although the state v decays at the desired rate, the equilibrium point $\theta_1 = 0$ of the system is unstable, since for $s = 0$ and $v = 0$

$$\lim_{t\to\infty} v(t) = 0 \rightarrow \ \dot{\theta}_1 = \frac{mgl}{K_2}\sin\theta_1 \tag{3.28}$$

and the state θ_1 is diverging. With regard to the control objective $s = 0$ unstable zero dynamics appears and the direct application of the proposed design methodology to an under-actuated system fails. ■

3.3 The Design Principle for Nonlinear Finite Systems

In this section the design approach given in [78] for interconnected systems of second order is extended. For a start, the resulting design principle- the GBCP- is introduced for systems consisting of two blocks of arbitrary order in canonical form.

Systems given in GBCF (3.18) consisting of two blocks of arbitrary order in canonical form are described by

$$\begin{aligned} \overset{(n_2)}{x}_{2,1} &= \overset{(n_2-1)}{x}_{2,2} = \ldots \ = \dot{x}_{2,n_2} = f_2(\boldsymbol{x}_2\,, \boldsymbol{x}_1) \\ \overset{(n_1)}{x}_{1,1} &= \overset{(n_1-1)}{x}_{1,2} = \ldots \ = \dot{x}_{1,n_1} = f_1(\boldsymbol{x}_2\,, \boldsymbol{x}_1) + \boldsymbol{g}_1^T(\boldsymbol{x}_2\,, \boldsymbol{x}_1)\boldsymbol{u} \end{aligned} \tag{3.29}$$

or summarized for substates

$$\begin{aligned} \dot{\boldsymbol{x}}_2 &= \boldsymbol{f}_2(\boldsymbol{x}_2\,, \boldsymbol{x}_1) \\ \dot{\boldsymbol{x}}_1 &= \boldsymbol{f}_1(\boldsymbol{x}_2\,, \boldsymbol{x}_1) + \mathbf{G}_1(\boldsymbol{x}_2\,, \boldsymbol{x}_1)\boldsymbol{u} \end{aligned} \tag{3.30}$$

where $\boldsymbol{x}_i^T = [x_{i,1} \ldots x_{i,n_i}] \in \mathbb{R}^{n_i}$ for $i = 1, 2$, $\boldsymbol{u} \in \mathbb{R}^m$, and $\boldsymbol{g}_1(\boldsymbol{x}_2\,, \boldsymbol{x}_1)) \neq \mathbf{0}$, or respectively $\mathbf{G}_1(\boldsymbol{x}_2\,, \boldsymbol{x}_1) \neq \mathbf{0}$. In Figure 3.3 the structure of the system is illustrated. It is assumed that the origin in the state space is an equilibrium point of the system, meaning

$$\mathbf{0} = \boldsymbol{f}_2(\boldsymbol{x}_2 = \mathbf{0}\,, \boldsymbol{x}_1 = \mathbf{0}) \tag{3.31}$$

$$\mathbf{0} = \boldsymbol{f}_1(\boldsymbol{x}_2 = \mathbf{0}\,, \boldsymbol{x}_1 = \mathbf{0})\,. \tag{3.32}$$

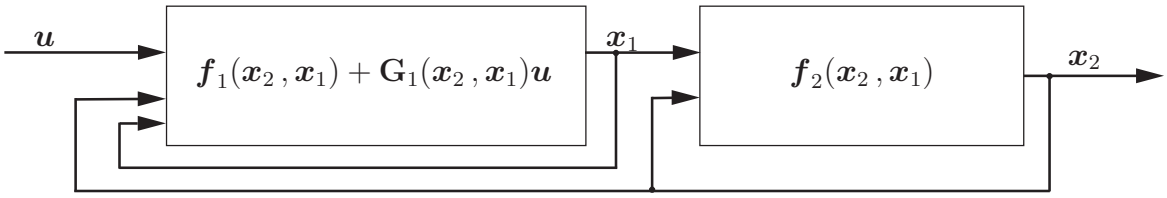

Figure 3.3: Structure of a system in GBCF consisting of two blocks of arbitrary order in canonical form. In contrast to the BCF the condition $\dim(\boldsymbol{x}_i) \leq \dim(\boldsymbol{u})$ for $i = 1, 2$ is not required. The dimension of the substates $\boldsymbol{x}_1$ or $\boldsymbol{x}_2$ can be higher than that of the control input $\boldsymbol{u}$.

As long as the dimension of the dimension of the state of the first block $\boldsymbol{x}_2$ is not higher than the dimension of the intermediate control input $\boldsymbol{x}_1$ - $n_1 \geq n_2$ - the GBCP is directly applicable, because there are no internal dynamics which can become unstable. But, as explained in the preceding section, if the dimension of the intermediate control input $\boldsymbol{x}_1$ is less than the dimension of the first block $\boldsymbol{x}_2$ - $n_1 < n_2$ - the direct application of the GBCP may lead to unstable zero dynamics. Regarding (3.29), this happens, because the block dynamics $\dot{\boldsymbol{x}}_2$ may not only depend on the first time derivative of the control input of the preceding block $\boldsymbol{u}$ but also on its higher time derivates of $\dot{\boldsymbol{u}}\,, \ddot{\boldsymbol{u}}\,, \ldots$. In the following, aspects of the control design based on the GBCP are explained. Systems for which the the zero dynamics with substate $\boldsymbol{x}_1$ as output is stable or with substate $\boldsymbol{x}_2$ as output is stable as well as system for which the dynamics $\dot{\boldsymbol{x}}_2$ does not depend on the time derivatives of the subspace $\boldsymbol{x}_1$ are discussed in detail.

Case 1: The Zero Dynamics with Substate x_1 as Output Is Stable

The zero dynamics with the substate $\boldsymbol{x}_1$ as output is given by the first equation of (3.30) with $\boldsymbol{x}_1 = \mathbf{0}$:

$$\dot{\boldsymbol{x}}_2 = \boldsymbol{f}_2(\boldsymbol{x}_1 = \mathbf{0},\, \boldsymbol{x}_2) \tag{3.33}$$

It is of the same order as the substate $\boldsymbol{x}_2$. In case it is stable, the overall system is stabilized by enforcing

$$s = x_{1,n_1} - x^*_{1,n_1} = 0 \tag{3.34}$$

e.g. with

$$\dot{x}^*_{1,n_1} = \sum_{i=1}^{n_1-1} \lambda_i\, x_{1,i} \tag{3.35}$$

where the coefficients λ_i satisfy the Hurwitz conditions. The control objective (3.34) can be realized in finite time if a discontinuous control input

$$\boldsymbol{u} = -\boldsymbol{m}\,\mathrm{sign}(s)\,, \quad \boldsymbol{m} \in \mathbb{R}^m \tag{3.36}$$

is chosen with selecting vector $\boldsymbol{m}$ based on the design methodology of sliding mode control. Hereby, condition $\mathrm{rank}(\mathbf{G}_1) = m$ has to be fulfilled. Then, if $\boldsymbol{s} = \mathbf{0}$ the state $\boldsymbol{x}_1$ decays to zero and due to the stability of the zero dynamics (3.33) the substate $\boldsymbol{x}_2$ decays as well.

Case 2: The Zero Dynamics with Substate $\boldsymbol{x}_2$ as Output Is Stable

The zero dynamics with the substate $\boldsymbol{x}_2$ as output is given by the first equation of (3.30) with $\boldsymbol{x}_2 = \mathbf{0}$:

$$\boldsymbol{f}_2(\boldsymbol{x}_2 = \mathbf{0}\,, \boldsymbol{x}_1) = \mathbf{0} \tag{3.37}$$

This dynamics is of less order than the one governed in (3.33). In case it is stable, the overall system is stabilized by enforcing

$$s = f_2(\boldsymbol{x}_2\,, \boldsymbol{x}_1) - x^*_{2,n_2} = 0 \tag{3.38}$$

e.g. with

$$\dot{x}^*_{2,n_2} = \sum_{i=1}^{n_2-1} \lambda_i\, x_{2,i} \tag{3.39}$$

where the coefficients λ_i satisfy the Hurwitz conditions. Then the control objective (3.38) can be realized in finite time if a discontinuous control input

$$\boldsymbol{u} = -\boldsymbol{m}\,\mathrm{sign}(s)\,, \quad \boldsymbol{m} \in \mathbb{R}^m \tag{3.40}$$

is chosen with selecting vector $\boldsymbol{m}$ based on the design methodology of sliding mode control. Hereby, condition $\mathrm{rank}(\mathbf{G}_1) = m$ has to be fulfilled. Then, if $\boldsymbol{s} = \mathbf{0}$

$$\dot{x}_{2,n_2} = f_2(\boldsymbol{x}_2\,, \boldsymbol{x}_1) = \sum_{i=1}^{n_2-1} \lambda_i\, x_{2,i} \tag{3.41}$$

and the state variable x_{2,n_2} decays to zero. Consequently, the subspace $\boldsymbol{x}_2$ decays to zero and due to the stability of the zero dynamics (3.37) the substate $\boldsymbol{x}_1$ decays as well. The assumption $\dim(\boldsymbol{x}_2) \leq \dim(\boldsymbol{x}_1)$ guarantees that all components of $\dot{\boldsymbol{s}}$ can be influenced by the control input $\boldsymbol{u}$.

Case 3: The Dynamics $\dot{x}_2$ Does Not Depend on the Time Derivatives of the Substate $\boldsymbol{x}_1$

If the dynamics of the subspace $\boldsymbol{x}_2$ does not depend on the time derivatives of the state variable x_{1,n_1},

$$\overset{(n_2)}{x}_{2,1} = \overset{(n_2-1)}{x}_{2,2} = \ldots = f_2(\boldsymbol{x}_2\,, x_{1,n_1}) \tag{3.42}$$

the system of the new class (3.29) can be stabilized similar to [78]. Sliding mode is enforced on the manifold

$$s_1 = \sum_{i=0}^{(n_2-1)} c_i\, \overset{(i)}{s} = 0\,, \tag{3.43}$$

where the coefficients c_i satisfy the Hurwitz conditions. Hereby

$$s = f_2(\boldsymbol{x}_2\,, x_{1,n_1}) - x^*_{2,n_2} = 0 \tag{3.44}$$

e.g. with

$$\dot{x}^*_{2,n_2} = \sum_{i=1}^{n_2-1} \lambda_i \, x_{2,i} \tag{3.45}$$

where the coefficients λ_i satisfy the Hurwitz conditions. For this case stability of zero dynamics is not required. Regarding (3.45), if $\boldsymbol{s} = \boldsymbol{0}$, s tends to zero and based on (3.44)

$$\sum_{i=1}^{n_2-1} \lambda_i \, x_{2,i} = f_2(\boldsymbol{x}_2 \, , \boldsymbol{x}_1) = \dot{x}_{2,n_2} \tag{3.46}$$

is obtained. As a result the state variable x_{2,n_2} decays to zero. Consequently, the subspace $\boldsymbol{x}_2$ decays to zero. Finally, the substate $\boldsymbol{x}_1$ is calculated from the algebraic equations $0 = f_2(\boldsymbol{x}_2 \, , x_{1,n_1})$. Because the origin of the state space is an equilibrium point of the system, the substate $\boldsymbol{x}_1$ decays to zero as well. As in Case 2 the assumption $\dim(\boldsymbol{x}_2) \leq \dim(\boldsymbol{x}_1)$ guarantees that all components of $\dot{\boldsymbol{s}}$ can be influenced by the control input $\boldsymbol{u}$.

Remark 3.2 (How to Find the Right System Transformation) There are special systems of the class (3.29) with unstable zero dynamics for which system transformations exist that transform the system into a form that fits in Case 3. It is assumed that $\boldsymbol{f}_1$ is an affine function with respect to $\dot{\boldsymbol{x}}_1$,

$$\begin{aligned} \dot{\boldsymbol{x}}_2 &= \boldsymbol{f}_{21}(\boldsymbol{x}_2, \boldsymbol{x}_1) + \boldsymbol{f}_{22}(\boldsymbol{x}_1)\dot{\boldsymbol{x}}_1 \\ \dot{\boldsymbol{x}}_1 &= \boldsymbol{f}_1(\boldsymbol{x}_2, \boldsymbol{x}_1) + \boldsymbol{g}_1^T(\boldsymbol{x}_2 \, , \boldsymbol{x}_1)\boldsymbol{u} \, . \end{aligned} \tag{3.47}$$

Now even if the zero dynamics with $\boldsymbol{x}_2$ as output

$$\boldsymbol{0} = \boldsymbol{f}_{21}(\boldsymbol{x}_2 = \boldsymbol{0} \, , \boldsymbol{x}_1) + \boldsymbol{f}_{22}(\boldsymbol{x}_1)\dot{\boldsymbol{x}}_1 \tag{3.48}$$

is unstable, the system can be stabilized based on the GBCP. The state transformation

$$(\boldsymbol{x}_2 \, , \boldsymbol{x}_1) \mapsto (\boldsymbol{v} = \boldsymbol{x}_2 - \boldsymbol{\phi}(\boldsymbol{x}_1) \, , \boldsymbol{x}_2) \tag{3.49}$$

yields the system equations

$$\begin{aligned} \dot{\boldsymbol{v}} &= \boldsymbol{f}_{21} \left(\boldsymbol{x}_2 \, , \boldsymbol{v} + \boldsymbol{\phi}(\boldsymbol{x}_2)\right) + \boldsymbol{f}'_{22}(\boldsymbol{x}_2)\dot{\boldsymbol{x}}_2 - \frac{\partial \boldsymbol{\phi}(\boldsymbol{x}_2)}{\partial \boldsymbol{x}_2}\dot{\boldsymbol{x}}_2 \\ \dot{\boldsymbol{x}}_1 &= \boldsymbol{f}_1(\boldsymbol{x}_2 \, , \boldsymbol{x}_1) + \boldsymbol{g}_1^T(\boldsymbol{x}_2 \, , \boldsymbol{x}_1)\boldsymbol{u} \, . \end{aligned} \tag{3.50}$$

If the transformation function $\boldsymbol{\phi}(\boldsymbol{x}_2)$ is chosen in such a way that $\frac{\partial \boldsymbol{\phi}(\boldsymbol{x}_2)}{\partial \boldsymbol{x}_2} = \boldsymbol{f}_{22}(\boldsymbol{x}_2)$, the first block does not depend on the derivative of the state of the second block. The GBCP is applicable to the resulting reduced order system

$$\begin{aligned} \dot{\boldsymbol{v}} &= \boldsymbol{f}_{21} \left(\boldsymbol{x}_2, \boldsymbol{v} + \boldsymbol{\phi}(\boldsymbol{x}_2)\right) \\ \dot{\boldsymbol{x}}_1 &= \boldsymbol{f}_2(\boldsymbol{x}_2 \, , \boldsymbol{x}_1) + \boldsymbol{g}_2^T(\boldsymbol{x}_1 \, , \boldsymbol{x}_2)\boldsymbol{u} \end{aligned} \tag{3.51}$$

The state $\boldsymbol{x}_2$ is handled as an intermediate control input. It is realized after a finite time transient by enforcing sliding mode in the manifold

$$\boldsymbol{s} = \boldsymbol{x}_2 - \boldsymbol{x}_2^* = \boldsymbol{0} \, . \tag{3.52}$$

■

Remark 3.3 The described design methods are applicable to systems fulfilling the condition $n_2 \leq n_1$. If this condition does not hold, the design procedure explained in [45, 44] can be used. ■

Example 3.6 (Application of the Proposed Coordinate Transformation [78])
The inverted rotational pendulum will be considered again. As illustrated in Remark 3.1 direct application of the GBCP to system (3.25) yields unstable zero dynamics. This problem can be solved by applying a coordinate transformation such that the first block after decomposition does not depend on the derivative as offered in [78] and explained in Remark 3.2. The state transformation

$$(v, \theta_1) \mapsto (w = \dot{v} - \frac{K_2}{K_3}\theta_1, \theta_1) \tag{3.53}$$

yields to

$$\begin{aligned} \dot{w} &= -\frac{mgl}{K_3}\sin\theta_1 \\ \ddot{\theta}_1 &= -\frac{K_1K_3}{J_0J_1}w - (\frac{K_2}{J_1} + \frac{K_1}{J_0})\dot{\theta}_1 + \frac{mgl}{J_1}\sin\theta_1 - \frac{K_1K_2}{J_0J_1}\theta_1 + \frac{K_1K_2}{J_0J_1}u\,. \end{aligned} \tag{3.54}$$

In the system equations (3.54) the dynamics of the first block is independent of the derivatives of the state of the second block with respect to time and the in Case 3 described design procedure is applicable. Following the proposed GBCP a virtual control θ_1^* is determined such that the state variable w follows desired dynamics

$$\dot{w}^* = -c_1 w \qquad c_1 \in \mathbb{R}^+\,. \tag{3.55}$$

The derivative of the error between the real and the desired dynamics of w

$$s = \dot{w} - \dot{w}^* = \frac{mgl}{K_3}\sin\theta_1 + c_1 w = 0\,. \tag{3.56}$$

with respect to time does not depend on the control input u. But the derivative of

$$s_1 = \dot{s} + c_2 s = 0 \qquad c_2 \in \mathbb{R}^+ \tag{3.57}$$

with respect to time depends on the control input u. Therefore sliding mode can be enforced in the manifold $s_1 = 0$. The condition for existence of sliding mode can be found in [78]. In sliding mode according to (3.57) $\lim_{t\to\infty} s = 0$ and regarding (3.55) and (3.56) also $\lim_{t\to\infty} w(t) = 0$. Consequently

$$\lim_{t\to\infty}\left(\frac{mgl}{K_3}\sin\theta_1\right) = 0 \tag{3.58}$$

meaning $\lim_{t\to\infty}\theta_1 = 0$. Following (3.53) and (3.24) the dynamics of the state variables v and θ_0 tend to zero as well,

$$\lim_{t\to\infty}\dot{v} = \lim_{t\to\infty}(w + \frac{K_2}{K_3}\theta_1) = 0 \tag{3.59}$$

and

$$\lim_{t\to\infty}\dot{\theta}_0 = \lim_{t\to\infty}(v + \frac{J_1}{K_3}\theta_1) = 0\,. \tag{3.60}$$

The offered solution suppresses instability, but it cannot be taken as the final one, because the coordinate θ_0 is not diverging, but tends to some final value, which will generally be different from zero. Asymptotic stability can be achieved by slightly modifying the function s on the switching surface $s = \sin\theta_1 + c_1(w + v) = 0$.

The application of the GBCP to two interconnected systems of arbitrary order in canonical form proves to be fruitful. As long as a coordinate transformation into the system class described in Case 1, 2 or 3 exists, the problem of unstable zero dynamics can be solved.

3.4 The Design Principle for Infinite Dimensional Systems

The objective of this section is to illustrate the application of the GBCP to infinite dimensional systems. As an example, the control of the rotation angle of a torsion bar with torque as control input is considered. The idea of this control concept is based on a system transformation into a system with delay and can be found in [23] and [79]. This section forms the basis for the discussion of the practical issues of the GBCP and the extension of the existing sliding mode control in order to reject disturbances.

The following control unit design procedure points out two advantages of the GBCP. Firstly, it shows, that the GBCP is applicable to systems, where the BCP fails. The motion equations of the flexible shaft system cannot be transformed into a set of blocks governed by differential equations of the same order as the control input. Secondly, it illustrates that the GBCP offers an alternative to design control for infinite dimensional systems base on the accurate model. In contrast to commonly used control strategies which are based on modal forms, the GBCP does not deal with approximations.

The model of the flexible shaft is introduced in Section 3.4.1. In Section 3.4.2 the model is changed in order to receive a form that is appropriate for the application of the GBCP. Finally, the control is designed in Section 3.4.3.

3.4.1 Model of a Flexible Shaft

The system considered is a torsion bar, see Figure 3.4, which belongs to the class of distributed and therefore infinite dimensional systems. The bar's length is l, the position on it is described by the variable x. At position $x = 0$ the torque M is the input to the shaft. On the opposite side there is a load with inertia J. The degree of rotation at each position x is given by the angle

$$q(x,t) = e(t) + f(x,t)\,. \tag{3.61}$$

Angle e is proportional to the torque input M, angle f results from additional torsion effects.

The dynamics of the flexible shaft is given by the partial differential equation

$$\frac{\partial^2 q(x,t)}{\partial t^2} = a^2 \frac{\partial^2 q(x,t)}{\partial x^2} \tag{3.62}$$

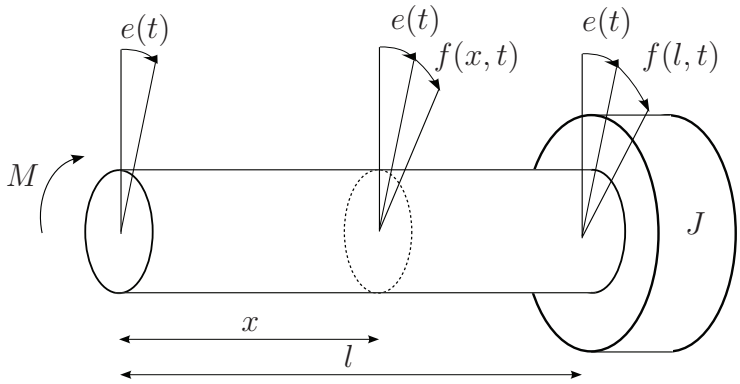

Figure 3.4: Flexible shaft.

where the material constant a is derived from the stiffness of the torsion bar. The boundary conditions for (3.62) are:

$$M(0,t) = -GI_p \frac{\partial q(0,t)}{\partial x} = -GI_p \nabla q(0,t) \quad \text{and} \tag{3.63}$$

$$J\frac{\partial^2 q(l,t)}{\partial t^2} = J\ddot{q}(l,t) = -GI_p \frac{\partial q(l,t)}{\partial x} = -GI_p \nabla^2 q(l,t)\ . \tag{3.64}$$

The first condition (3.63) describes that on the left side of the torsion bar, only the torque $M(0,t)$ attacks and causes a deflection $\nabla q(0,t)$. This deflection is directed against the movement generated by M, because M changes the position $q(0,t)$ whereas the rest of the shaft wants to remain in its original position. Thus M and ∇q have different signs. The parameter G is a material constant describing the necessary moment to evoke a certain torsion of the shaft. The parameter I_p is the geometrical moment of inertia of the bar depending on the shaft's shape. For the cylindrical shaft with the radius r it is calculated $I_p = \frac{\pi}{2}\, r^4$.

The second boundary condition (3.64) describes the torque attacking to the right side of the shaft. The torque given to the system by the load depends linear on the acceleration. With m_L as the mass of the load and r_L as its radius and assuming that the load has a massive cylindrical body th parameter J can be calculated as $J = \frac{m_L}{2}\, r_L^2$.

3.4.2 System Transformation into the Generalized Block Control Form

The objective is to control the rotation position $q(x,t)$ of the flexible shaft (3.62) at the position of the load $x = l$.

Before the control algorithm is developed in detail, in the following paragraphs some general considerations are done.

A partial differential equation is an equation containing operators of time and location.

$$A_t\left\{q(x,t)\right\} + A_x\left\{q(x,t)\right\} + B_t\left\{u(t)\right\} = 0 \tag{3.65}$$

where A_t and B_t are operators of time, e.g. derivatives, integrators or delays, and A_x is an operator which can provide derivatives, integrals or translations with respect to location. The variable $u(t)$ is a control input to this system. Equation (3.65) cannot be solved by conventional mathematical methods.

Therefore, the first goal is to transform the mathematical description of the torsion bar 3.62 in such a way that conventional methods are applicable. That is done in two steps which consist of a Laplace transformation with adjacent solution of the resulting equation and a retransformation into time domain at the position of the load.

When the Laplace transformation is applied, all operators of time change into the algebraic functions $g_1(p)$ and $g_2(p)$. Thus an ordinary differential equation with respect to x

$$g_1(Q(x,p)) + A_x\{Q(x,p)\} + g_2(U(p)) = 0 \tag{3.66}$$

is received. The solution of (3.66) can be transformed back into the time domain for the position $x = l$. The result is an equation that only contains operators of time forming an ordinary differential equation with partly delayed arguments in the case of the torsion bar. This equation is no longer dependent on the variable x.

$$\tilde{A}_t\{q(l,t)\} + \tilde{B}_t\{u(t)\} = 0 \tag{3.67}$$

To this system model conventional control design methods can be applied.

In the case of the flexible shaft this equation consists of derivatives and delays of the rotation $q(l,t)$ and therefore it is not trivial to solve.

The presented approach to control a distributed system is not universal because it may lead to dead ends. For example some transformations could not be possible or the ordinary differential equation into the Laplace domain could not be solvable. How to achieve the differential-difference equation that is less difficult to control than the the original description of the given sample system (3.62) is described in the following sections in detail.

Step 1: Transfer Function Approach

For applying the Laplace transformation to system (3.62) the initial conditions

$$q(x,0) = 0 \tag{3.68}$$

$$\dot{q}(x,0) = 0 \tag{3.69}$$

are assumed.

The position of the load $q(l,t)$ is considered as the system output and the input torque M as the control input $u(t)$. The latter is replaced during Laplace transformation by $U(p)$. Written in the Laplace domain, system (3.62) and the boundary conditions (3.63) and (3.64) are:

$$p^2 Q(x,p) = a^2 \frac{\partial^2 Q(x,p)}{\partial x^2} \tag{3.70}$$

$$U(p) = -GI_p \frac{\partial Q(0,p)}{\partial x} \tag{3.71}$$

$$p^2 JQ(l,p) = -GI_p \frac{\partial Q(l,p)}{\partial x}\,. \tag{3.72}$$

To solve the ordinary differential equation (3.70) the standard approach for finding a solution of a homogeneous differential equation $Q(x) = e^{\lambda x}$ is applied which delivers the characteristic polynomial of (3.70):

$$\lambda^2 - \frac{p^2}{a^2} = 0 \tag{3.73}$$

$$\Rightarrow \quad \lambda_{1/2} = \pm\frac{p}{a}\,. \tag{3.74}$$

The solution of the homogeneous differential equation (3.70) is:

$$Q(x,p) = c_1 e^{\frac{p}{a}x} + c_2 e^{-\frac{p}{a}x}\,. \tag{3.75}$$

To find out the parameters c_1 and c_2 the boundary conditions (3.71) and (3.72) have to by analyzed for the derivative of (3.75) with respect to x,

$$\frac{\partial Q(x,p)}{\partial x} = c_1\frac{p}{a}e^{\frac{p}{a}x} - c_2\frac{p}{a}e^{-\frac{p}{a}x}\,. \tag{3.76}$$

Putting (3.71) and (3.72) into (3.76) leads to the parameters c_1 and c_2,

$$c_1 = \frac{\left(1 - \frac{Jap}{GI_p}\right)e^{-\frac{l}{a}p}}{p\left(\left(Jp + \frac{GI_p}{a}\right)e^{\frac{l}{a}p} + \left(Jp - \frac{GI_p}{a}\right)e^{-\frac{l}{a}p}\right)}\,U(p) \tag{3.77}$$

$$c_2 = \frac{\left(1 + \frac{Jap}{GI_p}\right)e^{\frac{l}{a}p}}{p\left(\left(Jp + \frac{GI_p}{a}\right)e^{\frac{l}{a}p} + \left(Jp - \frac{GI_p}{a}\right)e^{-\frac{l}{a}p}\right)}\,U(p) \tag{3.78}$$

The solution of (3.75) can be written in the transfer function form $Q(x,p) = W(x,p)\,U(p)$ then,

$$Q(x,p) = \frac{\left(1 - \frac{Jap}{GI_p}\right)e^{-\frac{l-x}{a}p} + \left(1 + \frac{Jap}{GI_p}\right)e^{\frac{l-x}{a}p}}{p\left(\left(Jp + \frac{GI_p}{a}\right)e^{\frac{l}{a}p} + \left(Jp - \frac{GI_p}{a}\right)e^{-\frac{l}{a}p}\right)}\,U(p)\,. \tag{3.79}$$

To the system model (3.79) conventional control design methods based on transfer function system descriptions are applicable. Another option is to transform the system again and apply design methods into the time domain. Latter approach is is chosen here.

Step 2: Time Domain

The transformation of the transfer function (3.79) into the time domain is done at the position $x = l$,

$$Q(l,p) = \frac{2e^{-\frac{l}{a}p}}{p\left(\left(Jp + \frac{GI_p}{a}\right) + \left(Jp - \frac{GI_p}{a}\right)e^{-\frac{2l}{a}p}\right)}\,U(p)\,. \tag{3.80}$$

It yields

$$p\left(\left(Jp + \frac{GI_p}{a}\right) + \left(Jp - \frac{GI_p}{a}\right)e^{-\frac{2l}{a}p}\right) Q(l,p) = 2e^{-\frac{l}{a}p}\, U(p) \tag{3.81}$$

$$J\ddot{q}(t) + \frac{GI_p}{a}\,\dot{q}(t) + J\ddot{q}(t-2\tau) - \frac{GI_p}{a}\,\dot{q}(t-2\tau) = 2u(t-\tau)\,, \tag{3.82}$$

with $\tau = \frac{l}{a}$. By setting

$$s_1(t) = q(t) \tag{3.83}$$

$$s_3(t) = J\ddot{q}(t) + \frac{GI_p}{a}\,\dot{q}(t) \tag{3.84}$$

the difference-differential equation (3.82) can be transformed into the GBCF (3.18),

$$\ddot{s}_1(t) = -\frac{GI_p}{Ja}\dot{s}_1(t) + \frac{1}{J}s_3(t) \tag{3.85}$$

$$s_3(t) = 2\,\frac{GI_p}{a}\,\dot{s}_1(t-2\tau) - s_3(t-2\tau) + 2u(t-\tau)\,. \tag{3.86}$$

There are two blocks. The differential equation of second order (3.85) represents the first block. The scalar variable s_3 can be seen as virtual control input for it. The second order difference equation (3.86) forms the second block. It contains all state variables with delayed arguments but no derivatives. Its control input is $u(t)$.

The step response of the uncontrolled, free motion of system (3.85) can be seen in Figure 3.5 . A step input torque is applied to the unexcited shaft, so it moves with a constant acceleration after a possible transient process. A constant acceleration means that the position is a parabolic function of time, so the shaft's simulated behavior meets exactly the expectation.

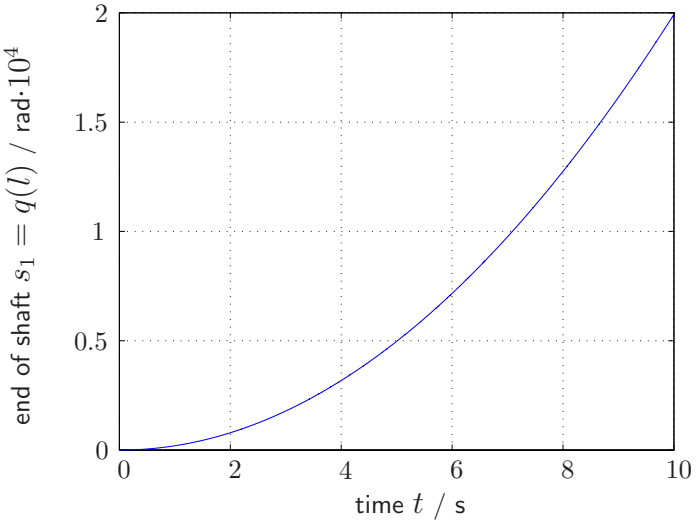

Figure 3.5: Simulation results: Trajectory of the rotational angle $q(l)$ at the end of the flexible shaft. The initial conditions are zero. At time $t = 0.01\,\mathrm{s}$ the shaft responses to a step in the moment from $0\,\mathrm{Nm}$ to $1\,\mathrm{Nm}$, which is given to the beginning of the shaft.

Now, the equations of the flexible shaft are retransformed into the time domain and the system is given in GBCF. In GBCF the differential and difference terms are separated. This way the control design can be simplified.

3.4.3 Sliding Mode Control Design

Following the GBCP, the control design for the system (3.85 - 3.86) is done in two steps. In the first step the state $s_3(t)$ of the second block (3.86) is considered as virtual control input for the first block (3.85). To assign desired dynamics for $s_1(t)$

$$\ddot{s}_1^*(t) = -\frac{GI_p}{Ja}\dot{s}_1^*(t) + \frac{1}{J}s_3^*(t) = -c_1 s_1^*(t) - c_2\dot{s}_1^*(t) \qquad (c_1, c_2 \in \mathbb{R}^+) \tag{3.87}$$

the state variable $s_3(t)$ has to be chosen as

$$s_3^*(t) = k_1 s_1^*(t) + k_2\dot{s}_1^*(t) \qquad \text{with} \quad k_1 = -Jc_1 \text{ and } k_2 = \frac{GI_p}{a} - Jc_2\,. \tag{3.88}$$

This choice of $s_3(t)$ corresponds with taking a PD-Controller to govern system (3.85). In the second step the real control input $u(t)$ has to be chosen such that

$$s(t) = s_3(t) - s_3^*(t) = 0 \tag{3.89}$$

is fulfilled. The control input $u_{eq}(t)$ can be calculated based on (3.89) and (3.88)

$$u_{eq}(t) = \frac{1}{2}\Big(k_1 s_1(t+\tau) + k_2 s_2(t+\tau) + s_3(t-\tau) - 2\frac{GI_p}{a}s_2(t-\tau)\Big)\,. \tag{3.90}$$

As system (3.86) is a discrete-time system, a continuous control input $u_{eq}(t)$ necessary to receive sliding mode in the manifold (3.89) after finite time, only $s_3^*(t)$ may show up discontinuities. It If the input is bounded, $u(t)$ should be of the form

$$u(t) = \begin{cases} u_{eq}(t) & |u_{eq}(t)| \le |M_{max}| \\ M_{max}\,\mathrm{sign}\,(u_{eq}(t)) & |u_{eq}(t)| > |M_{max}| \end{cases}\,, \tag{3.91}$$

where M_{max} is the maximal torque that can be given to the system.

Remark 3.4 (Identification of $s_1(t+\tau)$ and $s_2(t+\tau) = \dot{s}_1(t+\tau)$) For the implementation of the control $u_{eq}(t)$ all values are known, except those for $s_1(t+\tau)$ and $s_2(t+\tau)$ which have to be estimated. Therefore system (3.85) is needed again. With

$$s_2(t) = \dot{s}_1(t) \tag{3.92}$$

it can be written as

$$\begin{pmatrix} \dot{s}_1(t) \\ \dot{s}_2(t) \end{pmatrix} = \mathbf{A}\begin{pmatrix} s_1(t) \\ s_2(t) \end{pmatrix} + \frac{1}{J}\begin{pmatrix} 0 \\ s_3(t) \end{pmatrix} \tag{3.93}$$

where $\mathbf{A} = \begin{pmatrix} 0 & 1 \\ 0 & -\frac{GI_p}{aJ} \end{pmatrix}$. The analytical solution of the above system is:

$$\begin{pmatrix} s_1(t) \\ s_2(t) \end{pmatrix} = e^{\mathbf{A}t} \begin{pmatrix} s_1(0) \\ s_2(0) \end{pmatrix} + \frac{1}{J} \int_0^t e^{\mathbf{A}(t-\xi)} \begin{pmatrix} 0 \\ s_3(\xi) \end{pmatrix} d\xi \; p \tag{3.94}$$

Substituting t by $t + \tau$ in (3.94), it can easily be shown that the following extrapolator is reached and estimates the values of $s_1(t + \tau)$ and $s_2(t + \tau)$.

$$\begin{pmatrix} s_1(t+\tau) \\ s_2(t+\tau) \end{pmatrix} = e^{\mathbf{A}\tau} \begin{pmatrix} s_1(t) \\ s_2(t) \end{pmatrix} + \frac{1}{J} \int_t^{t+\tau} e^{\mathbf{A}(t+\tau-\xi)} \begin{pmatrix} 0 \\ s_3(\xi) \end{pmatrix} d\xi \tag{3.95}$$

with

$$s_3(\xi) = 2\frac{GI_p}{a}\, s_2(\xi - 2\tau) - s_3(\xi - 2\tau) + 2u(\xi - \tau) - T_L(\xi) - T_L(\xi - 2\tau)$$

and $t \leq \xi \leq t + \tau \; p$

Because of this definition of $s_3(t)$ with delayed variables, it is possible to solve the integral appearing in (3.95) and so the missing values of $s_1(t + \tau)$ and $s_2(t + \tau)$ can be found according to [79]. ■

There is no zero dynamics. If the error $s(t)$ gets zero in finite time, the desired dynamics (3.88) are realized. The resulting motion of the system is described by (3.87). If the parameters c_1 and c_2 fulfill the Hurwitz condition asymptotic stability is guaranteed.

The result of the sliding mode control applied to system (3.85), (3.86) is illustrated in Figure 3.6 . Initially the system is unexcited. At time 1s, the target position of the shaft jumps to 1rad and it can be seen how the system follows and reaches the new target position.

The derived control strategy for the flexible shaft has got two weak points: It requires information of all state variables, but in applications the variables $\dot{s}_1$ and s_3 cannot always be measured. Moreover, the GBCP calculates the desired dynamics based on a system model. Uncertain system parameters and unknown disturbances may lead to calculation errors and reduced control performance. In the following section these practical issues of the GBCP are discussed in detail.

3.5 Practical Issues

This section focuses on two practical issues of the GBCP. These are the necessity of complete state information and the problem of reduced robustness of sliding mode controls which are developed based on the GBCP. Both application challenges as are discussed examplarily for the system of the flexible shaft, which is in introduced in Section 3.4. In Section 3.5.1 required observers are derived. In Section 3.5.2 as a solution to the problem of reduced robustness, a disturbance rejection method is developed.

The BCP deals with the same implementation problems as the GBCP. The methods proposed in this section can be applied to BCP problems without any changes.

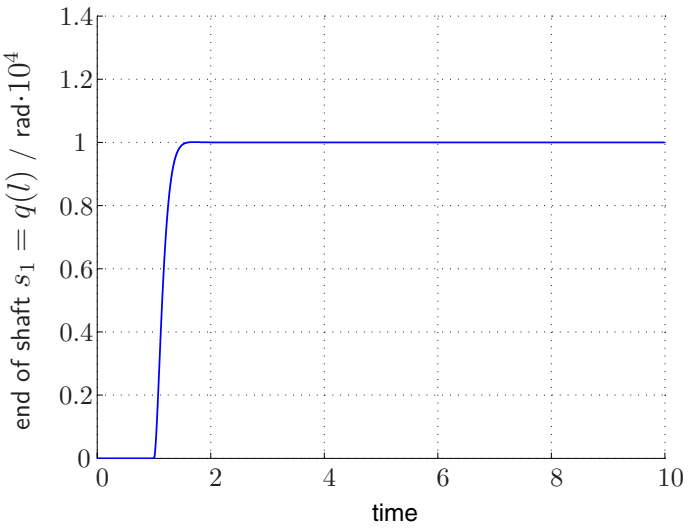

Figure 3.6: Simulation results: Sliding Mode controlled flexible shaft system. The initial conditions are zero. At time $t = 1\,\mathrm{s}$ the shaft response to a step in the input position $q(0,t)$ from 0 rad to 1 rad.

3.5.1 Observers

The in Section 3.4.3 presented sliding mode control needs the state variables s_1, $\dot{s}_1$ and s_3 as input variables at different times. It is assumed that only the current rotation position $s_1(t)$ of the torsion bar can be measured. Thus, to find the missing variables an observer is implemented. This thesis proposes a sliding mode observer that consists of a parallel model of the flexible shaft with approximated system parameters as illustrated in Figure 3.7.

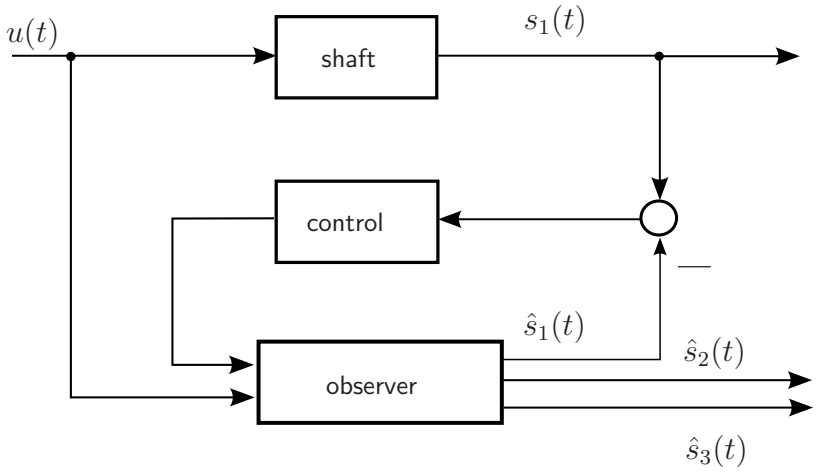

Figure 3.7: Observer architecture for the flexible shaft system.

Based on the system equations (3.85 - 3.86) the observer dynamics is assigned

$$\begin{aligned}\dot{\hat{s}}_1(t) &= \hat{s}_2(t) - V_1 \operatorname{sign}\left(\hat{s}_1(t) - s_1(t)\right)\\ \dot{\hat{s}}_2(t) &= -\frac{GI_p}{aJ}\,\hat{s}_2(t) + \frac{1}{J}\,\hat{s}_3(t) - V_2 \operatorname{sign}\left(\hat{s}_1(t) - s_1(t)\right)\end{aligned} \tag{3.96}$$

$$\hat{s}_3(t) = -\hat{s}_3(t-2\tau) + 2\,\frac{GI_p}{a}\,\hat{s}_2(t-2\tau) + 2u(t-\tau)$$

with $V_1 > 0$ and $V_2 = l\,V_1\,; l > 0$. The variables $\hat{s}_1(t)$, $\hat{s}_2(t)$ and $\hat{s}_3(t)$ are the estimates of the the variables $s_1(t)$, $s_2(t) = \dot{s}_1(t)$ and $s_3(t)$. If the estimation errors are defined as

$$\bar{s}_i(t) = \hat{s}_i(t) - s_i(t) \quad \text{for} \quad i = 1, 2, 3 \tag{3.97}$$

the error dynamics is

$$\dot{\bar{s}}_1(t) = \bar{s}_2(t) - V_1 \operatorname{sign}\left(\bar{s}_1(t)\right) \tag{3.98}$$

$$\dot{\bar{s}}_2(t) = -\frac{GI_p}{aJ}\,\bar{s}_2(t) + \frac{1}{J}\,\bar{s}_3(t) - V_2 \operatorname{sign}\left(\bar{s}_1(t)\right) \tag{3.99}$$

$$\bar{s}_3(t) = -\bar{s}_3(t-2\tau) + 2\,\frac{GI_p}{a}\,\bar{s}_2(t-2\tau)\,. \tag{3.100}$$

The stability of the sliding mode observer is shown in three steps. First, it is shown that $\bar{s}_1(t) = 0$ is reached in finite time. Then it is proved one after the other that $\bar{s}_2(t) = 0$ and finally $\bar{s}_3(t) = 0$ is reached asymptotically.

Observation of $s_1(t)$

To prove the stability of the observer for $s_1(t)$, it is shown, that sliding mode is enforced in the manifold

$$\bar{s}_1(t) = 0\,. \tag{3.101}$$

The continuously differentiable Lyapunov function

$$V(t) = \frac{1}{2}\,\bar{s}_1^2(t) \tag{3.102}$$

with

$$V \geq 0 \tag{3.103}$$

$$V = 0 \quad \text{for} \quad \bar{s}_1(t) = 0 \tag{3.104}$$

$$\lim_{s \to \infty} V = \infty \tag{3.105}$$

is considered. It's derivative with respect to time is

$$\dot{V}(t) = \bar{s}_1(t)\dot{\bar{s}}_1(t) = \bar{s}_1(t)\left(\bar{s}_2(t) - V_1 \operatorname{sign}(\bar{s}_1(t))\right). \tag{3.106}$$

Taking an appropriate choice of V_1,

$$V_1 > |\bar{s}_2(t)| + \frac{\varepsilon}{|\bar{s}_1(t)|}\,, \tag{3.107}$$

follows

$$\dot{V}(t) < -\varepsilon \quad \text{with} \quad \varepsilon > 0 \tag{3.108}$$

and $\bar{s}_1(t) = 0$, that is $\hat{s}_1(t) = s_1(t)$, is reached in finite time.

Observation of $s_2(t)$

To demonstrate that $\hat{s}_2(t)$ approaches $s_2(t)$ asymptotically, the equation (3.99) is transformed into an ordinary homogeneous differential equation of first order. Then the stability of this differential equation is proved.

From (3.99) follows

$$\bar{s}_3(t-2\tau) = \frac{GI_p}{a}\,\bar{s}_2(t-2\tau) + J\dot{\bar{s}}_2(t-2\tau) + JV_2\,\mathrm{sign}\,(\bar{s}_1(t-2\tau))\,. \tag{3.109}$$

Replacing $\bar{s}_3(t-2\tau)$ in (3.100) using (3.109) yields

$$\bar{s}_3(t) = \frac{GI_p}{a}\,\bar{s}_2(t-2\tau) - J\dot{\bar{s}}_2(t-2\tau) - JV_2\,\mathrm{sign}\,(\bar{s}_1(t-2\tau)) \tag{3.110}$$

and (3.99) can be written as

$$\dot{\bar{s}}_2(t) = -\frac{GI_p}{aJ}\,\bar{s}_2(t) + \frac{GI_p}{Ja}\,\bar{s}_2(t-2\tau) - \dot{\bar{s}}_2(t-2\tau) - V_2\,\mathrm{sign}\,(\bar{s}_1(t-2\tau)) - V_2\,\mathrm{sign}\,(\bar{s}_1(t))\,. \tag{3.111}$$

Based on the equivalent control method [74, 75], the discontinuous terms in (3.111) can be replace by continuous terms

$$V_1\,\mathrm{sign}(s(t)) = v_{1,eq}(t) \tag{3.112}$$

$$V_2\,\mathrm{sign}(s(t)) = l v_{1,eq}(t)\,. \tag{3.113}$$

If sliding mode is enforced in the manifold $\bar{s}_1(t) = 0$, equation (3.100) yields

$$v_{1,eq}(t) = \bar{s}_2(t) \tag{3.114}$$

and

$$V_1\,\mathrm{sign}(s(t)) = \bar{s}_2(t) \tag{3.115}$$

$$V_2\,\mathrm{sign}(s(t)) = l\bar{s}_2(t)\,. \tag{3.116}$$

Finally, the dynamics for s_2 can be described by

$$\dot{\bar{s}}_2(t) = -\left(l + \frac{GI_p}{aJ}\right)\bar{s}_2(t) + \left(\frac{GI_p}{aJ} - l\right)\bar{s}_2(t-2\tau) - \dot{\bar{s}}_2(t-2\tau)\,. \tag{3.117}$$

If the ordinary homogeneous differential equation (3.117) provides stable, that is decreasing, solutions, then $\lim_{t\to\infty}\bar{s}_2(t) = 0$. This proof of stability is demonstrated first for the case of τ approaching zero, which represents a stiff shaft. Then the flexible shaft is considered. In this case the stability proof is based on a contradiction between the assumption of the system being instable and the resulting condition of the system being stable.

Theorem 3.1 In case of a stiff shaft, solutions to (3.117) are stable.

Proof: In case of a stiff shaft

$$\lim_{\tau \to 0} \bar{s}_2(t - 2\tau) = \bar{s}_2(t)$$

holds. Applied to (3.117) follows

$$\dot{\bar{s}}_2(t) = -l\bar{s}_2(t), \tag{3.118}$$

which has stable solution $\forall\, l > 0$. ■

Theorem 3.2 In case of a flexible shaft, for a certain range of l with $l > 0$, solutions to (3.117) are stable.

Proof: To solve the ordinary differential equation (3.117) the standard approach $\bar{s}_2(t) = ce^{\lambda t}$ is applied. The stability of $\bar{s}_2(t)$ only depends on the real part of the generally complex number $\lambda = \sigma + j\upsilon$, which is

$$\Re(\bar{s}_2(t)) = ce^{\sigma t}\cos(\upsilon t) \tag{3.119}$$

The imaginary part does not have any influence on the stability. Therefore, it is sufficient to base the following proof on the assumption that λ would be real. If the proof is successful, the system will also be stable in the case of a complex eigenvalue λ.

With λ being real number, the solution $\bar{s}_2(t)$ shows monotonic behavior. Then system (3.117) can be considered to be monotonic as well, thus,it is not oscillating. So $\dot{\bar{s}}_2(t)$ and its delayed equivalent have the same signs, which also applies to $\bar{s}_2(t)$ and its delayed correspondent. That means

$$\begin{aligned} \dot{\bar{s}}_2(t) \cdot \dot{\bar{s}}_2(t - 2\tau) &> 0 \\ \bar{s}_2(t) \cdot \bar{s}_2(t - 2\tau) &> 0\ . \end{aligned} \tag{3.120}$$

It is assumed that the system (3.117) is unstable or periodically stable but not asymptotically stable. Then, following the consideration above, the condition

$$|\dot{\bar{s}}_2(t - 2\tau)| \leq |\dot{\bar{s}}_2(t)| \tag{3.121}$$

$$|\bar{s}_2(t - 2\tau)| \leq |\bar{s}_2(t)| \tag{3.122}$$

holds. Additionally, the variable $\bar{s}_2(t)$ has the same sign as $\dot{\bar{s}}_2(t)$ in case of an instability. This also applies to $\bar{s}_2(t - 2\tau)$ and $\dot{\bar{s}}_2(t - 2\tau)$,

$$\begin{aligned} \bar{s}_2(t)\dot{\bar{s}}_2(t) &> 0 \\ \bar{s}_2(t - 2\tau)\dot{\bar{s}}_2(t - 2\tau) &> 0\,. \end{aligned} \tag{3.123}$$

Looking at the continuous differential equation in a certain time interval $t_1 \leq t \leq t_2$ with $t_1, t_2 \in [0; \infty)$, it is possible to find in such an interval with an appropriate choice of t_1 and t_2 an upper limit of difference between the state variables and their delayed equivalents. Replacing the actual differences at each time $t \in [t_1; t_2]$ by this maximum deviation for the whole time interval, this represents the worst case of instability. Another similar and conservative proceeding is achieved, if at each time $t \in [t_1; t_2]$ a factor describing a linear relation between $\bar{s}_2(t)$ and $\bar{s}_2(t - 2\tau)$ like $\bar{s}_2(t - 2\tau) = c\bar{s}_2(t)$ can be set up. Taking the lowest factor appearing in this interval as a constant factor for all relations in this time interval, the worst case of instability is assumed. When the factor goes versus zero, then the difference between $\bar{s}_2(t)$ and its delayed form approaches infinity. So for the estimation error $\bar{s}_2(t-2\tau)$, its derivative with respect to time $\dot{\bar{s}}_2(t)$ and its delayed equivalent $\dot{\bar{s}}_2(t-2\tau)$, linear relations can be introduced for the special time interval $[t_1; t_2]$,

$$|\dot{\bar{s}}_2(t - 2\tau)| \geq c_1 \, |\dot{\bar{s}}_2(t)| \tag{3.124}$$

$$|\bar{s}_2(t - 2\tau)| \geq c_2 \, |\bar{s}_2(t)| \; . \tag{3.125}$$

Knowing that $\bar{s}_2(t)$ and $\bar{s}_2(t - 2\tau)$ have the same signs, which is also true for their derivatives, $c_1 > 0$ and $c_2 > 0$. The upper limit of c_1 and c_2 has the value one, which describes the periodically stable system. Applying relation (3.124) and (3.125) on the differential equation (3.117), the following result is obtained:

$$\dot{\bar{s}}_2(t) = - \frac{l\,(1 + c_2) + \frac{GI_p}{aJ}\,(1 - c_2)}{1 + c_1}\, \bar{s}_2(t) \; . \tag{3.126}$$

Considering $0 < c_1 \leq 1\,,\;\; 0 < c_2 \leq 1$ and $l > 0$,

$$\frac{l\,(1 + c_2) + \frac{GI_p}{aJ}\,(1 - c_2)}{1 + c_1} > 0 \; . \tag{3.127}$$

Therefore, $\dot{\bar{s}}_2(t)$ and $\bar{s}_2(t)$ have different signs, which is contradictory to condition (3.123). Equation (3.126) describes an asymptotically stable, homogeneous differential equation. This is controversial to the assumption (3.121), (3.122) that the equation is unstable or periodically stable.

Thus, resulting from the monotonic properties of $\bar{s}_2(t)$, equation (3.126) must be asymptotically stable in the time interval $t \in [t_1; t_2]$. As equation (3.126) is asymptotically stable in one time interval, it is asymptotically stable in $[0; \infty]$ because of its monotony and the inability of $\bar{s}_2(t)$ with the approach (3.119) to change its sign. ■

The asymptotic stability of the dynamics $\dot{\bar{s}}_2(t)$ is proved and

$$\lim_{t \to \infty} \bar{s}_2(t) - \hat{s}_2(t) = s_2(t) = 0 \, . \tag{3.128}$$

Observation of $s_3(t)$

If $\lim_{t\to\infty} \bar{s}_2(t) = 0$, for the time derivative $\lim_{t\to\infty} \dot{\bar{s}}_2(t) = 0$ holds as well. Moreover, if sliding mode is enforced in the manifold $\bar{s}_1(t) = 0$, $V_1 \operatorname{sign}(s(t)) = \bar{s}_2(t)$ With these assumptions (3.117) leads to

$$\bar{s}_3(t) = \frac{GI_p}{a}\, \bar{s}_2(t) + J\dot{\bar{s}}_2(t) + Jl\bar{s}_2(t) \tag{3.129}$$

follows $\bar{s}_3(t) = 0$, and $\hat{s}_3(t) = s_3(t)$.

Now, the stability of the observer (3.96) is proved. Enforcing sliding mode in the manifold $\bar{s}_1(t) = 0$ implies $\bar{s}_2(t) = \bar{s}_3(t) = 0$, and thereby $\hat{s}_1(t) = s_1(t)$, $\hat{s}_2(t) = s_2(t)$ and $\hat{s}_3(t) = s_3(t)$. All not measurable system state variables are now available for the control design. The transient process of the observer is illustrated in Figures 3.8 - 3.10 and below. In each figure, the real system state variables $s_1(t)$, $s_2(t)$ and $s_3(t)$ are compared to the corresponding estimates. It can be seen that the observer is able to reach the variables $s_1(t)$, $s_2(t)$ and $s_3(t)$ quite fast with $s_3(t)$ having the slowest approximation process.

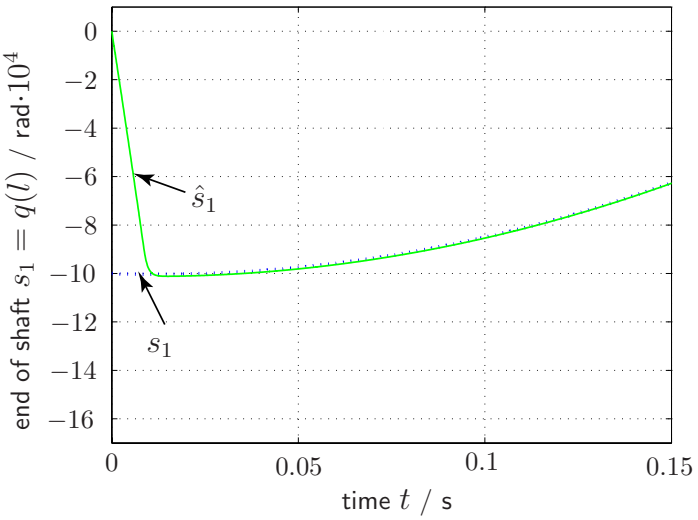

Figure 3.8: Simulation results: Sliding mode observer output $\hat{s}_1(t)$ following the uncontrolled system output $s_1(t)$ of the flexible shaft. The initial values of the state variables of the observer and the shaft system are zero, except for $s_1(0) = -10$.

3.5.2 Estimation of Disturbances

This section discusses the problem of reduced robustness of sliding mode control algorithms that are derived based on the GBCP and the BCP. As a solution, this section presents disturbance rejections methods. As an example, the in the last section explained sliding mode control is extended in order to reject disturbances. The developed rejection method provides a stable, fast and very robust control of the flexible mechanical system. The proposed control compensates the effects of perturbations completely.

Problem Statement

Generally, sliding mode control is known for its high robustness. But the sliding mode control algorithm developed in Section 3.4.3 cannot control the flexible shaft system with disturbances, as illustrated in Figure 3.11. At first, the transient process of the flexible shaft controlled by sliding mode, known from Figure 3.6, can be seen. When a constant disturbance in form of torque attacks at the load a constant control error appears. This happens, because a discrete-time system is considered and there is a continuous control

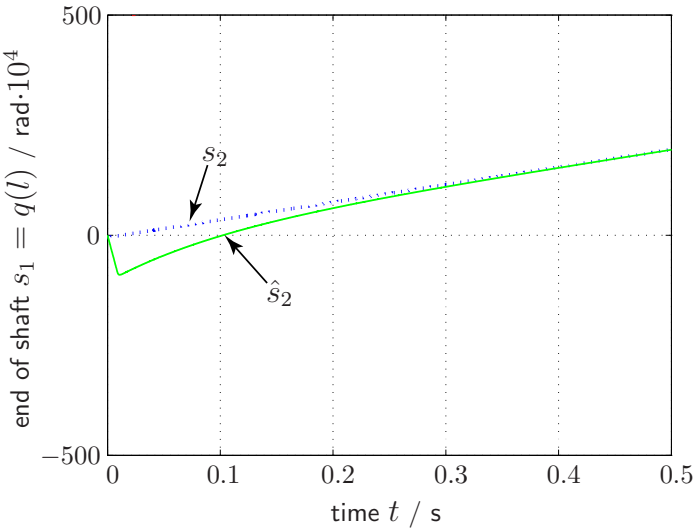

Figure 3.9: Simulation results: Sliding mode observer output $\hat{s}_2(t)$ following the uncontrolled system output $s_2(t)$ of the flexible shaft. The initial values of the state variables of the observer and the shaft system are zero, except for $s_2(0) = -5$.

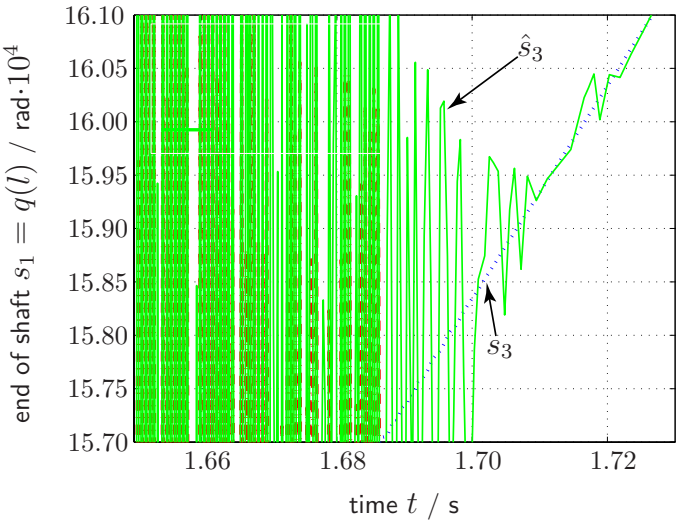

Figure 3.10: Simulation results: Sliding mode observer output $\hat{s}_3(t)$ following the uncontrolled system output $s_3(t)$ of the flexible shaft. The initial values of the state variables of the observer and the shaft system are zero.

input, thus in contrast to discontinuous control inputs the capability of tolerating errors is much lower. The control input $u(t-\tau)$ is calculated based on modeled system dynamics, compare (3.90). Any additional unknown term in (3.135) leads to an error $s(t) \neq 0$ and consequently, the desired behavior of the system is not achieved.

The GBCP is robust only with respect to the state of the last block, because the discontinuous control is only used to assign desired dynamics in the last block. Nevertheless, if some informations of disturbances are given, they can be estimated and control gets more robust.

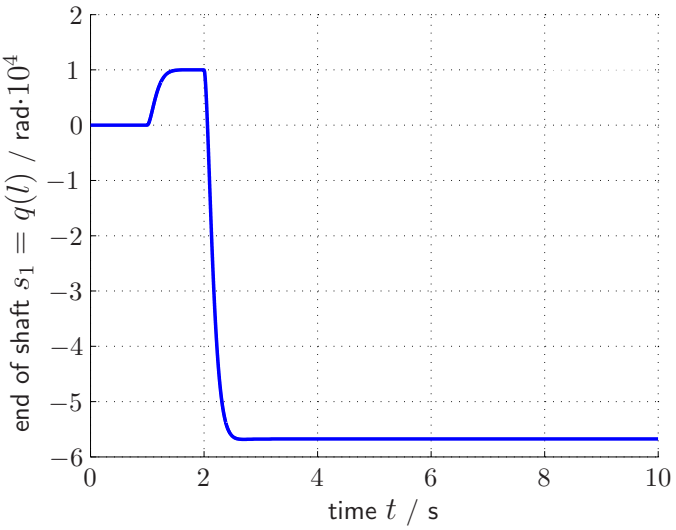

Figure 3.11: Simulation results: Sliding mode controlled system. The initial conditions are zero At time 1s the shaft's response on a step in the input position $q(0,t)$ from 0 rad to 1 rad. At time 2s a disturbance in form of a 1Nm step is given to the end of the bar. A constant control error appears.

In literature two main approaches to reject the influence of perturbations on any system are mentioned [24], [6]. The first is to utilize high gain and the second is to compensate the disturbances by measuring or knowing them. This thesis follows the second approach. A control concept is developed, that estimates the unknown disturbances at first and then compensates them. For that purpose the existing sliding mode control is extended accordingly.

It is assumed that an additional torque attacks at the end of the shaft. The partial differential equation describing the behavior of the flexible shaft remains the same

$$\ddot{q}(x,t) = a^2 \frac{\partial^2 q(x,t)}{\partial x^2} \ . \tag{3.130}$$

But the boundary condition at position $x = l$ changes to

$$\begin{aligned} M(0,t) &= -GI_p \frac{\partial q(0,t)}{\partial x} \\ T_L(l,t) + J\ddot{q}(l,t) &= -GI_p \frac{\partial q(l,t)}{\partial x} \end{aligned} \tag{3.131}$$

whereas the initial conditions are still zero.

$$q(x,0) = 0$$
$$\dot{q}(x,0) = 0$$

The variable T_L represents a disturbance that attacks in form of torque at the load.

As done in Section 3.4.2 the equations (3.130) and (3.131) may be rewritten as a transfer function in the Laplace domain,

$$\begin{aligned} Q(x,p) =& \frac{\left(1 - \frac{Jap}{GI_p}\right)e^{-\frac{l-x}{a}p} + \left(1 + \frac{Jap}{GI_p}\right)e^{\frac{l-x}{a}p}}{p\left(\left(Jp + \frac{GI_p}{a}\right)e^{\frac{l}{a}p} + \left(Jp - \frac{GI_p}{a}\right)e^{-\frac{l}{a}p}\right)} U(p) \\ &+ \frac{-\left(e^{\frac{x}{a}p} + e^{-\frac{x}{a}p}\right)}{p\left(\left(Jp + \frac{GI_p}{a}\right)e^{\frac{l}{a}p} + \left(Jp - \frac{GI_p}{a}\right)e^{-\frac{l}{a}p}\right)} T_L(l,p)\,. \end{aligned} \tag{3.132}$$

Evaluating (3.132) at position $x = l$ delivers the transfer function which can be transformed back into the time domain.

$$\begin{aligned} Q(l,p) =& \frac{2e^{-\frac{l}{a}p}}{p\left(\left(Jp + \frac{GI_p}{a}\right) + \left(Jp - \frac{GI_p}{a}\right)e^{-\frac{2l}{a}p}\right)} U(p) \\ &- \frac{1 + e^{-\frac{2l}{a}p}}{p\left(\left(Jp + \frac{GI_p}{a}\right) + \left(Jp - \frac{GI_p}{a}\right)e^{-\frac{2l}{a}p}\right)} T_L(l,p) \end{aligned} \tag{3.133}$$

Completing the retransformation, the differential equation with delay

$$\begin{aligned} J\ddot{q}(t) + \frac{GI_p}{a}\dot{q}(t) + J\ddot{q}(t-2\tau) - \frac{GI_p}{a}\dot{q}(t-2\tau) \\ = 2u(t-\tau) - T_L(t) - T_L(t-2\tau) \end{aligned} \tag{3.134}$$

is achieved. Writing (3.134) as a differential-difference system in block-control form, the following result is obtained:

$$\ddot{s}_1(t) = -\frac{GI_p}{aJ}\dot{s}_1 + \frac{1}{J}s_3 \tag{3.135}$$

$$s_3(t) = 2\frac{GI_p}{a}\dot{s}_1(t-2\tau) + s_3(t-\tau) - s_3(t-2\tau) + 2u(t-\tau) - T_L(t) - T_L(t-2\tau) \tag{3.136}$$

Remark 3.5 When developing a control architecture that compensates the disturbance applied to the load of the system, then at first it has to be shown that it is possible at all to reject such a perturbation. For this purpose, it is generally expected that the control input and the disturbance fulfill the so called matching condition.

So this matching condition is certainly not satisfied as the control input is added on the left side to the shaft and the disturbance attacks on the right side, see (3.131). This can be interpreted as control input vector and perturbation vector not being collinear. But this matching condition is too strong for only being interested in controlling the rotation degree $q(l,t)$ at the position of the load. There, the control input $u(t)$ and the perturbation $T_L(t)$ are collinear. According to (3.134), an input $u(t)$ can be found that compensates the disturbance $T_L(t)$ and leads to the desired output $q(l,t)$. So the sufficient matching condition only valid for the position of the load is fulfilled.

Physically speaking, this means that it is only possible to control the rotation at one position x_c, whereas all other state variables $q(x,t)$ cannot be governed. To achieve the desired rotation $q(x_c,t)$ at the load ($x_c = l$) under influence of perturbations, e.g. keep $q(l,t)$ equal to zero, it is necessary to apply a certain $u(t)$ at the beginning of the shaft. This input leads to uncontrollable oscillations along the bar. Only at the end of the shaft the rotation remains zero and the required torque $-T_L(t)$ to compensate the effect of the disturbance turns up. The disturbed system can be controlled at the position $x = l$. ■

Rejecting any kinds of perturbations is a difficult task. In order to simplify the problem, this thesis assumes that differential equations of the disturbances attacking the system of the flexible shaft exist and that they are known except of their initial conditions.

In this thesis an observer is built, that estimates the disturbance and then compensates it. This approach is mathematically speaking similar to extending the existing PD-Controller $s_3^*(t) = k_1 s_1(t) + k_2 s_2(t)$. Depending on the differential equation of the disturbance to be rejected, different extensions would be necessary. For a constant perturbation for example, the existing PD-Controller would be supplemented by an I-Component.

Remark 3.6 The assumption, that disturbances are known except of their initial conditions, is not totally unrealistic because it is usually known what types of perturbations appear in the area the torsion bar is used. These influences could for example be friction, oscillations, start-up procedures or torque. With these reflections a wide range of functions of disturbances can be covered, e.g. polynomials, products, exponential and sinusoidal functions etc. ■

Sliding Mode Control of the System with Disturbances

The proposed sliding mode control architecture can be seen in Figure 3.12. In contrast to the architecture presented in Section 3.4.3, a perturbation $T_L(t)$ influences the system of the flexible shaft. The observer equals that of the real system. In order to work correctly, it requires the value of the disturbance as well. It receives this value $\hat{T}_L(t)$ from the estimator which estimates the unknown perturbation. This estimated value is also put into the sliding mode control of the whole system to compensate the effect of the real disturbance. The not yet in detail described blocks are discussed in the paragraphs below.

In the following paragraphs three kinds of disturbances are discussed, all of them attacking in form of additional torque at the end of the torsion bar, at the load.

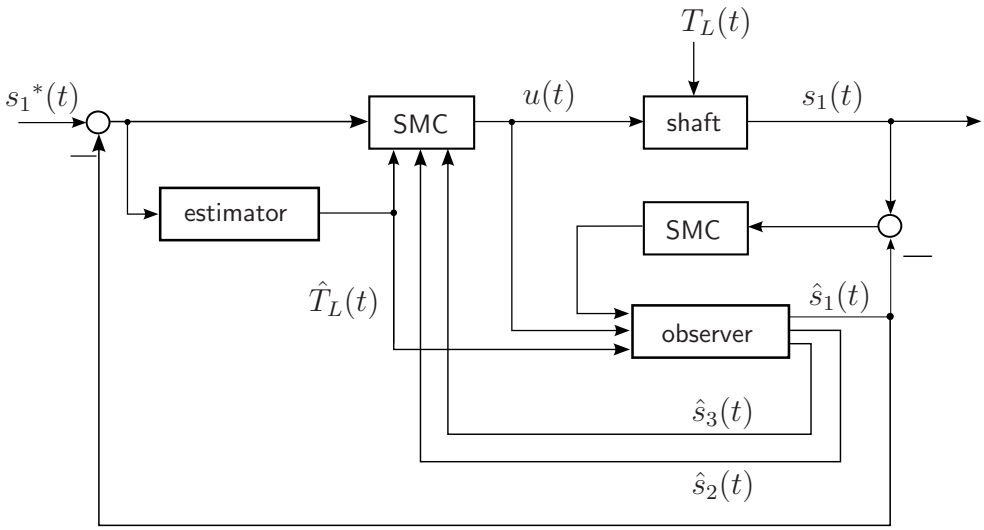

Figure 3.12: Sliding mode control architecture with disturbance rejection.

At first *constant disturbances*, e.g. a constant torque applied to the end of the bar which starts at a certain time t_1 with amplitude $\tilde{T}_L$, are examined. So it can be described as a step function

$$T_L(t) = \tilde{T}_L \sigma(t - t_1)\,, \tag{3.137}$$

whose Laplace transformation is

$$T_L(p) = \tilde{T}_L \frac{e^{-t_1 p}}{p} \qquad (t_1 \geq 0)\,. \tag{3.138}$$

The torque could for example result from friction between the load and the environment or a mass, which is clutched in at time t_1 and shall be lifted by a rotation of the shaft. In this case the friction is independent of the load's rotation speed.

The second type to be looked at are *linear disturbances* which consist of a ramp function, that begins at time t_1 with slope $\tilde{T}_L$

$$T_L(t) = \tilde{T}_L\,(t - t_1)\sigma(t - t_1)\,, \tag{3.139}$$

where

$$\mathcal{L}\left\{T_L(t)\right\} = \tilde{T}_L \frac{e^{-t_1 p}}{p^2} \qquad (t_1 \geq 0)\,. \tag{3.140}$$

Such linear disturbance function may be caused by a device, which is pressed increasingly stronger against the load of the shaft. Applications could be brake processes or start-up procedures.

At last, *sinusoidal disturbances* are analyzed. The sine-function is again time controlled with the peak value $\tilde{T}_L$.

$$T_L(t) = \tilde{T}_L \sin(t)\sigma(t - t_1)\,, \tag{3.141}$$

Such disturbances appear, if the load is influenced by some irregularitive device that oscillates. Thus, the torque of the perturbation would increase and decrease periodically with time t.

With the proposed approach to reject disturbances a really wide range of different perturbations can be covered. The amount dealt with here has been limited to the three cases of constant, linear and sinusoidal disturbances. Although most perturbations will consist of nonlinear functions, the choice of the three kinds corresponds with the dominating behavior of a lot of mechanical perturbations in a certain interval. Moreover, the general idea of rejecting disturbances can be illustrated very good with these three examples.

The sliding mode control design for system (3.135 - 3.136) follows, the proceeding in Section 3.4.3. To assign desired dynamics for $s_1(t)$ (3.87) , the state variable $s_3(t)$ has to be chosen as in (3.88). To guarantee that

$$s(t) = s_3(t) - s_3^*(t) = 0 \tag{3.142}$$

in a finite time interval, the control input $u(t)$ must satisfy the following equation:

$$\begin{aligned} u_{eq}(t) =& \frac{1}{2}\Big(k_1 s_1(t+\tau) + k_2 s_2(t+\tau) + s_3(t-\tau) - 2\frac{GI_p}{a} s_2(t-\tau) \dots \\ &+ T_L(t+\tau) + T_L(t-\tau)\Big) \end{aligned} \tag{3.143}$$

The calculation of the control input now requires informations about the value of the disturbance.

The values of $s_1(t)$ and $s_2(t) = \dot{s}_1(t)$ can be estimated with the extrapolator introduced in Remark 3.4,

$$\begin{pmatrix} s_1(t+\tau) \\ s_2(t+\tau) \end{pmatrix} = e^{\mathbf{A}\tau} \begin{pmatrix} s_1(t) \\ s_2(t) \end{pmatrix} + \frac{1}{J}\int_t^{t+\tau} e^{\mathbf{A}(t+\tau-\xi)} \begin{pmatrix} 0 \\ s_3(\xi) \end{pmatrix} d\xi \tag{3.144}$$

where

$$s_3(\xi) = 2\frac{GI_p}{a}\, s_2(\xi - 2\tau) - s_3(\xi - 2\tau) + 2u(\xi - \tau) - T_L(\xi) - T_L(\xi - 2\tau)$$

and $t \le \xi \le t + \tau\, p$

Equations (3.143) and (3.144) contain values of T_L at several times. That means, if the disturbances are not known, values of T_L have to be found in a different way. Assuming the differential equations of the disturbances are known, an observer can be designed to find the influences on the shaft.

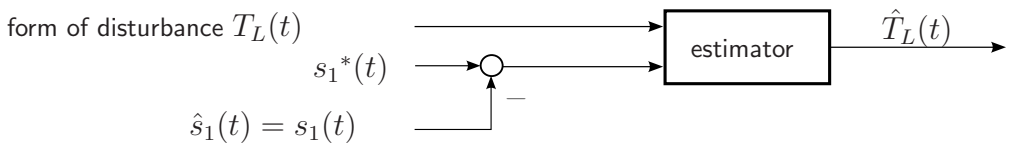

Figure 3.13: Estimator of disturbances

As shown in Figure 3.13, the proposed estimator requires two inputs to calculate the missing value of a disturbance, The first is some information about the form of the disturbance. The second is the difference between the reference value and the observer or real system output

$$s_1{}^*(t) - \hat{s}_1(t) = s_1^*(t) - s_1(t)\,. \tag{3.145}$$

In the undisturbed system no steady state error exists. So if a remaining difference occurs, then it can be concluded that a disturbance attacks the flexible shaft. Based on this error, the estimator can find the real value of the disturbance. When the perturbation is approximated, this deviation will vanish. A necessary requirement is that the disturbance is estimated with a structure that corresponds with the structure of the disturbance. Therefore the type of perturbation and so its differential equations except their initial conditions have to be known, so that the accurate structure is provided for the estimator to calculate the disturbance. This structure is shown below for the three types of perturbations dealt with in this thesis.

A constant disturbance's first derivative with respect to time is zero ($\dot{T}_L(t) = 0$). Thus an integrator is necessary to find the height of this unknown input. For a ramp-like perturbation two integrators are needed, because its second derivative is zero ($\ddot{T}_L(t) = 0$). No time derivative of a sinusoidal disturbance is zero for all times, so a slightly different form of estimator is used here. The second time derivative is defined as follows: $\ddot{T}_L(t) = -\omega^2 T_L(t)$. Therefore two integrators with a feedback loop, which form a PT2-function, are applied to estimate the disturbance. So it is possible that the input of this PT2-function becomes zero as in the cases before, but, however, the disturbance is estimated accurately. Additionally, the denominator of the PT2-function should be without damping. Otherwise an input difference between the reference value $s_1^*(t)$ and the system output $\hat{s}_1(t) = s_1(t)$ remaining on the value zero would not be achieved.

This way the disturbance at time t can be found. The control input $u_e q(t)$ also depends on several values of T_L in the past. To receive these delayed values of T_L, the present $T_L(t)$has to be stored and then may be used when it is necessary. Future disturbances $T_L(t+\tau)$ have to be approximated with the knowledge of its previous behavior.

Future values of a perturbation can only be found in continuous parts of a disturbance's function. At times of discontinuity, the future values cannot be found. But that is not a too serious problem, because the error in governing the shaft at this time is primarily caused by the transient process of the estimator trying to find the disturbance. The not suitable future value $T_L(t+\tau)$ only plays a subordinate role in this situation. After the transient process however, the value of the perturbation lying ahead is necessary to reduce the difference between the target position and the actual position to zero. Here the future value of the disturbance is approximated by developing $T_L(t+\tau)$ in a Taylor Series starting from $T_L(t)$.

$$T_L(t+\tau) = \sum_{i=0}^{n} \frac{1}{i!} \frac{\partial^i T_L(t)}{\partial t^i}\, \tau^i \tag{3.146}$$

If $n \to \infty$, the Taylor Series is exact, of course, but as τ is very small ($\tau < 1 \cdot 10^{-3}$s) it is sufficient for simulation purposes to take $n = 2$. In order to find $T_L(t+\tau)$ the first

and second time derivative of $T_L(t)$ must be calculated. To avoid problems with the derivatives at times of discontinuities, they are filtered. For the purposes of quickness and stability, a different filter is used for each derivative. A filter of first order is applied to the first time derivative of $T_L(t)$ and a filter of second order to the second time derivative.

Observer

To find the system state variables that are necessary for implementing the sliding mode control algorithm with disturbance rejection, the in Section 3.5.1 introduced observer has to be expanded. The perturbation dynamics is added to the observer dynamics.

$$\begin{aligned}
\dot{\hat{s}}_1(t) &= \hat{s}_2(t) - V_1 \operatorname{sign}\left(\hat{s}_1(t) - s_1(t)\right) \\
\dot{\hat{s}}_2(t) &= -\frac{GI_p}{aJ}\,\hat{s}_2(t) + \frac{1}{J}\,\hat{s}_3(t) - V_2 \operatorname{sign}\left(\hat{s}_1(t) - s_1(t)\right) \\
\hat{s}_3(t) &= -\hat{s}_3(t-2\tau) + 2\,\frac{GI_p}{a}\,\hat{s}_2(t-2\tau) + 2u(t-\tau) - T_L(t) - T_L(t-2\tau)
\end{aligned} \tag{3.147}$$

This observer is also controlled by sliding mode based on the difference between observer and real output $\hat{s}_1(t) - s_1(t)$. The stability of this observer can be proved in the same way as in Section 3.5.1. This time, the real disturbance and the estimated one compensate each other, so that $\bar{s}_3(t)$ approaches zero. Otherwise, $\bar{s}_3(t)$ would become equal to the value of the disturbance.

Simulation Results

In this section, the theoretically discussed results of the above developed disturbance rejection are validated in numerical simulations with Matlab/Simulink.

Firstly, simulation results are given for step-like and ramp-like disturbance functions. Initially the flexible shaft is unexcited, only the end of the shaft is not zero, $s_1(t = 0) = 0.5\,\text{rad}$. At time $t = 1\,\text{s}$ the reference value jumps from 0 to 1 rad. At time $t = 2\,\text{s}$ the different disturbances attack the system.

In case of constant disturbances, see Figure 3.14, the fast response of the observer can be seen. When the target value changes the sliding mode controlled system (3.135 - 3.136) follows immediately. The trajectory $\hat{T}_L(t)$ shows the quick approximation of the perturbation by the estimator. The step-like disturbance is estimated with an I-controller, which corresponds to the structure of $T_L(t)$ and leads to a control error zero. For reasons of fast performance and stability, a proportional and a derivative component are added to the estimator. Because of the transient process of the estimator approximating the new value $T_L(t)$ at the time of the perturbation's jump, the system output $s_1(t)$ reacts slowly to the disturbance. After a short time period the system approaches the target value again. During the whole process, the trajectory $\bar{s}_1 = \hat{s}_1 - s_1$ demonstrates the abilities of the observer.

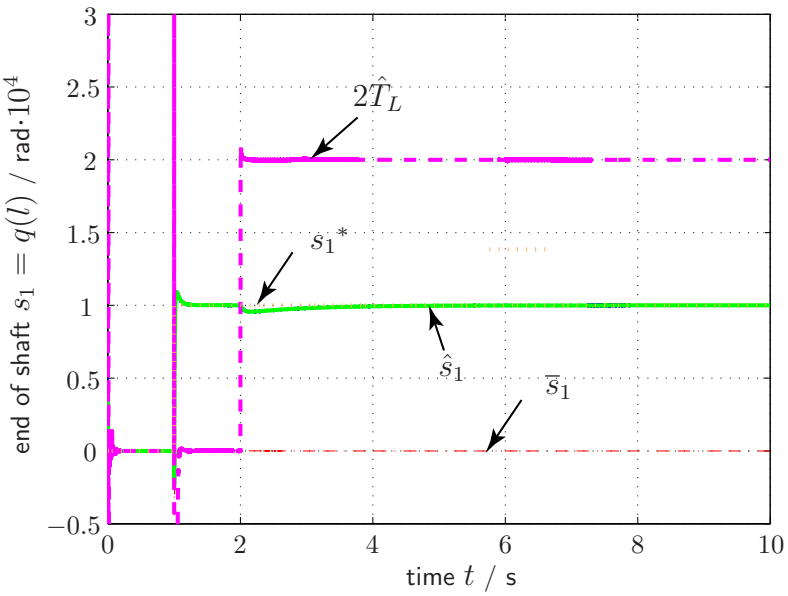

Figure 3.14: Simulation results: Sliding mode controlled system. The initial conditions are zero. The system responses to a step in the input position $q(0,t)$ from 0 rad to 1 rad at time $t = 1\,\mathrm{s}$ is shown. Additionally, a step-like disturbance attacks at the end of the torsion bar at time $t = 2\mathrm{s}$.

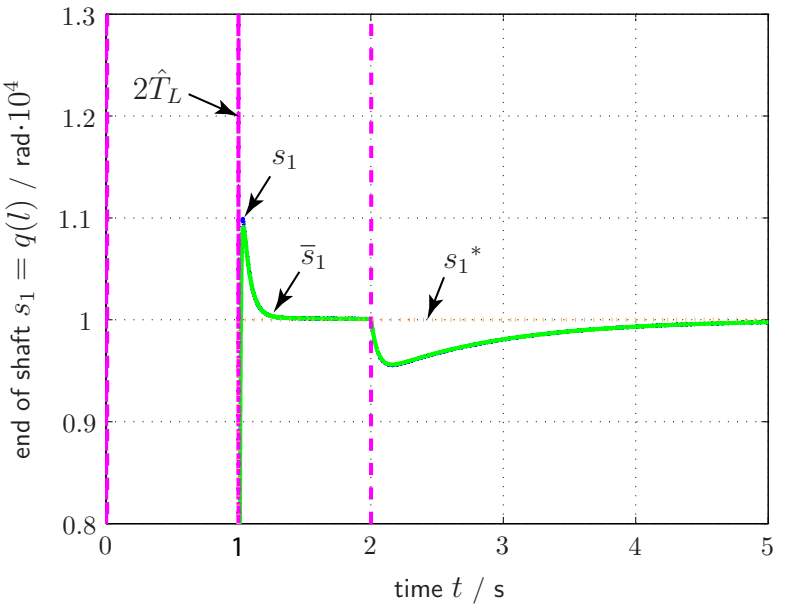

Figure 3.15: Simulation results: Close-up of Figure 3.14.

Figure 3.16 illustrates the behavior of system (3.135) when a ramp-like disturbance attacks. The disturbance is estimated quickly due to a PD-controller added to the necessary double I-controller.

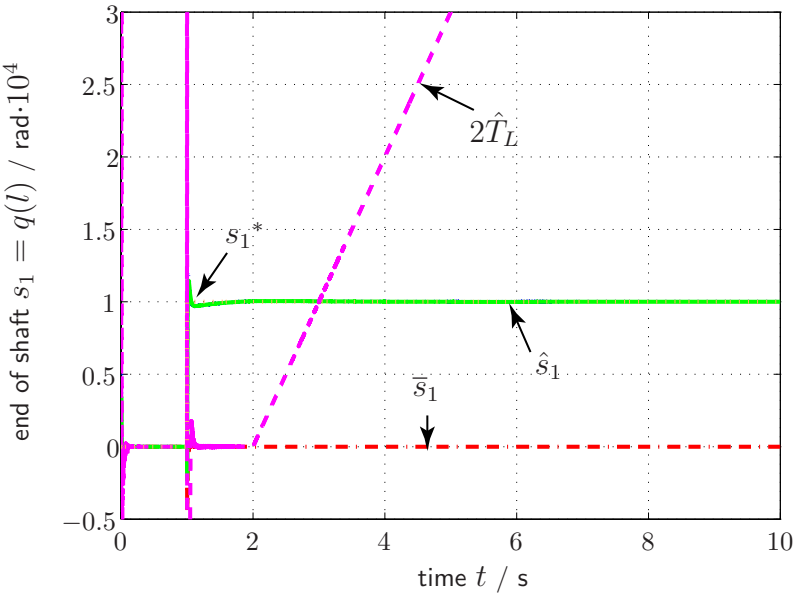

Figure 3.16: Simulation results: Sliding mode controlled system. The initial conditions are zero. At time $t = 1\,\mathrm{s}$ the shaft responses to a step in the input position $q(0,t)$ from 0 rad to 1 rad. Additionally, a ramp-like disturbance with slope $\tilde{T}_L(t) = 1\,\frac{\mathrm{rad}}{\mathrm{s}}$ attacks at the load of the torsion bar at time $t = 2\,\mathrm{s}$.

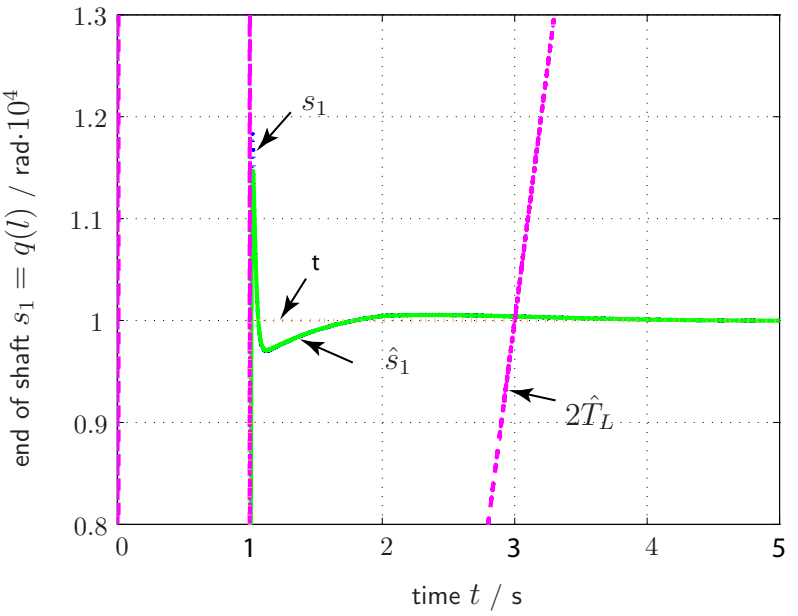

Figure 3.17: Simulation results: Close-up of Figure 3.16.

Figure 3.18 shows the simulation result if a sinusoidal disturbance functions attacks. Initially the flexible shaft is unexcited, only the end of the shaft is not zero, $s_1(t=0) = 0.5\,\text{rad}$. There is a sinusoidal reference value with frequency $\omega = 2\text{s}^{-1}$ and amplitude $\tilde{T}_L = 1\text{rad}$ starting at time $t = 1\text{s}$. The system output $s_1(t) = \hat{s}_1(t)$ oscillates with decreasing amplitude around the trajectory of the target value and tends toward it. At time 2s, a sinusoidal disturbance with frequency $\omega = 1\text{s}^{-1}$ and amplitude $\tilde{T}_L = 1\text{rad}$ attacks the flexible shaft. Its oscillations around the target value increase a bit at first and then becomes smaller again. This time, the estimation process of the disturbance features huge oscillations, which result from the choice of parameters of the PT2-function supported by a P- and D-component in its nominator.

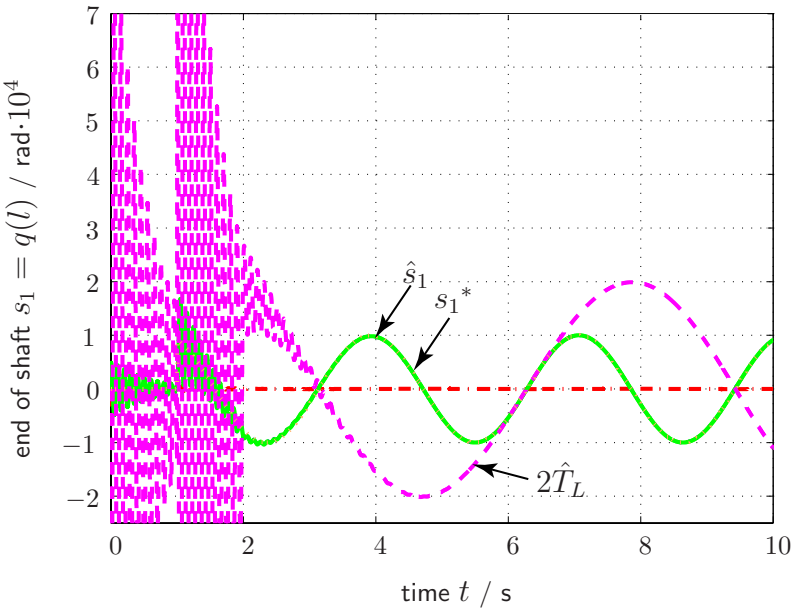

Figure 3.18: Simulation results: Sliding mode controlled system. The initial conditions are zero, At time $t = 1\,\text{s}$ the shaft responses to a sinusoidal reference value with amplitude $A_d = 1\,\text{rad}$ and frequency $\omega = 2\,\text{s}^{-1}$. Additionally, a sinusoidal disturbance with amplitude $\tilde{T}_L = 1\,\text{rad}$ and frequency $\omega = 1\text{s}^{-1}$ attacks the load of the torsion bar at time $t = 2\,\text{s}$.

3.5.3 Discussion

In this section the implementation of the sliding mode control algorithm, which was developed in Section 3.4 was discussed. A concept for the estimation of disturbances and the observation of not measurable system state variables has been developed. It assumes that the forms of the disturbances are known, only their initial conditions are not known. Simulation results illustrated the abilities of the developed control architecture.

The proposed disturbance estimation concept meets the drawback of the GBPC/ BCP of reduced robustness. By estimating the disturbances and using this information in the observer and control algorithm the the control performance improves significantly.

Up to now, the estimator has to be told manually which structure to use for the estimation process dependent on the form of the differential equation of the disturbance. A switching logic could be implemented that recognizes the type of perturbation and choose automatically a suitable structure to calculate this unknown influence. This switching logic could also be extended in a way, that different kinds of disturbances could appear synchronously and would be estimated accurately.

At the moment, the frequency of a sinusoidal perturbation has to be known to be able to estimate this disturbance correctly. If the frequency was taken as an additional state variable of the perturbation, it could be found in a similar way as the estimator of the disturbances works. When the unknown frequency is constant, then an integrator would be able to find its value. Thus the PT2-function that is used to approximate sinusoidal disturbances could have an adaptive frequency, so different values and different forms of frequencies could be covered.

3.6 Conclusion

In this chapter an existing design procedure was extended to the GBCP, which presents a closed methodology for the systematic control unit design for electromechanical systems. Compared to the existing BCP, the GBCP simplifies the control design and does not require equal dimension of block states and intermediate controls.

Based on the in [23] presented sliding mode control of an flexible shaft an application example of the GBCP to infinite dimensional systems was given. That proved the applicability of GBCP to a larger system class than the BCP. For the first time, solutions to implementation problems of sliding mode control based on the GBCP and respectively the BCP, were given. A new method for disturbance rejection was contributed.

Supplementary to the theoretical considerations in this chapter, in this thesis the GBCP is tested in experiments. They show the performance of the newly derived theory. It is applied to control inverted pendulum systems, which are driven by different electric motors. Chapter 4 considers a DC motor (Section 4.1) and a synchronous motor (Section 4.1) as actuators. Chapter 5 discusses an induction machine as actuator to control the position of a mechanical system.

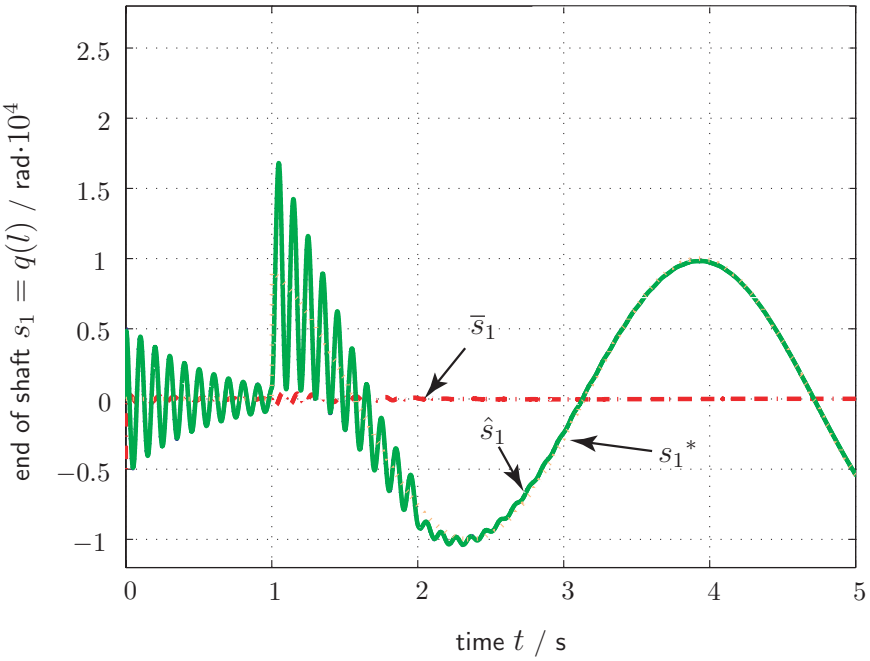

Figure 3.19: Simulation results: Close-up of Figure 3.18.

4 The Benefits of Sliding Mode Control of Electromechanical Systems

Conventional architectures for the trajectory control of mechanical systems use torque or force -the actual control input of the mechanical subsystem- as the control input of the feedback loop. Such a control scheme is illustrated in Figure 4.1. The inner control loop, which regulates the desired torques $\boldsymbol{\tau}^*$, comprises a control unit and a power amplifier that provides the supply voltages $\boldsymbol{u}_a$ for the electric motor. In most implementations the power amplifier is based on pulse-width modulation (PWM). It is assumed that the inner control loop, which provides the desired torques or forces, is fast compared to the outer control loop of the mechanical system. This inner loop is therefore supposed to be an ideal source in the ansatz, implying that the given reference torques will be tracked ideally. In an outer control loop the mechanical part of the system is controlled to follow the reference signal $\boldsymbol{\tau}^*$, which represents the desired position and velocity trajectories. The control law generates desired motor torques $\boldsymbol{\tau}^*$ that are computed based on the knowledge of the mechanical variables $\boldsymbol{x}_{mech}$ only.

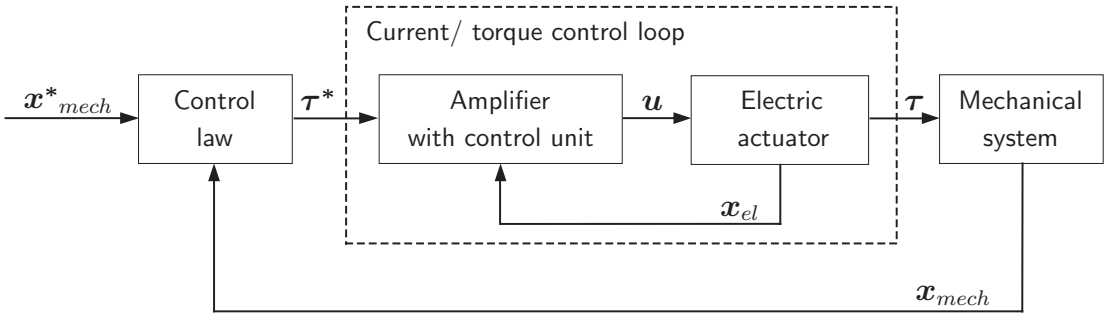

Figure 4.1: Schematic diagram of a conventional control scheme for a mechanical system driven by an electric motor.

The application of sliding mode control theory to the shown control loop promises insensitivity to parameter variations and compensation of disturbances. However, it involves a difficulty:

Forces or torques provided by electric motors are always time-continuous signals. The is because the current in the motor coil cannot change instantaneously when the voltages at the coil are limited. A conventional sliding mode controller implemented into the control scheme of Figure 4.1 would produce force/control output signals $\boldsymbol{\tau}^*$ that are time-discontinuous on the timescale of the sampling time. The conversion of the time-discontinuous controller output signals to an actually continuous input signal of the mechanical system $\boldsymbol{\tau}$, which is given by the characteristic dynamics of the current/torque control loop would mean to neglect dynamics in the control loop which results in chatter-

Controller	Controller output $\boldsymbol{\tau}^*$	Control variable
PID controller	continuous	continuous (torques/forces $\boldsymbol{\tau}^*$)
Conventional control architecture with sliding mode controller	discontinuous	continuous (torques/forces $\boldsymbol{\tau}^*$)
Sliding mode controller that takes actuator dynamics into account	discontinuous	discontinuous (impressed voltages $\boldsymbol{u}_a$)

Table 4.1: Comparison of control schemes for electromechanical systems.

ing. If the the conventional control structure of Figure 4.1 is thus used to implement a discontinuous control, the control loop inherently comprises unmodeled dynamics.

This problem can be dealt with by including actuator dynamics in the system model and by using voltages as discontinuous control inputs. This idea is shown in Figure 4.2. In addition to the mechanical variables $\boldsymbol{x}_{mech}$, the variables of the electrical subsystem $\boldsymbol{x}_{el}$ are fed back to the controller.

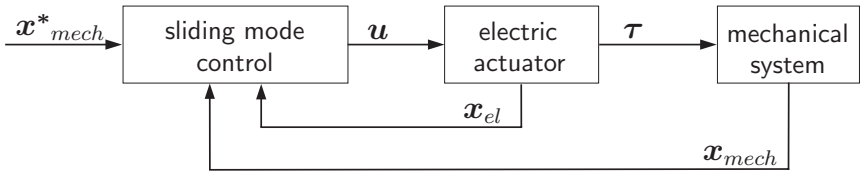

Figure 4.2: Schematic diagram of the proposed sliding mode control scheme for a mechanical system driven by an electric motor.

This chapter faces the challenge of sliding mode control for mechanical systems driven by electric actuators in order to improve robustness of these systems. The key problem of an increased complexity of the design process due to a more detailed system model is met by applying the GBCP to the design problems. The application of the proposed control concept is demonstrated for two sample systems: The position control of an inverted pendulum system driven by a DC motor is considered in Section 4.1. A novel position control of a synchronous motor is derived in Section 4.2. The benefits of the proposed sliding mode control are demonstrated in numerical simulations and experiments. Section 4.3 concludes this chapter.

4.1 Position Control of a DC Motor

Sliding mode control for electromechanical systems is discussed and validated for an inverted pendulum as introduced in section A.1 driven by a DC motor and compared to a linear control structure. First, the state of the art of sliding mode control of DC motors is summarized in Section 4.1.1 and the model of the electric actuator is given in Section 4.1.2. Then a sliding mode position control is developed. Subsequently in Section 4.1.4 a linear control algorithm is derived and an observer is designed in Section 4.1.5. Finally, the

results of numerical simulations and experimental results are given in Sections 4.1.6 and discussed in 4.1.7.

4.1.1 State of the Art

Utkin deals with the problem of controlling a DC motor using a sliding mode control approach in [77] and designs a control algorithm based on a cascaded control structure and proves that this control structure provides strong robustness. This method only considers the mechanical part of the system and assumes that the torque can be switched, which is not possible in practice. However, the neglected electrical dynamics can be excited by the discontinuous control input leading to the so called chattering phenomenon. In [79] Utkin also discusses an integrated structure for speed control accomplishing current control implicitly based on numerical simulations. For the implementation of this control algorithm angular acceleration in the mechanical system is needed. Cavallo et al. propose in [10] a sliding mode control with a partial state feedback where only the mechanical variables of the motor are considered. This approach provides robustness and avoids large peaks in the input signal of the PWM unit and consequently constant current ripples occur. The efficiency of sliding mode control approach for a complete electromechanical system driven by a DC motor has not been analyzed yet.

Several applications of sliding mode control of DC motors, induction motors and synchronous motors have been proposed, e.g. in [77]. In the outer control loop of the control scheme shown in Figure 4.1 PD or PID control is usually implemented. Moreover, in order to improve robustness, tracking problems for position and angular speed of a DC motor also have been solved based on a sliding mode control approach [10]. Improvement of robustness by adding sliding mode control of mechanical system for an induction motor drive with forced dynamics has been shown [86]. Nevertheless, this approach still is based on a cascade control structure assuming fast ideal low-level feedback loops.

4.1.2 Modeling

The dynamics of the electrical system is given by

$$L\dot{i} = u_a - R_a i - K_n \omega \tag{4.1}$$

where i is the armature current, u_a the supplied voltage, R_a the armature resistance and L the armature inductance; K_n represents the induction constant of the DC motor and ω the angular velocity. The generated torque of the motor is defined by $\tau = K_m i$, where K_m represents the torque constant.

4.1.3 Sliding Mode Control Algorithm

The electromechanical system consists of a mechanical subsystem

$$J\ddot{\theta} = mgl \sin\theta - \gamma\omega + K_m i \tag{4.2}$$

and an electrical subsystem (4.1) as illustrated in Figure 4.3. The control input of the whole system is the voltage applied to the DC motor, u_a. This real control input does not influence the dynamics of the mechanical subsystem directly, but only the dynamics of the electrical subsystem. The current i can be treated as intermediate control input of the mechanical subsystem.

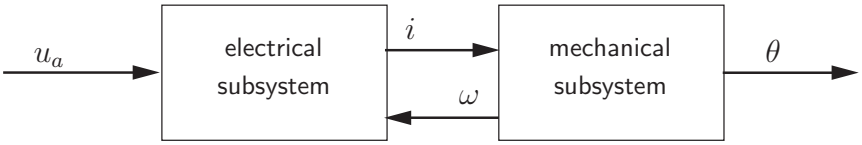

Figure 4.3: Decomposition into subsystems (inverted pendulum driven by a dc motor).

Based on this decomposition, a control algorithm can be assigned based on the GBCP. In the first step the intermediate control input current i or the proportionate torque $\tau = K_m i$ is chosen such that the mechanical system follows desired dynamics. Then in the second step, the real control input, voltage u_a, is utilized in order to enforce sliding mode such that the real torque equals the desired torque.

Desired dynamics for the mechanical system

$$\ddot{\theta} = -c_1\theta - c_2\dot{\theta} \quad c_1\,, c_2 \in \mathbb{R}^+ \tag{4.3}$$

is obtained if

$$-c_1\theta - c_2\omega \stackrel{!}{=} \frac{mgl}{J}\sin\theta - \frac{\mu}{J}\omega + \frac{K_m}{J}i^* \tag{4.4}$$

$$\leftrightarrow i^* = -\frac{mgl}{K_m}\sin\theta - \frac{J}{K_m}c_1\theta + \frac{\mu - Jc_2}{K_m}\omega \tag{4.5}$$

Finally, the discontinuous control input u_a is chosen to set the error between the real and the desired dynamics of the armature current to zero after a finite time

$$u_a = -\bar{u}_a\,\mathrm{sign}(s) \quad \bar{u}_a \in \mathbb{R}^+ \tag{4.6}$$

where

$$s = i^* - i = 0\,. \tag{4.7}$$

When sliding mode is reached, implying $s = 0$, the system state will converge to

$$i = i^* \tag{4.8}$$

and the assigned dynamics is realized. This chosen dynamics (4.3) corresponds to the characteristic polynom

$$\Delta s = s^2 + c_2 s + c_1\,. \tag{4.9}$$

Choosing the constants of the characteristic polynom as follows

$$c_1 = \omega_0^2 \tag{4.10}$$

$$c_2 = 2D\omega_0 \tag{4.11}$$

leads to the desired dynamics of a second order system with the damping ratio D and the characteristic frequency ω_0.

Theorem 4.1 The control law (4.6) enforces sliding mode after a finite time.

Proof: To prove that control law (4.6) fulfills the sliding mode reaching condition (2.14), variable s is derived with respect to time

$$\dot{s} = \dot{i^*} - \dot{i} = \dot{i^*} - \frac{R_a}{L}\dot{i} + \frac{K_n}{L}\omega - \frac{1}{L}u_a \tag{4.12}$$

$$\rightarrow s\dot{s} = s(\dot{i^*} - \frac{R_a}{L}i + \frac{K_n}{L}\omega) - \frac{s}{L}u_a \tag{4.13}$$

$$= s(\dot{i^*} - \frac{R_a}{L}i + \frac{K_n}{L}\omega) - \frac{\bar{u}}{L}|s|\,. \tag{4.14}$$

There exists a $\bar{u} > 0$ fulfilling the inequation $s\dot{s} < 0$, since

$$s\dot{s} < 0 \leftrightarrow s(\dot{i^*} - \frac{R_a}{L}i + \frac{K_n}{L}\omega) < \frac{\bar{u}}{L}|s| \tag{4.15}$$

$$\leftrightarrow \frac{s}{|s|}(L\dot{i^*} - R_a i + K_n\omega) < \bar{u} \tag{4.16}$$

where term $\frac{s}{|s|}$ is equal to 1 or -1, the terms $L\dot{i^*}$ and $\frac{R_a}{L}i$ are limited because the current of the actuator and its slope are limited and the voltage drop $K_n\omega$ is restricted as well. ■

4.1.4 Linear Control Algorithm

In this section the proposed sliding mode control is compared to the linear control scheme described in Figure 4.1. In the outer control loop of the electromechanical system only the state variables representing the angle and angular velocity are included in the control law. The third variable, the current, is considered as a manipulated variable and controlled by PWM in the inner electrical control loop. The control law for the mechanical system is implemented as a feedback linearization control.

The feedback linearization with respect to the output, $y = \theta$, can be realized introducing the virtual control input

$$v = \frac{u - \frac{Km}{J}}{\frac{mgl\sin\theta}{J}} \tag{4.17}$$

leading to the integrator chain below

$$y = x_1' \tag{4.18}$$

$$\dot{x}_1' = x_2' \tag{4.19}$$

$$\dot{x}_2' = u\,. \tag{4.20}$$

The parameters of the linear feedback loop are calculated based on the ITAE (Integral Time Multiplied Absolute Error) criterion. As before, damping rate and characteristic frequency can be assigned.

4.1.5 Observer Design

In the experimental setup a sliding mode observer is used to estimate the angular velocity ω, see Figure 4.4.

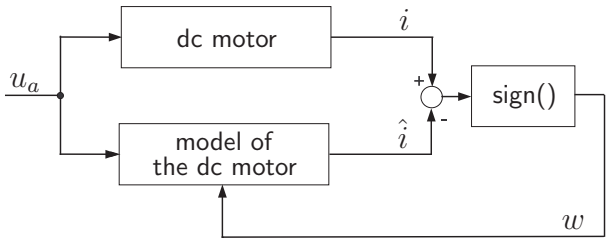

Figure 4.4: Schematic diagram of the observer.

Assuming that the current i can be measured, based on the dc motor equation (4.1), the observer dynamics is designed using the following formulation

$$L\dot{\hat{i}} = u_a - R_a\hat{i} - w \tag{4.21}$$

where $\hat{i}$ is the observed current. If the term w is defined as a switching function of the tracking error of the observer $\bar{i} = \hat{i} - i$

$$w = \bar{w}\,\mathrm{sign}\,(\bar{i}) \qquad \bar{w} \in \mathbb{R}^+\,, \tag{4.22}$$

the error dynamics is

$$L\dot{\bar{i}} = -R_a\bar{i} + K_n\omega - \bar{w}\,\mathrm{sign}(\bar{i})\,. \tag{4.23}$$

The constant $\bar{w}$ is chosen in such a way that sliding mode is enforced in the manifold $s = \hat{i} - i = 0$ and $\bar{i}$ is set to zero after a finite time. Using the concept of equivalent control in sliding mode

$$0 = K_n\omega - \left(\bar{w}\,\mathrm{sign}(\bar{i})\right)_{eq} \tag{4.24}$$

is obtained and the angular velocity $\hat{\omega}$ can be estimated as

$$\omega = \frac{\left(\bar{w}\,\mathrm{sign}\,(\bar{i})\right)_{eq}}{K_n}\,. \tag{4.25}$$

Theorem 4.2 The control law(4.22) enforces sliding mode after a finite time.

Proof: The sliding mode existence condition can be derived based on (4.1):

$$\begin{aligned} L\dot{s} &= L\dot{\hat{i}} - Li \\ &= -R_a s + K_n\omega - \bar{w}\,\mathrm{sign}(s) \end{aligned} \tag{4.26}$$

Next to the sliding manifold $s = 0$ the term $R_a s$ is very small and so it can be neglected. That implies

$$\begin{aligned} \bar{w} &> K_n\omega \quad \text{for} \quad s > 0 \\ \bar{w} &> -K_n\omega \quad \text{for} \quad s < 0\,, \end{aligned} \tag{4.27}$$

summarizing $\bar{w} > |K_n\omega|$, the existence condition for sliding mode is fulfilled. ■

Remark 4.1 In the experimental setup the value of $(\bar{w}\,\mathrm{sign}\,(\bar{i}))_{eq}$ can be determined by a low pass filter ■

4.1.6 Results

Figure 4.5 shows the trajectories of the angle θ, and angular position ω. Detailed trajectories of the angle can be seen in Figure 4.6. Figure 4.7 illustrates influence of the control parameters on the transient response of the system. Figure 4.8 shows trajectories of angular and angular speed if sliding mode is applied and actuator dynamics is taken into account and if it is not considered.

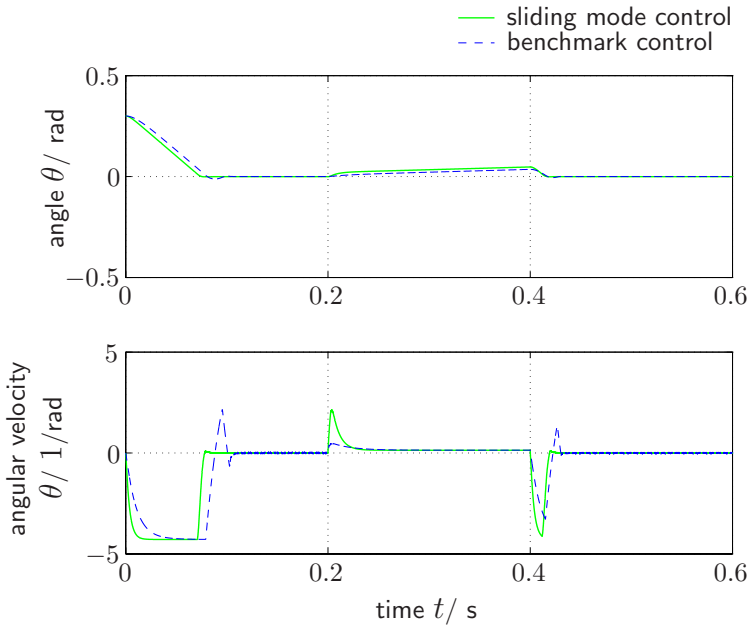

Figure 4.5: Simulation results: Sliding mode control and linear control of the electromechanical system with disturbances and parameter variations. Numerical simulations are carried out using variable stepsize while the minimal stepsize is $T_a = 10^{-6}$ s. The sampling time of the controller is assigned as $T_{sample} = 10^{-4}$s. In order to provide comparability of simulation results, the same dynamics for all methods is specified. That means for all control strategies the dynamics of the closed loop is characterized by $\omega_0 = 500$ and $D = \frac{1}{\sqrt{2}}$. In case of linear control law the current is simulated by PWM control based on 20 kHz sampling rate. For all systems the control objective is $\theta = 0$ and the initial angle is $\theta_0 = -0.1$ rad. In simulations a disturbance of 1 Nm is added at time $t = 0.06$ s for a time period of 0.02 s and the inertia of the mechanical system is set to 110% of the inertia J used in control design. Friction is neglected ($\mu = 0$). A zero order hold, sampling time $T = 0.0001$ s, was added in order to simulate discrete control. In the simulations the observer is not used.

Figure 4.9 and 4.10 present the trajectories of angle as well as measured current if the proposed sliding mode control is applied to the electromechanical system described in Appendix A.1 and A.2. Measurements were repeated for different loads.

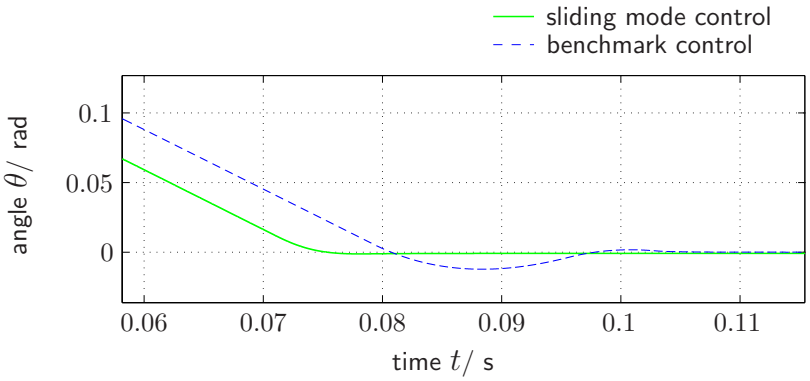

Figure 4.6: Simulation results: Sliding mode control and linear control of the electromechanical system and benchmark control with disturbances and parameter variations- Close up.

4.1.7 Discussion

The efficiency of the sliding mode controller is proved by means of numerical simulations as well as experiments. The sliding mode control for the electromechanical system, which was derived based on the GBCP, offers high robustness and fast dynamics.

- *Robustness*

  The sliding mode controlled system proved to be very robust against parameter variations. Changing the load approximately 5% does not effect performance considerably. The control objective is achieved without steady state error. The feedback linearization as well as pole placement with the help of the ITAE criterion require well known models. Therefore while using sliding mode control, it is easier to compensate a perturbation of the torque load.

- *Simple Implementation*

  Implementation of the proposed sliding mode control is simple and stability analysis can be carried out seamlessly using the sliding mode condition (2.13). Nevertheless, fast hardware is required: A control unit offering at least 1 kHz sampling rate is necessary to achieve acceptable results concerning current and angle ripple.

4.2 Position Control of a Synchronous Motor

This section focuses on sliding mode position control of a three-phase permanent magnet synchronous motor. Firstly, the motor and inverter model are derived in Section 4.2.1. Then in Section 4.2.2 following the control concept proposed in Figure 4.2 a sliding mode position control is derived based on the GBCP. Finally the experimental results are presented in Section 4.2.3 and discussed in Section 4.2.4.

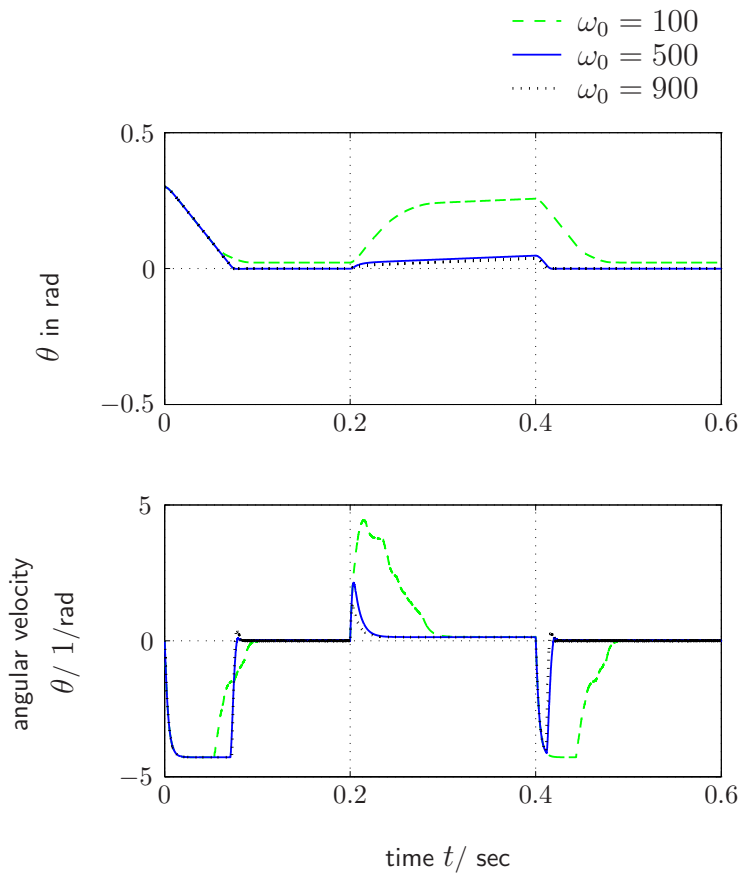

Figure 4.7: Simulation results: Sliding mode control of the electromechanical system with disturbances. Transient response for different design parameters. When ω_0 is increased the transient system response is achieved faster.

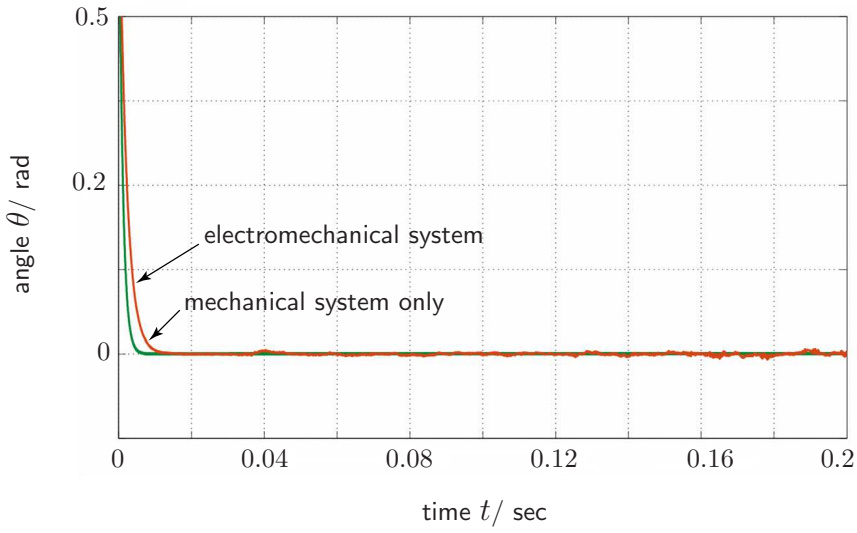

Figure 4.8: Simulation results: Sliding mode control of the electromechanical compared to sliding mode control of the mechanical system. If actuator dynamics is taken into account, chattering effects are reduced.

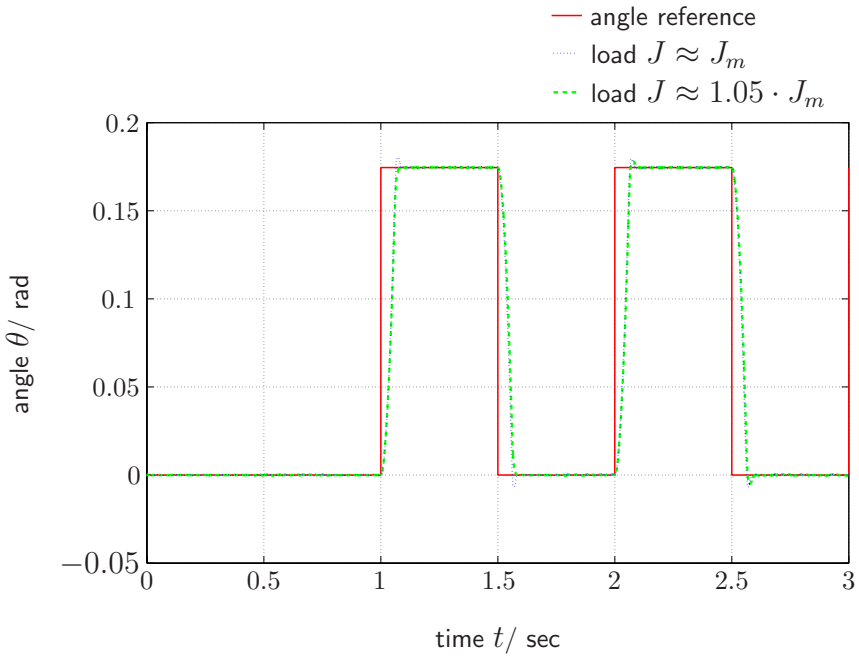

Figure 4.9: Experimental results: Sliding mode control of the electromechanical system. Position control with different, not assignable loads.

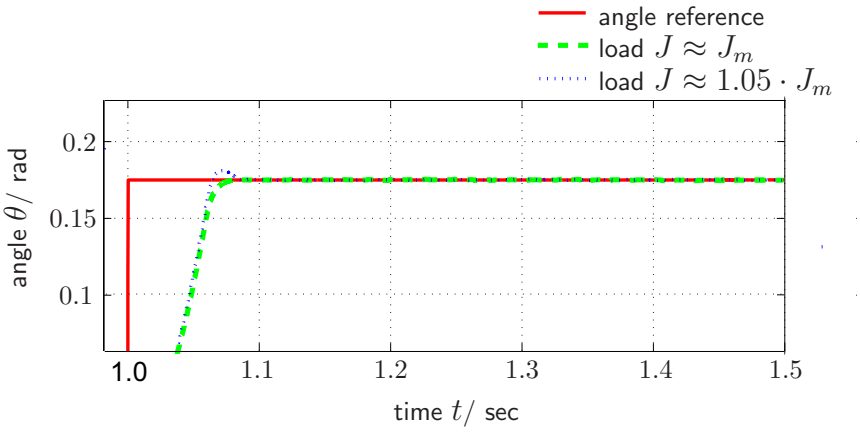

Figure 4.10: Experimental results: Sliding mode control of the electromechanical system. Position control with different, not assignable loads- Close up.

4.2.1 Modeling

In a permanent magnet synchronous motor a rotating magnetic field is generated by an alternating current in the motor windings, which are usually located on the stator. Mechanical torque is then generated by attraction and repulsion of one or several permanent magnets, that are usually located on the rotor. The rotor then starts to rotate with the permanent magnets aligned to the rotating magnetic field of the motor windings. If an external resisting torque is applied to the shaft, the rotating permanent magnets lag behind the motion of the rotating field.

Motor Model

For control unit design the synchronous motor is modeled in rotating rotor coordinates $\{d, q\}$. Unlike in stator coordinates $\{a, b, c\}$ or $\{\alpha, \beta\}$, where the signals have to be modulated on sine waves in order to propel the machine, the waveform of all variables in rotor coordinates is unconstrained and the modulation is carried out implicitly during transformation from rotor to stator coordinates. The model is given by the following differential equations

$$\begin{aligned} L\dot{i}_d &= -Ri_d + p\omega L i_q + u_d \\ L\dot{i}_q &= -Ri_q + -p\omega L i_d + \frac{2}{3} k\omega u_q \end{aligned} \tag{4.28}$$

$$\begin{aligned} J\dot{\omega} &= ki_q - \mu\omega + \tau_L \\ \dot{\theta} &= \omega\,. \end{aligned} \tag{4.29}$$

Here u_d and u_q are rotor voltages in $\{d, q\}$ coordinates, i_d and i_q are rotor currents in $\{d, q\}$ coordinates, θ is the angular position and ω is the angular velocity of the motor shaft. Parameters R and L represent respectively the winding resistance and the inductance; J is the rotor and shaft inertia, p is the number of permanent magnet pole pairs, k is a machine constant and μ represents the coefficient of friction. Variable τ_L represents the disturbing external torque.

Inverter Model

The real control input of the synchronous motor are the switch commands $\boldsymbol{g}$ not the voltages u_d and u_q. Based on the inverter model given in Section 5.2.1 the transformations from switch commands $\boldsymbol{g}$ to voltage $\boldsymbol{u}_{qd}$ and vice versa can be carried out seamlessly. Besides the transformations described in Section 5.2.1, the transformation from $\{\alpha, \beta\}$ coordinates to $\{d, q\}$ coordinates is required for control unit design

$$\boldsymbol{u}_{dq} = \begin{bmatrix} \cos\theta & \sin\theta \\ -\sin\theta & \cos\theta \end{bmatrix} \boldsymbol{u}_{\alpha\beta} \tag{4.30}$$

$$\boldsymbol{u}_{\alpha\beta} = \begin{bmatrix} \cos\theta & -\sin\theta \\ \sin\theta & \cos\theta \end{bmatrix} \boldsymbol{u}_{dq} \tag{4.31}$$

where θ represents the rotor angle. The backward transformation matrix in (4.31) is the transposed forward transformation matrix in (4.30). The same transformations can be applied for transformations between stator and rotor currents. The direct transformation from phase voltage $\boldsymbol{u}_{abc}$ to rotor voltage $\boldsymbol{u}_{qd}$ can be calculated using the matrices in (4.31), (5.9) and resulting as follows (4.30)

$$\boldsymbol{u}_{dq} = \frac{2}{3} \begin{bmatrix} \cos\theta & \cos(\theta - \frac{2}{3}\pi) & \cos(\theta - \frac{4}{3}\pi) \\ -\sin\theta & -\sin(\theta - \frac{2}{3}\pi) & -\sin(\theta - \frac{4}{3}\pi) \end{bmatrix} \boldsymbol{u}_{abc} \tag{4.32}$$

$$\boldsymbol{u}_{abc} = \begin{bmatrix} \cos\theta & -\sin\theta \\ \cos(\theta - \frac{2}{3}\pi) & -\sin(\theta - \frac{2}{3}\pi) \\ \cos(\theta - \frac{4}{3}\pi) & -\sin(\theta - \frac{4}{3}\pi) \end{bmatrix} \boldsymbol{u}_{dq}\,, \tag{4.33}$$

after substituting $\frac{1}{2} = -\cos(\frac{2}{3}\pi) = -\cos(\frac{4}{3}\pi)$ and $\frac{\sqrt{3}}{2} = \sin(\frac{2}{3}\pi) = -\sin(\frac{4}{3}\pi)$. The backward transformation matrix in (4.33) is the Moore-Penrose pseudo inverse of the forward transformation matrix in (4.32).

4.2.2 Sliding Mode Control Design

The position control design for the synchronous motor is accomplished based on the GBCP. The desired dynamics is chosen so as to provide optimal system dynamics with respect to a given cost functional.

As illustrated in Figure 4.11, the electromechanical system consists of two subsystems that are the electrical (4.28) and the mechanical (4.29) ones. The electromagnetic force of the motor is generated by magnetic attraction and repulsion between the rotating magnetic field and the permanent magnets. If the system model is given in field oriented coordinates, the current component i_q is oriented parallel to the peak flux of the permanent magnets and it does not generate any torque. But if the current component i_d is oriented perpendicular to the peak flux, it generates torque. This torque is proportional to the current component i_q as long as the machine's iron is not saturated.

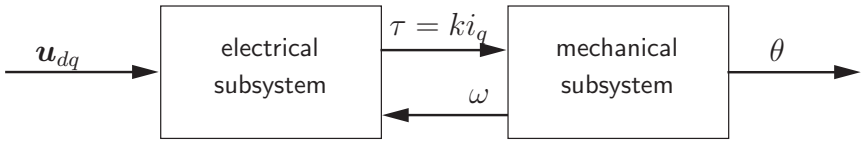

Figure 4.11: Decomposition into subsystems (synchronous motor with load).

Dynamics of the mechanical subsystem described by the state variables

$$\boldsymbol{x}_{mech} = \begin{pmatrix} \theta \\ \omega \end{pmatrix} \tag{4.34}$$

depends only on the current component i_q only and it does not depend on the control input

$$\boldsymbol{u}_{dq} = \begin{pmatrix} u_d \\ u_q \end{pmatrix}, \tag{4.35}$$

but the dynamics of the electrical subsystem described by the state variables

$$\boldsymbol{x}_{el} = \boldsymbol{i}_{dq} \begin{pmatrix} i_d \\ i_q \end{pmatrix} \tag{4.36}$$

depends on $\boldsymbol{u}_{dq}$.

Based on this decomposition into subsystems following the GBCP a control algorithm can be designed as follows: In the first step desired optimal dynamics for the mechanical subsystem with respect to a given cost functional is assigned. The state of the electrical subsystem is then handled as a virtual control input for the mechanical subsystem in order to assign that desired dynamics. In the second step the dynamics of the error between the desired and real values of the electrical state is assigned to be asymptotically stable. Therefore the control input $\boldsymbol{u}_{dq}$ is used to enforce sliding mode in a manifold, which is

defined by the error between the real value $\boldsymbol{x}_{el}$ and the desired value $\boldsymbol{x}_{el}^*$ of the electrical state:

$$\boldsymbol{s} = \boldsymbol{x}_{el}^* - \boldsymbol{x}_{el} = \boldsymbol{0}\,. \tag{4.37}$$

If sliding mode is enforced, the error $\boldsymbol{s}$ is set to zero after a finite time and the desired dynamics for the mechanical subsystem is realized.

The resulting control structure is shown in Figure 5.5. In the outer control loop desired continuous dynamics for the mechanical subsystem is calculated, producing desired continuous dynamics $\boldsymbol{s}_{el}^*$ for the state of the inner control loop. This desired dynamics is exerted on the synchronous motor by using a sliding mode control with discontinuous control input $\boldsymbol{u} \in \mathbb{R}^3$ (switched voltages), that is provided by an inverter which itself is controlled by on/off signals $\boldsymbol{g}$ for the switching devices.

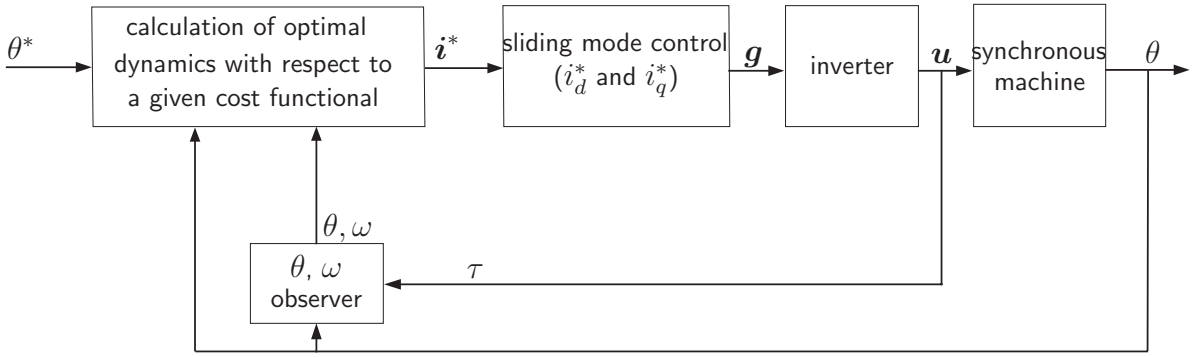

Figure 4.12: Sliding mode position control for a synchronous motor based on the GBCP.

Desired dynamics of the mechanical system is chosen in such a way that the dissipative power loss of the synchronous motor is minimized during operation. In Appendix B the approach how the desired dynamics $\boldsymbol{x}_{mech}^*$ is found is explained in detail. The result is then desired acceleration

$$\begin{aligned}\dot{\omega}^*(t) = Q\omega_0 \left[\sinh(Qt) - \frac{C}{S}\cosh(Qt)\right] + \frac{Q\omega_T}{S}\cosh(Qt) + \ldots \\ \ldots + \frac{Q^2 S(\theta_T - \theta_0) - QD(\omega_0 + \omega_T)}{2D - QTS}\left[\sinh(Qt) - \frac{D}{S}\cosh(Qt)\right]\,,\end{aligned} \tag{4.38}$$

which leads to the desired current component following (4.29)

$$\begin{aligned} i_d^* &= \frac{J}{k}\dot{\omega}^* + \mu\omega\tau_L && (4.39)\\ &= f_{i_d}(\theta_0, \omega_0, \theta_T, \omega_T, T, t) && (4.40)\end{aligned}$$

Finally, the discontinuous control input $\boldsymbol{u}_{dq}^T = (u_d, u_q)$ is chosen to set the error between real and desired dynamics for the stator current components to zero after a finite time.

$$\boldsymbol{u}_{dq} = \begin{pmatrix}\operatorname{sign}(s_1)\\ \operatorname{sign}(s_2)\end{pmatrix} = -U_0 \operatorname{sign}(\boldsymbol{s}) \tag{4.41}$$

where

$$\begin{aligned} s_1 &= i_d^* - i_d = 0 \\ s_2 &= i_q^* - i_q = 0\,. \end{aligned} \tag{4.42}$$

When sliding mode is reached, $\boldsymbol{s} = \binom{s_1}{s_2} = \mathbf{0}$, the system will converge to

$$i_d = i_d^* \tag{4.43}$$

$$i_q = i_q^* \tag{4.44}$$

and the assigned dynamics described by the formulas (B.10) and (B.11) is realized.

Nevertheless, switching takes place in stator coordinates $\{a, b, c\}$, while the motor phase voltages take values from the limited set $\{-u_0, u_0\}$. The switching control law must therefore be in the form of

$$\boldsymbol{u}_{123} = U \operatorname{sign} \boldsymbol{s}_{123} \tag{4.45}$$

where $|U| = u_0$ and $\tilde{\boldsymbol{s}} \in \mathbb{R}^3$ being a transformation of (4.42) in stator coordinates

$$\boldsymbol{s}_{123} = \begin{bmatrix} s_d \cos(p\theta) - s_q \sin(p\theta) \\ s_d \cos\left(p\theta - \frac{2}{3}\pi\right) - s_q \sin\left(p\theta - \frac{2}{3}\pi\right) \\ s_d \cos\left(p\theta - \frac{4}{3}\pi\right) - s_q \sin\left(p\theta - \frac{4}{3}\pi\right) \end{bmatrix} \tag{4.46}$$

with $[s_d\, s_q]^T = \boldsymbol{s}^*$ from (4.42). ■

4.2.3 Experiments

Since the proposed sliding mode controller requires complete state information, an observer is used to reconstruct the missing state variables ω, $\dot{\omega}$ and i_d.

Figures 4.13 and 4.14 show the trajectories of the angular position θ if the proposed control is applied to the test bench which is explained in Appendix A.3. Two different transition times T were set. Figure 4.13 illustrates the optimal trajectory due to a longer transition time better whereas Figure 4.14 demonstrates the performance of the controlled motor. There is no visible difference in the resulting trajectories when the disturbance is considered, as long as the disturbing torque does not surpass the maximal torque the motor can handle.

4.2.4 Discussion

The GBPC can be used to design a sliding mode position controller that provides optimal system dynamics with respect to a given cost functional. During sliding mode the system dynamics follows an optimal trajectory which is calculated based on well known methods of constrained continuous dynamic optimization. The developed control algorithm proved working on a test system. Despite exerting external disturbing torques, the motor reaches a target position on an optimal path, minimizing its dissipative power losses on the way.

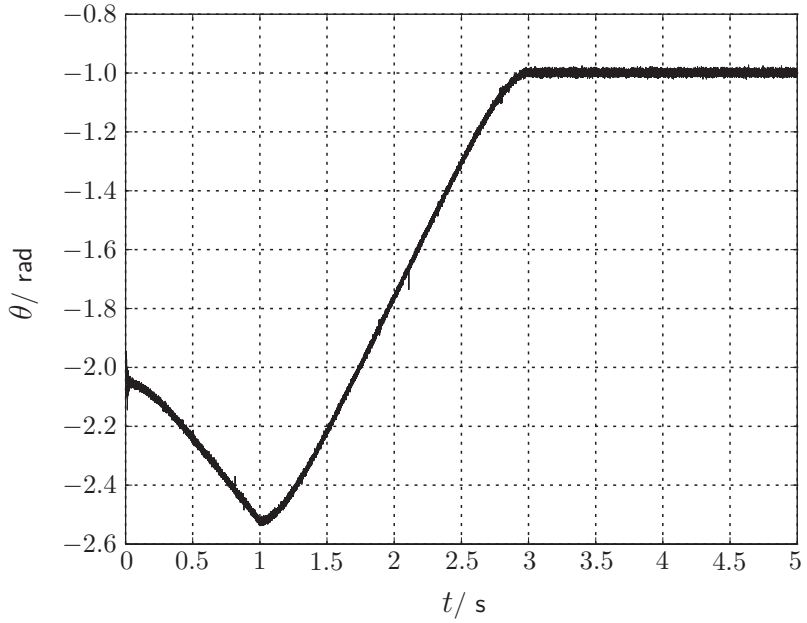

Figure 4.13: Experimental result: Trajectory of the change of the angular position θ when cost functional minimizing sliding mode control for $T = 2\,\mathrm{s}$ is applied. Control starts at time $t = 0\,\mathrm{s}$ for the condition that the target angle is set to $\theta_T = -3\,\mathrm{rad}$. At $t = 1\,\mathrm{s}$ the target angle is changed to $\theta_T = -1\,\mathrm{rad}$.

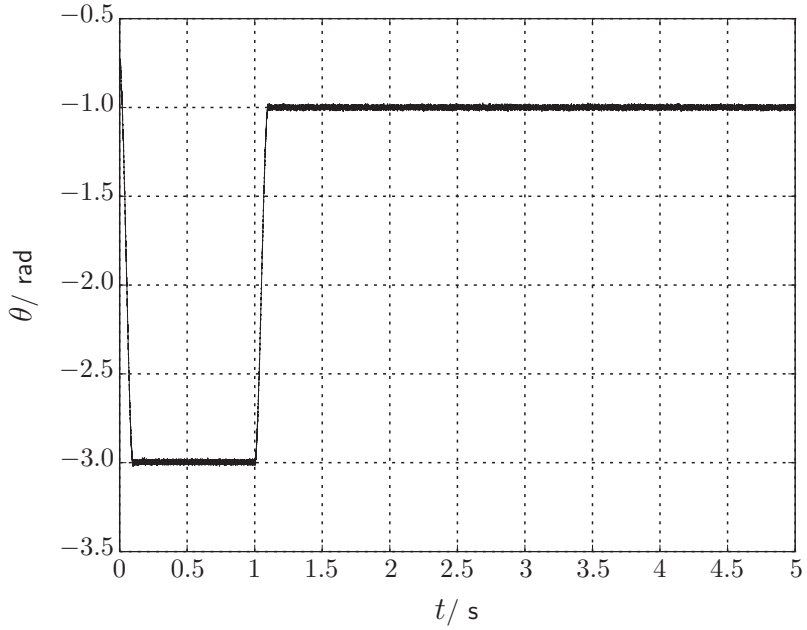

Figure 4.14: Experimental result: Trajectory of the change of the angular position θ when cost functional minimizing sliding mode control for $T = 0.1\,\mathrm{s}$ is applied. Control starts at time $t = 0\,\mathrm{s}$ for the condition that the target angle is set to $\theta_T = -3\,\mathrm{rad}$. At $t = 1\,\mathrm{s}$ the target angle is changed to $\theta_T = -1\,\mathrm{rad}$.

4.3 Conclusion

In this chapter the problem of chattering, which remains the main obstacle for sliding mode control theory to be used in modern control applications, was approached. A sliding mode control concept for mechanical systems that takes actuator dynamics into account was successfully applied to two electromechanical systems. Numerical simulations and experimental results prove, that if the control law incorporates the dynamics of the electrical and mechanical subsystem, chattering effects are reduced while robustness and disturbance rejection, the main benefits of sliding mode control, are retained. The GBCP allows to handle the control unit design process for more complex system models that include the actuator dynamics. The implementation of the control law is simple, since the control signals are discontinuous and digital to analog converters are not required.

Based on th tools of constrained continuous dynamic optimization, the application of the GBCP can be extended. In this chapter a three-step control unit design method was developed to design a sliding mode control strategy, that provides optimal system dynamics with respect to a given cost functional. It allows a systematic control unit design and therefore reduces the time to find an appropriate sliding mode control law.

The proposed control scheme reaches its limit, if the switching frequency is too low with respect to the systems inertia. Then the system gets excited by the switching frequency. For mechanical systems, this can be audible in the best case, but it also may lead to vibration which eventually fatigues the material. But meanwhile, new switching devices providing higher frequencies have been developed. Provided that the necessary computations including both, control law and state estimation, can be handled on-line at a high enough rate or the control law and state estimation can be implemented using analog devices, pure sliding mode control algorithms using switching control laws are a viable and extremely high performance option if controllers for electromechanical systems have to be found.

5 Position Control of an Induction Machine

The advantages of induction machines, compared to other electric drives, are their reliability, low-maintenance and their low cost. They are mechanically robust actuators. Their compactness, small mass moment of inertia and high efficiency are the reasons to employ them for high-precision position control tasks. However, the control of induction machines is far from trivial, because even very simplified models are high-dimensional and non-linear.

Sliding mode control theory simplifies control design and uses applied voltages as real discontinuous control inputs. It meets requirements for high-precision position control, which is applied in different areas of robotics and industrial machinery, like good dynamical response, disturbance rejection and low sensitivity to machine and load parameter variations. Existing applications of sliding mode control to induction machines show an excellent performance, including insensitivity to parameter variations and rejection of disturbances. However, the chattering problem is a major obstacle in implementation.

In this chapter two novel sliding mode position control strategies of induction machines are developed and validated by an experimental setup. The first control unit design is based on the GBCP, which is explained in Section 3 of this thesis. The second control approach is an extension of an existing sliding mode torque control schemes for induction machines. In Section 5.1 an overview of control schemes for the position control of induction machines and existing sliding mode controllers and observer concepts for induction machines is given. Within the same chapter the significance of induction machines in robotics is discussed shortly. Section 5.2 includes how the novel position control units are designed. At the beginning of this section the used models for the induction machine and the inverters are given. Then the respective control designs are explained. Finally the chosen observers are presented and experimental results are given and discussed. Section 5.3 discusses the use of multilevel inverters in order to reduce chattering effects. Two different solutions to realize multilevel controls are developed and tested in numerical simulations. Section 5.4 concludes this chapter.

5.1 State of the Art

Generally, closed loop control schemes for the position control of induction machines can be divided into two classes, field oriented control and direct torque control.

Field oriented control, also known as vector control, has been researched since 1972 [8, 35]. It is a cascaded control model based on rotor, stator or main flux oriented motor models. Due to the chosen motor model, flux as well as torque generating current may be controlled decoupled in an inner control loop. The corresponding reference signals are generated in the outer control loop. Due to the utilization of PWM-units in the inner control loop the field oriented control offers the advantage of constant switching

frequencies. Furthermore, the direct current control enables simple current limiting. While the coordinate transformation of the machine variables in flux oriented signals provides a very simple control, which is comparable to that of dc motors, it requires very complicated on-line computations. This transformation is dependent on precise determination of the flux angle and precise knowledge of the induction machine parameters. Variations of the parameters and improper flux angle data influence the decoupling of flux and torque generating currents and lead to reduced torque and decreased control performance.

Direct torque control [71, 72] or direct self control [15] are intended to control torque and flux of an induction machine by direct selecting the power converter voltage space vectors through a look-up table. Since it is based on stator coordinates oriented motor models, direct torque control avoids coordinate transformations which depend on exact knowledge of the machine parameters and the frequency. Therefore this control scheme is very robust. Moreover, its implementation is very simple, because no current controllers are needed. Direct torque control achieves quick and precise torque control response. But in steady-state operations notable torque pulsation and current ripple appear. These ripples may be reduced by improving the look-up tables and hysteresis controllers or by using PWM-units [33, 34]. Latter method corresponds to the implementation of a stator flux oriented control and leads to reduced dynamics increasing sensitivity against parameters and reduced dynamics. The direct torque control is the establish cause of variable switching frequencies, because the switching devices are directly controlled by hysteresis controllers. To achieve high performance direct torque control requires high sampling frequencies. If the same average switching frequencies are used, the performance of direct torque control is worse than that of field oriented control concerning current and torque ripple.

Sliding Mode Control of Induction Machines

Sliding mode control of induction machines was developed first by [64]. Speed control was successfully applied to an experimental setup for the case when the references were chosen out of the nominal rotation speed range. In [77] besides the non cascaded speed and rotor flux control, an extension of the traditional field oriented control benefiting from the above mentioned advantages of sliding mode control is discussed. Sophisticated semiconductor technologies achieve high commutation frequencies, increasing efficiency and decreasing the cost of modern switching devices. They allow realization of fast control units for sliding mode control, required for implementation. Thus, sliding mode control of induction machines is a current field of research.

To increase robustness in existing field oriented speed control schemes, linear speed and flux controllers were replaced by sliding mode controllers [16, 86, 87, 43, 4]. Nevertheless, the cascaded structure of field oriented control (there is an inner control loop for current, which requires exact knowledge of the magnetic flux) is still used in these concepts.

The implementation of discontinuous control may lead to undesired high frequency oscillations in the closed loop, which result in excessive use and mechanical wear of the actuators. Discontinuous current control results in high current ripples. There are many publications that investigate the problem of reduction of current and torque ripple. They use either the explained cascaded control structure with linear current control or the concept of equivalent control, in order to control PMW–units [65, 53, 61]. In [13] the minimization of chattering effects by modification of switching manifolds was discussed. Among others a

sliding mode speed controller without inner current control loop is developed in [7]. Experimental results are satisfying for the control of moderate speeds, when a sliding mode observer is used to keep track of magnetic flux.

In [31] a different sliding mode position control strategy is discussed. However, their approaches are also based on rotor flux oriented machine models and cascaded control structures, which require precise estimation of flux. Parameter deviations affect dynamic performance and stability significantly.

Observer Concepts

For the control of induction machines, parameter identification algorithms as well as state variables observers are very important. For instance, magnetic flux in induction machines can be measured only after expending high efforts. In squirrel cage induction machines without changing the mechanical construction, it is not measurable at all. But it is required in almost all control algorithms.

Especially for field oriented control many observer concepts for magnetic flux, rotor resistance and load were developed. Here observers, based on parallel models, which calculate speed and magnetic flux based on dynamic motor models measuring applied voltages and stator currents prove to be efficient for speeds above to 1.8 rev/min [56, 55, 66]. If additional syste, and harmonic content in control input and state variables can be provided, new researches may realize high dynamic control loops possessing low speed objectives as well as zero speed control [37].

Actual research focuses on sensorless control of induction machines, which means control of induction machines without sensors for mechanical signals like speed and position. Sensorless control is highly reliable and low-priced. If speed can not be measured, it must be calculated based on the measurements of the stator voltages based on excellent machine models. Therefore, especially for sensorless control, Kalman-filters or Luenberger -observers with variable parameters were investigated and developed. [60, 18, 85]. In low speed range there are only small losses compared to the dynamics of control with mechanical sensors depending on the used parameter identification algorithm. In zero speed control, precision of systems with sensors are not achieved.

Many publications deal with the problem of sliding mode observers for induction machine control. Controllers derived by [41, 49] are based on non-linear adaptive flux observers with rotor resistance estimators. They require transformations of control variables from stator to rotor coordinates requiring high computational efforts. Moreover this approach increases sensitivity against model uncertainties. Therefore [46] suggests a concept, that uses stator-oriented signals for both control and observers. There also exist an observer for the friction forces in the machine [1]. In [17], the other observer concepts can be found, which are based on field oriented control. Precision of discontinuous observers may be increased by using adaptive algorithms [73].

With only some exceptions in publications there are not any stability analysis for observer based control algorithms. Stability analysis for sensorless control in [51] and [50] are valid only for concepts, which are based on current fed electromechanical motor models.

Induction Machines in Robotics

Basic discussions about induction machines as actuators in robotics began in the 1990s. Field oriented control was judged as inefficient, because it is sensitive against parameter variations when low speed should be controlled. Implementation of switching control based on static characteristics led to promising results [12].

For the time being, induction machines are widespread and of great importance in industrial applications. Sensorless drives are employed under operation conditions of low speed forshor duration.

Advantages of induction machines compared to other electric actuators are their low cost. Moreover, they are low-maintenance. Using them in hazardous environments is possible, because there are neither sparkling nor corrosion problems, leading to early wear. They do not have any disturbance torques, as for instance synchronous machines develop due to magnetic hysteresis and inhomogeneous distributed magnetic resistances. Although there are many other advantages of induction machines they are not used very often in robotic applications. In the author's opinion, the reason for this unavailability is only nonexistence of simple implementable control concepts. Sliding mode control of induction machines has a high application potential in robotics to improve the capability of robots significantly

5.2 Control Design

This section begins with the presentation of the model of an induction machine and the drive system applied for control. Based on this fundamental modeling, in Section 5.2.2 two novel position controllers are developed. In Section 5.2.3 experimental results are presented. The flux and angular velocity observers employed, are introduced. Finally, advantages and disadvantages of the developed sliding mode position control algorithms are discussed in Section 5.2.4.

5.2.1 Modeling

Induction machines belong to the category of alternating current drives. The stator consists of three inductors oriented by 120°. Each inductor is fed by an alternating input current generating a rotating magnetic field inside the motor. This field induces current in the rotor, inducing itself an opposite magnetic field. A torque is then generated accordin to the Lenz law.

Motor Model

For the control unit design a motor model in the stator fixed coordinate system with indices (α, β), where stator current components and rotor flux components are the state variables is used. The dynamical equations are

$$\begin{aligned} \dot{\lambda}_{\alpha r} &= -\eta\lambda_{\alpha r} - \omega_e\lambda_{\beta r} + \eta L_h i_{\alpha s} \\ \dot{\lambda}_{\beta r} &= -\eta\lambda_{\beta r} + \omega_e\lambda_{\alpha r} + \eta L_h i_{\beta s} \end{aligned} \tag{5.1}$$

$$\begin{aligned}\dot{i}_\alpha &= \beta\eta\lambda_{\alpha r} + \beta\omega_e\lambda_{\beta r} - \gamma i_\alpha + \frac{1}{\sigma L_s}u_\alpha \\ \dot{i}_\beta &= \beta\eta\lambda_{\beta r} - \beta\omega_e\lambda_{\alpha r} - \gamma i_\beta + \frac{1}{\sigma L_s}u_\beta\end{aligned} \tag{5.2}$$

with

$$\eta = \frac{R_r}{L_r} \qquad \sigma = 1 - \frac{{L_h}^2}{L_s L_r} \qquad \beta = \frac{L_h}{\sigma L_s L_r} \qquad \gamma = \frac{1}{\sigma L_s}(R_s + \frac{{L_h}^2}{{L_r}^2}R_r)\,. \tag{5.3}$$

Within that equation set $\lambda_{\alpha r}$ and $\lambda_{\beta r}$ are rotor flux components in (α, β) coordinates, i_α and i_β are stator currents in (α, β) coordinates, and u_α and u_β are stator voltages in (α, β) coordinates. Parameters L_r, L_s and L_h represent rotor, stator and mutual inductance. Parameters R_r and R_s represent rotor and stator resistance, and ω represents the rotor angular velocity. The number of pole pairs N_r influences the motor torque τ

$$\tau = \frac{3}{2}N_r\frac{L_h}{L_r}(i_\beta\lambda_{\alpha r} - i_\alpha\lambda_{\beta r})\,, \tag{5.4}$$

and the electrical rotor angular velocity is defined by

$$\omega_e = N_r\omega\,. \tag{5.5}$$

Choosing the load torque τ_l and the mass moment of inertia J, the electrical state space description is completed by equations for mechanical motion

$$\begin{aligned}\dot{\omega} &= \frac{1}{J}(\tau - \tau_L) \\ \dot{\theta} &= \omega\end{aligned} \tag{5.6}$$

where θ represents the rotor angle.

The model is based on the assumption of balanced phase and unsaturated operation, short-circuited rotor windings, and symmetrical construction. Further assumptions are that iron losses are zero and all parameters like inductances and resistances are constant. Those assumptions may lead to errors in a real system as the inductors change depending on the rotor position and the resistances depending on motor temperature.

Inverter Model

The three-phase two-level inverter shown in Figure 5.1 is the commonly used circuit for vector control of the induction motor. With this circuit, a DC voltage can be transformed into three AC voltages feeding the three stator inductors of the motor. Using star connection the output voltage of this converter is either $\frac{\sqrt{3}}{2}U_0$ or $-\frac{\sqrt{3}}{2}U_0$ for each phase, where U_0 is the maximum value of the supplied voltage.

Three-phase multilevel inverters as described in [67] and the circuit shown in Figure 5.2 is an extension for chattering reduction. Using star connection, the output voltage of this converter is either $\frac{\sqrt{3}}{2}U_0$, $-\frac{\sqrt{3}}{2}U_0$ or 0 V for each phase.

The output voltage of the inverters is controlled by the switch command vector $\boldsymbol{g}$. As the inverters have three phases, this vector has three elements:

$$\boldsymbol{g} = \begin{pmatrix} g_1 \\ g_2 \\ g_3\,. \end{pmatrix} \tag{5.7}$$

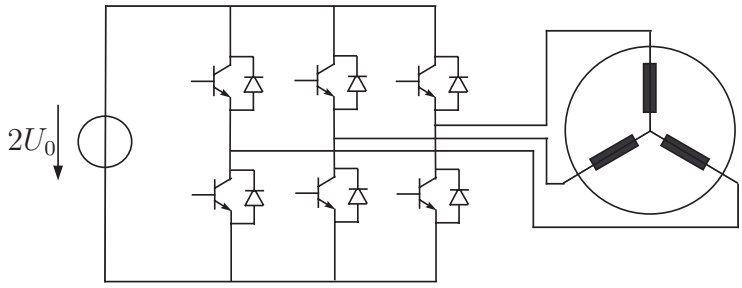

Figure 5.1: Two-level inverter.

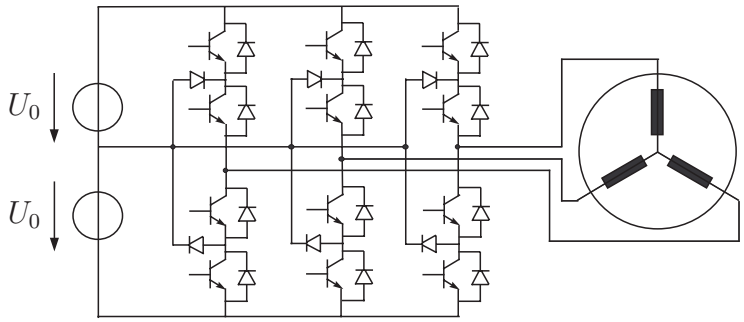

Figure 5.2: Three-level neutral point clamped inverter.

The switch command vector vector $\boldsymbol{g}$ takes discrete values between -1 and 1. Therefore the output voltage for each phase i is $g_i\, U_0$. For a two-level inverter, the three elements of $\boldsymbol{g}$ take values from the discrete set $\{-1, 1\}$. For a three-level inverter, the three elements of $\boldsymbol{g}$ take values from the discrete set $\{-1, 0, 1\}$.

The control input for the motor model is defined as the stator voltage vector $\boldsymbol{u} = \binom{u_\alpha}{u_\beta}$. This is a fictive voltage vector and for its calculation from the switch command vector $\boldsymbol{g}$, the inverter model is necessary.

The relationship between the switch command vector $\boldsymbol{g}$ and the three stator phase voltages $\boldsymbol{u}_{abc}$ is given by:

$$\boldsymbol{u}_{abc} = \begin{pmatrix} u_a \\ u_b \\ u_c \end{pmatrix} = \frac{U_0}{3}\mathbf{G}\boldsymbol{g} \quad \mathbf{G} = \begin{pmatrix} 2 & -1 & -1 \\ -1 & 2 & -1 \\ -1 & -1 & 2 \end{pmatrix} . \tag{5.8}$$

The relationship between the stator voltage vector $\boldsymbol{u}_{\alpha\,\beta}$ and the three phase voltages $\boldsymbol{u}_{abc}$ is given by:

$$\begin{pmatrix} u_\alpha \\ u_\beta \end{pmatrix} = \mathbf{A}^{a,b,c}_{\alpha,\beta}\boldsymbol{u}_{a,b,c} \quad \mathbf{A}^{a,b,c}_{\alpha,\beta} = \frac{2}{3}\begin{pmatrix} 1 & -\frac{1}{2} & -\frac{1}{2} \\ 0 & \frac{\sqrt{3}}{2} & -\frac{\sqrt{3}}{2} \end{pmatrix} . \tag{5.9}$$

When (5.8) is written in (5.9), the relation between the switch command vector $\boldsymbol{g}$ and the stator voltage vector $\boldsymbol{u}_{\alpha\,\beta}$ is given by

$$\boldsymbol{u}_{\alpha\,\beta} = \begin{pmatrix} u_\alpha \\ u_\beta \end{pmatrix} = \mathbf{A}^{a,b,c}_{\alpha,\beta}\,\frac{U_0}{3}\mathbf{G}\,\boldsymbol{g} = \frac{U_0}{3}\begin{pmatrix} 2 & -1 & -1 \\ 0 & \sqrt{3} & -\sqrt{3} \end{pmatrix}\begin{pmatrix} g_1 \\ g_2 \\ g_3 \end{pmatrix} . \tag{5.10}$$

With this forward model, and the knowledge that the elements of the switch command vector takes values from a discrete set, all possible stator voltages can be calculated.

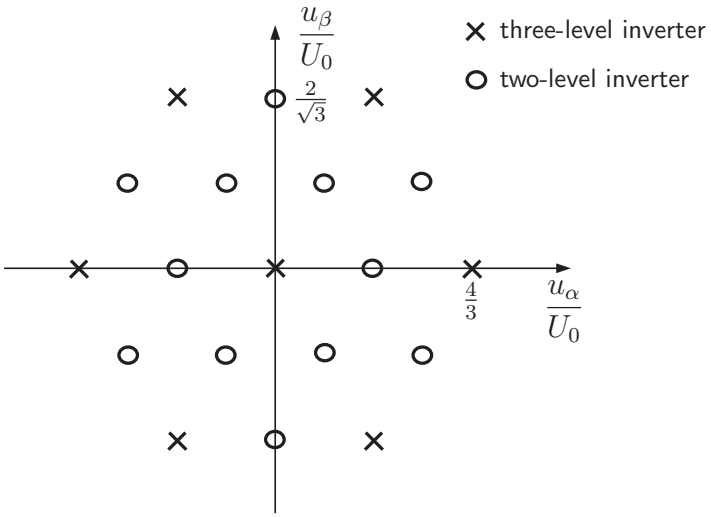

Figure 5.3: Stator voltages for the two-level (x) and three-level (o) inverter.

For a two-level inverter, the elements of $\boldsymbol{g}$ take values from $\{-1, 1\}$, therefore eight switch combinations are possible. As there is one redundancy, there are seven possible stator voltages, marked by an 'x' in Figure 5.3. The redundancy appears when all three switches are at the same position, either $\boldsymbol{g}^T = (1, 1, 1)$ or $\boldsymbol{g}^T = (-1, -1, -1)$, leading to the stator voltage vector $\boldsymbol{u}_{\alpha\,\beta} = \binom{0}{0}$.

For a three-level inverter, the elements of $\boldsymbol{g}$ take values from $\{-1, 0, 1\}$, therefore twenty seven switch combinations are possible. Eight of those twenty seven switch combinations are redundancies, therefore ninteen stator voltages are possible, marked by 'x' and 'o' in Figure 5.3. The same stator voltage vectors are possible for the three-level inverter as were for the two-level inverter.

5.2.2 Control Unit Design

In this section two novel sliding mode position control algorithms of the induction machine are developed. The first approach is based on the GBCP as explained in detail in Section 3. It takes advantage of the special structure of the electromechanical system. Based on a decomposition of the system into mechanical, magnetical and electrical subsystems, the control unit design can be simplified. The discontinuous control input of the overall system is directly used, which is the phase voltages in this case.

The second control approach is based on the existing sliding mode speed control algorithm of induction machines. This control method is extended. Using the chattering reduction methods, which were shown in Section 2.2, a robust position control is derived, that offers acceptable chattering and high control accuracy. Because voltages are used directly as control input, no complicated hardware is required.

Sliding Mode Position Control Algorithm based on the Generalized Block Control Principle

As illustrated in Figure 5.4, the induction machine system consists of three subsystems, which are the magnetical (5.1), the electrical (5.2), and the mechanical (5.6) subsystems. Dynamics of the state of the mechanical subsystem

$$\boldsymbol{x}_{mech} = \begin{pmatrix} \theta \\ \omega \end{pmatrix} \tag{5.11}$$

depends on the states of the magnetical and electrical subsystems

$$\boldsymbol{x}_{mag} = \boldsymbol{\lambda}_r = \begin{pmatrix} \lambda_{\alpha r} \\ \lambda_{\beta_r} \end{pmatrix} \quad \text{and} \quad \boldsymbol{x}_{el} = \boldsymbol{i}_s = \begin{pmatrix} i_{\alpha s} \\ i_{\beta s} \end{pmatrix}, \tag{5.12}$$

dynamics of the state of the mechanical and magnetical subsystems does not depend on the control input

$$\boldsymbol{u} = \begin{pmatrix} u_\alpha \\ u_\beta \end{pmatrix}, \tag{5.13}$$

but is dependent on the dynamics of the state of the electrical subsystem.

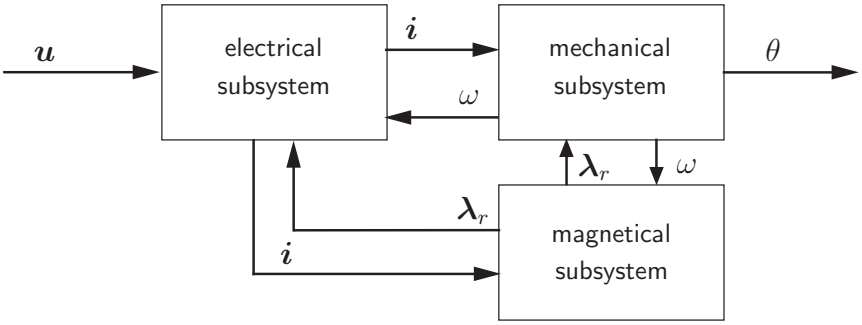

Figure 5.4: Decomposition into subsystems (induction machine with load).

Based on this decomposition into subsystems, following the GBCP, the control algorithm can be designed as follows: In the first step desired dynamics for the magnetical and mechanical subsystem are determined. The state of the electrical subsystem is handled as virtual control input for theses subsystems in order to assign theses desired dynamics. In the second step the dynamics of the error between the desired and real values of the electrical state is assigned to be asymptotically stable. Therefore, the discontinuous control input $\boldsymbol{u}$ is used to enforce sliding mode in a manifold, which is defined by the error between the real value $\boldsymbol{x}_{el}$ and the desired value $\boldsymbol{x}_{el}^*$ of the electrical state:

$$\boldsymbol{s} = \boldsymbol{x}_{el}^* - \boldsymbol{x}_{el} = \boldsymbol{0}\,. \tag{5.14}$$

If sliding mode is enforced, the error $\boldsymbol{s}$ takes the value zero in finite time and the desired dynamics for the mechanical subsystem is realized.

The resulting control unit design is shown in Figure 5.5. In the outer control loop desired continuous dynamics for the magnetical and mechanical subsystem is controlled, producing desired continuous dynamics for the state of the inner control loop. These desired dynamics is routed to the induction machine by using a sliding mode control with discontinuous control input $\boldsymbol{u} \in \mathbb{R}^3$ (switched voltages), which is provided by an inverter which itself is controlled by the on/ off signals $\boldsymbol{g}$ of the switching devices.

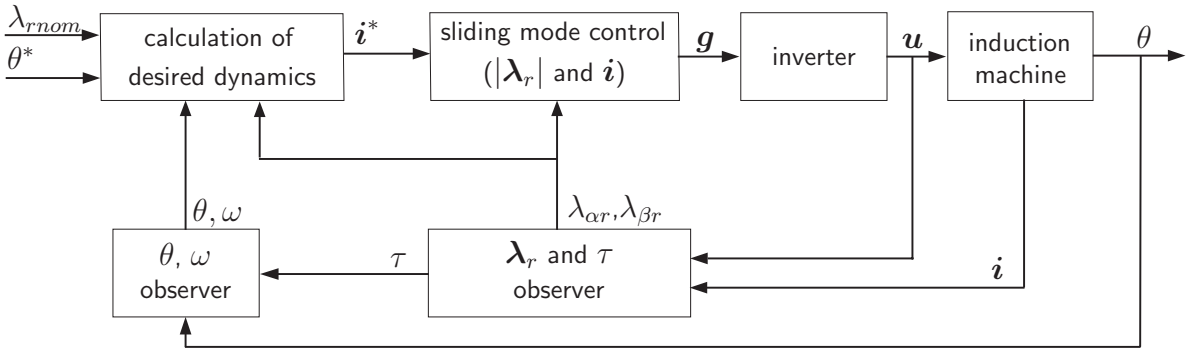

Figure 5.5: Sliding mode position control for an induction machine based on the GBCP.

Based on the induction machine equation (5.1), with λ_{rnom} as nominal value for the modulus of the rotor flux, desired dynamics for the magnetical subsystem

$$\|\dot{\boldsymbol{\lambda}}_r\| = \lambda_{rnom} - c_3\|\boldsymbol{\lambda}_r\| \quad c_3 \in \mathbb{R}^+ . \tag{5.15}$$

is given, if

$$\lambda_{rnom} - c_3\|\boldsymbol{\lambda}_r\| \stackrel{!}{=} \sqrt{\dot{\lambda}_{\alpha r}^2 + \dot{\lambda}_{\beta r}^2} \tag{5.16}$$

$$= \sqrt{(-\eta\lambda_{\alpha r} - \omega_e\lambda_{\beta r} + \eta L_h i_{\alpha s})^2 + (-\eta\lambda_{\beta r} + \omega_e\lambda_{\alpha r} + \eta L_h i_{\beta s})^2} . \tag{5.17}$$

This condition leads to a current component i_α, which depends on not only the machine parameters but also the rotor flux components and as well as the stator current component i_β

$$i_\alpha^* = f_{i_\alpha}(\lambda_{\alpha r}\,, \lambda_{\beta r}\,, i_\beta) . \tag{5.18}$$

Based on the induction machine equation (5.4), desired dynamics for the mechanical subsystem

$$\dot{\omega}^* = -c_1\theta^* - c_2\omega^* \quad c_1\,, c_2 \in \mathbb{R}^+ \tag{5.19}$$

is given, if

$$-c_1\theta - c_2\omega \stackrel{!}{=} \frac{1}{J}(\tau - \tau_L) \tag{5.20}$$

$$\leftrightarrow \quad -J(c_1\theta + c_2\omega) + \tau_L = \frac{3}{2}N_r\frac{L_h}{L_r}(i_\beta\lambda_{\alpha r} - i_\alpha\lambda_{\alpha r}) \tag{5.21}$$

which leads to a current component i_β, which depends on not only the machine parameters but also the rotor flux components and as well as the stator current component i_α

$$\begin{aligned} \leftrightarrow i_\beta^* &= \frac{-J(c_1\theta + c_2\omega) + \tau_L + \frac{3}{2}N_r\frac{L_h}{L_r}\lambda_{\beta r} i_\alpha}{\frac{3}{2}N_r\frac{L_h}{L_r}\lambda_{\alpha r}} \\ &= f_{i_\beta}(\lambda_{\alpha r}\,, \lambda_{\beta r}\,, \theta\,, \omega)\,. \end{aligned} \tag{5.22}$$

Regarding (5.18) and (5.22) the stator current components, which produce desired dynamics for the magnetical and mechanical subsystem, can be calculated as functions of the actual angular position θ, rotor speed ω and rotor flux:

$$i_\alpha^* = f'_{i_\alpha}(\lambda_{\alpha r}\,, \lambda_{\beta r}\,, \theta\,, \omega) \tag{5.23}$$

$$i_\beta^* = f'_{i_\beta}(\lambda_{\alpha r}\,, \lambda_{\beta r}\,, \theta\,, \omega) \tag{5.24}$$

Finally, the discontinuous control input $\boldsymbol{u}^T = (u_\alpha, u_\beta)$ is chosen to set the error between real and desired dynamics of the stator current components to zero after a finite time.

$$\boldsymbol{u}_{\alpha\beta} = \begin{pmatrix} \operatorname{sign}(s_1) \\ \operatorname{sign}(s_2) \end{pmatrix} = -U_0 \operatorname{sign}(\boldsymbol{s}) \tag{5.25}$$

with

$$s_1 = i_\alpha^* - i_\alpha = 0 \tag{5.26}$$

$$s_2 = i_\beta^* - i_\beta = 0\,. \tag{5.27}$$

When sliding mode is reached, yielding $\boldsymbol{s} = \binom{s_1}{s_2} = \boldsymbol{0}$, the stator current components will converge to

$$i_\alpha = i_\alpha^* \tag{5.28}$$

$$i_\beta = i_\beta^* \tag{5.29}$$

and the assigned dynamics (5.15) and (5.19) are realized.

Theorem 5.1 The control equation (5.25) enforces sliding mode after a finite time.

Proof: The continuously differentiable Lyapunov function

$$V = \frac{1}{2}\boldsymbol{s}^T\boldsymbol{s}\,, \qquad \boldsymbol{s} = \begin{pmatrix} s_1 \\ s_2 \end{pmatrix} \tag{5.30}$$

with

$$V \geq 0 \tag{5.31}$$

$$V = 0 \quad \text{for } \boldsymbol{s} = \boldsymbol{0} \tag{5.32}$$

$$\lim_{\boldsymbol{s}\to\infty} V = \infty \tag{5.33}$$

is chosen. When the derivative of V is taken with respect to time

$$\dot{V} = \boldsymbol{s}^T\dot{\boldsymbol{s}} \tag{5.34}$$

$$= \boldsymbol{s}^T(\boldsymbol{e} + \mathbf{C}\boldsymbol{u}) \; < 0\,, \tag{5.35}$$

where vector $\boldsymbol{e}$ depends on the state variables $\boldsymbol{\lambda}_r$ and $\boldsymbol{i}_s$, and on the machine parameters, due to the the sliding manifolds (5.51) and (5.52) and machine equations (5.1)-(5.6). Besides machine parameters, matrix $\mathbf{C}$ depends on rotor flux componenets $\lambda_{\alpha r}$ and $\lambda_{\alpha r}$ only. Let

$$(\tilde{\boldsymbol{s}})^T := \boldsymbol{s}^T \mathbf{C}\ \mathbf{A}_{\alpha,\beta}^{a,b,c}\ \mathbf{G} \tag{5.36}$$

$$\leftrightarrow \qquad \tilde{\boldsymbol{s}} = (\mathbf{C}\ \mathbf{A}_{\alpha,\beta}^{a,b,c}\ \mathbf{G})^T \boldsymbol{s} \tag{5.37}$$

with vector $\tilde{\boldsymbol{s}} \in \mathbb{R}^3$ and $\boldsymbol{s} \in \mathbb{R}^2$. Since the matrix $(\mathbf{C}\ \mathbf{A}_{\alpha,\beta}^{a,b,c}\ \mathbf{G})^T \in \mathbb{R}^{3\times 2}$ is not invertablke, to express $\boldsymbol{s}$ in terms of $\tilde{\boldsymbol{s}}$, the pseudoinverse $\left((\mathbf{C}\ \mathbf{A}_{\alpha,\beta}^{a,b,c}\ \mathbf{G})^T\right)^+$ has to be used

$$\boldsymbol{s} = \left((\mathbf{C}\ \mathbf{A}_{\alpha,\beta}^{a,b,c}\ \mathbf{G})^T\right)^+ \tilde{\boldsymbol{s}} \tag{5.38}$$

$$\leftrightarrow \qquad \boldsymbol{s}^T = (\tilde{\boldsymbol{s}})^T (\mathbf{C}\ \mathbf{A}_{\alpha,\beta}^{a,b,c}\ \mathbf{G})^+ . \tag{5.39}$$

Based on (5.10) equation (5.35) can be rewritten as

$$\dot{V} = \boldsymbol{s}^T \boldsymbol{e} + \boldsymbol{s}^T \mathbf{C}\ \mathbf{A}_{\alpha,\beta}^{a,b,c}\ \frac{U_0}{3} \mathbf{G}\ \boldsymbol{g} \tag{5.40}$$

$$= (\tilde{\boldsymbol{s}})^T (\mathbf{C}\ \mathbf{A}_{\alpha,\beta}^{a,b,c} \mathbf{G})^+\ \boldsymbol{e} + (\tilde{\boldsymbol{s}})^T\ \frac{U_0}{3} \boldsymbol{g} . \tag{5.41}$$

If the switching commands are implemented as

$$\boldsymbol{g} = -\begin{pmatrix} \operatorname{sign}(\tilde{s}_1) \\ \operatorname{sign}(\tilde{s}_2) \\ \operatorname{sign}(\tilde{s}_3) \end{pmatrix} \qquad \tilde{\boldsymbol{s}} = \begin{pmatrix} \tilde{s}_1 \\ \tilde{s}_2 \\ \tilde{s}_3 \end{pmatrix} \tag{5.42}$$

equation (5.41) yields

$$\dot{V} = (\tilde{\boldsymbol{s}})^T (\mathbf{C}\ \mathbf{A}_{\alpha,\beta}^{a,b,c}\ \mathbf{G})^+\ \boldsymbol{e} - (\tilde{\boldsymbol{s}})^T\ \frac{U_0}{3} \operatorname{sign}(\tilde{\boldsymbol{s}}) \tag{5.43}$$

$$\leq \left|(\tilde{\boldsymbol{s}})^T\right|\ \left|(\mathbf{C}\ \mathbf{A}_{\alpha,\beta}^{a,b,c}\ \mathbf{G})^+)\right|\ |\boldsymbol{e}| - \frac{U_0}{3}\ |\tilde{\boldsymbol{s}}| \tag{5.44}$$

If the supply voltage is high enough: $U_0 \geq \left|(\mathbf{C}\ \mathbf{A}_{\alpha,\beta}^{a,b,c} \mathbf{G})^+)\right|\ |\boldsymbol{e}|$, holds $\dot{V} < 0$ so that sliding mode can occur. This proves, that if the inverter model is considered and the control input is $\boldsymbol{g}$, the control law takes the form

$$\boldsymbol{g} = -\operatorname{sign}(\mathbf{C}\ \mathbf{A}_{a,b,c}^{\alpha\beta}\ \mathbf{G}\boldsymbol{s}) , \tag{5.45}$$

which leads to $\boldsymbol{s} = \mathbf{0}$ after a finite time.

■

Remark 5.1 From the physical configuration of the inverter circuit it can be deduced, that the sum of the phase voltages has to be always equal to zero:

$$\int_0^t (u_a + u_b + u_c) \mathrm{d}t = 0 \tag{5.46}$$

This condition holds, if sliding mode is implemented directly in terms of switching commands $\boldsymbol{g}$. As it can be concluded from (5.8): There exist eight combinations for the on/off states of the three switches g_1, g_2 and g_3. For cases $g_1 = g_2 = g_3 = 1$ or $g_1 = g_2 = g_3 = -1$, $\boldsymbol{u} = \boldsymbol{0}$. For the other six combinations the value of one phase voltage is $\pm\frac{2}{3}U_0$ while the magnitude of the other two phase voltages is $\mp\frac{1}{3}U_0$. Obviously, all eight possible combinations satisfy the balance condition (5.46). Three phase voltages may be implemented only, if they satisfy the balance condition (5.46). ■

Sliding Mode Position Control Algorithm Based on Fast Torque and Flux Control

In this section a position control for induction machines is developed, based on theexisting sliding mode speed controller introduced in the works [64] and [79] . The new concept is illustrated in Figure 5.6. The induction machine is controlled by the discontinuous control input $\boldsymbol{u} \in \mathbb{R}^3$, which is provided by an inverter which itself is controlled by on/ off signals $\boldsymbol{g}$ of the switching devices. The control of the mechanical system is realized by the torque or force signals as the control action. It is assumed that there exists a fast inner control loop providing the desired torque.

In the outer control loop a super twisting algorithm is used to produce the continuous reference signals for the inner loop. In the inner control loop the torque $\boldsymbol{\tau}$ and the rotor flux $\boldsymbol{\lambda}_r$ are controlled using sliding mode control. To simplify control, the rotor flux is set to a constant nominal value λ_{rnom}.

Remark 5.2 Since the virtual control input for the mechanical system $\boldsymbol{v} = \begin{pmatrix} \boldsymbol{x}_{el} \\ \boldsymbol{x}_{mag} \end{pmatrix} \in \mathbb{R}^4$ is of higher order than the mechanical system $\boldsymbol{x}_{mech} \in \mathbb{R}^2$, two degrees of freedom exist in the system. They are used to reduce the order of the magnetical subsystem to its modulus

$$\boldsymbol{x}^*_{mag} = \|\boldsymbol{\lambda}_r\| = \sqrt{\lambda^2_{\alpha r} + \lambda^2_{\beta r}}\,. \tag{5.47}$$

■

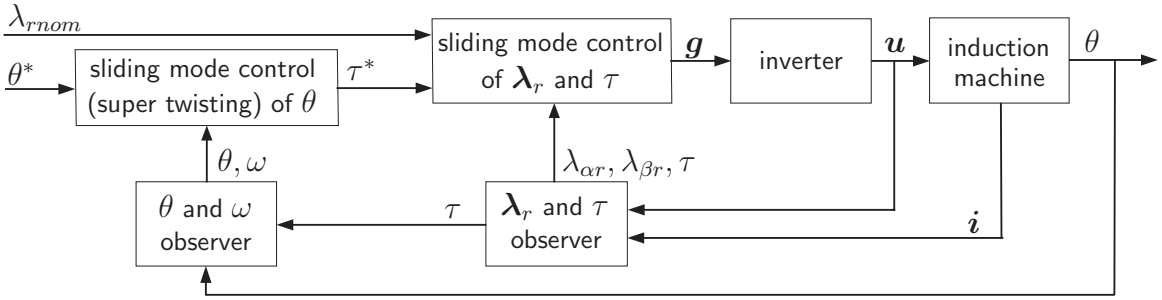

Figure 5.6: Control scheme: sliding mode position control of an induction machine based on fast torque and flux control.

The torque reference signal in the outer control loop can not be obtained by implenenting sliding mode control first, because if sliding mode were enforced in the manifold

$$s_3 = c_1(\theta^* - \theta) + c_2(\omega^* - \omega) = 0 \qquad c_1\,, c_2 \in \mathbb{R}^+\,. \tag{5.48}$$

where c_1 and c_2 are the control parameters, it would produce discontinuous referenced dynamics for the torque

$$\tau^* = \begin{cases} +\bar{\tau} & \text{for} \quad s_3 > 0 \\ -\bar{\tau} & \text{for} \quad s_3 < 0\,. \end{cases} \tag{5.49}$$

These can not be realized using sliding mode control in the inner control loop. As a solution the super twisting algorithm is applied to obtain the reference torque signal for the inner control loop:

$$\tau^* = -(c_{1_{STA}} \int \operatorname{sign}(s_3)\mathrm{d}t + c_{2_{STA}} \begin{cases} |s_3|^{\rho_{STA}} \operatorname{sign}(s_3) & \text{if}\,|s| \le \varepsilon_{STA} \\ |\varepsilon_{STA}|^{\rho_{STA}} \operatorname{sign}(s_3) & \text{if}\,|s| > \varepsilon_{STA} \end{cases}\,, \tag{5.50}$$

where $c_{1_{STA}}, c_{2_{STA}}, \varepsilon_{STA} > 0$ and $0 < \rho_{STA} \le 1$. This algorithm generates a smooth and continuous torque reference, so that the chattering phenomen is avoided and robustness is maintained.

The inner control loop for flux and torque is similar to that shown in [79]. The sliding manifolds are defined so that the torque τ is controlled to the desired value τ^* and the rotor flux is regulated to the nominal rotor flux λ_{rnom}, in order to avoid weak field operation. That yields

$$s_1 = \tau^* - \tau = 0 \tag{5.51}$$

$$s_2 = c_1(\lambda_{rnom} - |\boldsymbol{\lambda}_r|) + c_2(\dot{\lambda}_{rnom} - \left|\dot{\boldsymbol{\lambda}}_r\right|) = 0 \qquad c_1\,, c_2 \in \mathbb{R} \tag{5.52}$$

where c_1 and c_2 are representing positive control parameters. The discontinuous control input to enforce sliding mode are the phase voltages

$$\boldsymbol{u}_{\alpha\beta} = \begin{pmatrix} u_\alpha \\ u_\beta \end{pmatrix} = -U_0 \operatorname{sign}(\boldsymbol{s})\,, \tag{5.53}$$

more detailed

$$u_\alpha = \begin{cases} -U_0 & \text{for} \quad s_1 > 0 \\ +U_0 & \text{for} \quad s_1 < 0 \end{cases} \tag{5.54}$$

$$u_\beta = \begin{cases} -U_0 & \text{for} \quad s_2 > 0 \\ +U_0 & \text{for} \quad s_2 < 0\,. \end{cases} \tag{5.55}$$

When sliding mode is reached, $\boldsymbol{s} = \begin{pmatrix} s_1 \\ s_2 \end{pmatrix} = \mathbf{0}$, the system will converge to

$$|\boldsymbol{\lambda}_r| = \sqrt{{\lambda^2}_{\alpha r} + {\lambda^2}_{\beta r}} = \lambda_{rnom} \quad \text{and} \tag{5.56}$$

$$\tau = \tau^*\,. \tag{5.57}$$

As shown in [79] using a high enough peak voltage U_0 sliding mode can be reached in the inner control loop after a finite time. This proof takes into account, that in the experimental setup not the phase voltages u_α and u_β but the switching commands $\boldsymbol{g}$ are the control input. The inverter model, which enables the transformation from stator voltages to real control inputs, which are on/off-signals to the inverter switches, is considered in the stability proof as well.

Remark 5.3 The transformation matrix $(D\, A^{\alpha,\beta}_{a,b,c} G)^T$, which transform manifolds $\boldsymbol{s}$ to $\tilde{\boldsymbol{s}}$ performs a calculation of a desired stator flux change in rotor flux coordinates (d, q) followed by a transformation from rotor flux coordinates (d, q) to stator coordinates (α, β). Therefore the principle of this controller is similar to th eprinciple of the decoupling vector control algorithms. Vector $\tilde{\boldsymbol{s}}$ is in stator coordinates, which makes sense as the control input of the induction motor is also in stator coordinates. ■

5.2.3 Experiments

In this section the control algorithms, which were derived in the last section, are validated. Since not all of the state variables are measurable, first the observers used are introduced. Then, exerimental results of the control algorithm that is based on the GBCP as well as the results of the sliding mode position control algorithm based on fast flux and torque control are interpreted.

Flux Observer

Both proposed control approaches require knowledge of rotor flux, which is not measurable in off-the-shelf industry motors, since induction machines equipped with special sensors loose either one or both of the advantages of being cheap and reliable. That's why the proposed control concept includes a flux observer.

The observer used in the experimental setup is based on the work [79]. The original motion equations (5.1) are directly used as observer equations:

$$\frac{\mathrm{d}\hat{\lambda}_{\alpha r}}{\mathrm{d}t} = -\eta\hat{\lambda}_{\alpha r} - \omega_e\hat{\lambda}_{\beta r} + \eta L_h i_\alpha \tag{5.58}$$

$$\frac{\mathrm{d}\hat{\lambda}_{\beta r}}{\mathrm{d}t} = -\eta\hat{\lambda}_{\beta r} + \omega_e\hat{\lambda}_{\alpha r} + \eta L_h i_\beta \tag{5.59}$$

where $\hat{\lambda}_{\alpha r}$ and $\hat{\lambda}_{\beta r}$ are the estimates of the rotor flux components. If the estimation errors are defined as $\overline{\lambda}_{\alpha r} = \hat{\lambda}_{\alpha r} - \lambda_{\alpha r}$ and $\overline{\lambda}_{\beta r} = \hat{\lambda}_{\beta r} - \lambda_{\beta r}$ the error dynamics is

$$\frac{\mathrm{d}\overline{\lambda}_{\alpha r}}{\mathrm{d}t} = -\frac{R_r}{L_r}\overline{\lambda}_{\alpha r} - \omega_e\overline{\lambda}_{\beta r} \tag{5.60}$$

$$\frac{\mathrm{d}\overline{\lambda}_{\beta r}}{\mathrm{d}t} = -\frac{R_r}{L_r}\overline{\lambda}_{\beta r} + \omega_e\overline{\lambda}_{\alpha r}\,. \tag{5.61}$$

The stability of the observer can be proven with the help of the Lyapunov function

$$V = \frac{1}{2}(\overline{\lambda}^2_{\alpha r} + \overline{\lambda}^2_{\beta r}) > 0\,. \tag{5.62}$$

When it's derivate is taken with respect to time,

$$\dot{V} = -\eta(\overline{\lambda}_{\alpha r}^2 + \overline{\lambda}_{\beta r}^2) = -2\eta V < 0\,. \tag{5.63}$$

The rate of convergence depends on the rotor time constant $\frac{1}{\eta}$.

Speed Observer

Control performance may be effected strongly, if the velocity signal is not measured directly and instead a differentiated position signal. Especially if operation mode is slow discontinuous changes of the position signal cause high peaks in the velocity signal, which finally cause chattering. In order to solve this problem, the velocity signal is not calculated by differentiation of the position signal but reconstructed by a linear observer. The quality of an estimated signal may even be better than the one from a measured signal, as the measurement noise is avoided (e.g. tachometer signal for very low speeds). For the following observer design it is assumed, that the flux observer is sufficiently fast.

Based on the motion equations (5.6), dynamics of the observed state variables is described by the differential equations

$$\dot{\hat{\theta}} = \hat{\omega} + k_1(\hat{\theta} - \theta) \tag{5.64}$$

$$\dot{\hat{\omega}} = \frac{1}{J}(\tau - \tau_L) + k_2(\hat{\theta} - \theta) \quad k_1\,, k_2 \in \mathbb{R}^+ \tag{5.65}$$

where $\hat{\theta}$ and $\hat{\omega}$ are estimates of the angular position and velocity. If the estimation errors are defined as $\overline{\theta} = \hat{\theta} - \theta$ and $\overline{\omega} = \hat{\omega} - \omega$, error dynamics is expressed by the following equations

$$\dot{\overline{\theta}} = \overline{\omega} + k_1\overline{\theta} \tag{5.66}$$

$$\dot{\overline{\omega}} = k_2\overline{\theta}\,. \tag{5.67}$$

The stability of this linear observer can be garanteed by eigenvalue placement by choosing appropriate parameters k_1 and k_2. The rate of convergence can be determined by eigenvalue placement as well. The observer requires the torque signal as well as the measured position signal. The position signal garantees zero steady state error, the torque signal increases dynamics of the observer.

Results

The advantages and disadvantages of the presented control methods are evaluated and compared in experiments. As load an inverted pendulum is charged to the system. The control objective is to change the angular position of the pendulum from 0^o to 50^o at time $t = 0\,\mathrm{s}$ and than after $2.5\,\mathrm{s}$ back to 0^o.

In Figure 5.7 step responses of the angular position θ for the control algorithm that is based on the GBCP are shown. Three different desired dynamics are assigned by choosing the parameters in (5.19). The chattering effect is low, the stationary accuracy deviating relatively from the target position by a maximum angle of $\pm 0.5\,^{\circ}$. In order to achieve the given accuracy, the position control algorithm based on the GBCP requires a tuning of the model parameters to get the average of the steady state error zero. The accuracy decreases if the machine parameters and the load are not known exactly.

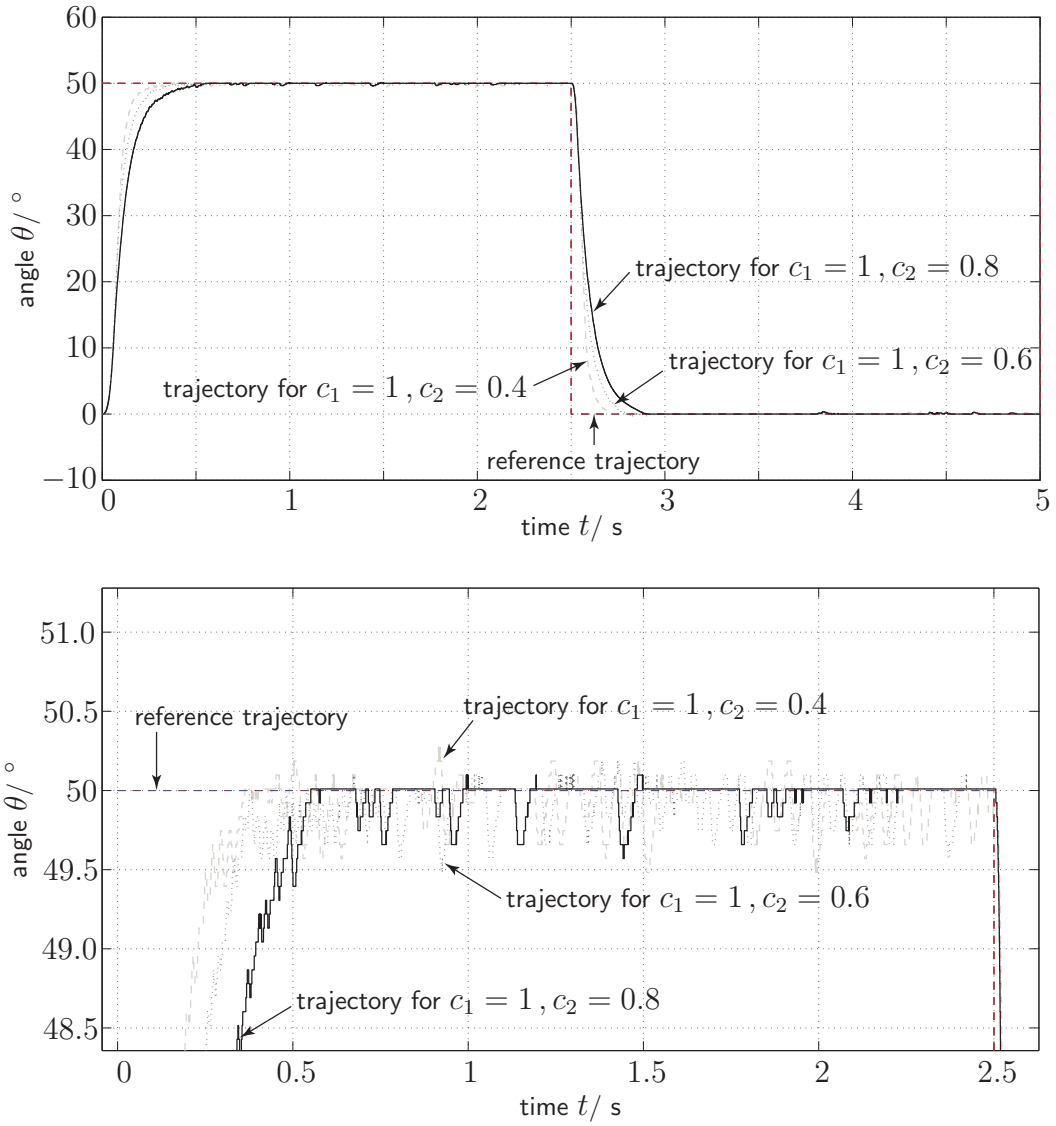

Figure 5.7: Experimental results: Position trajectories if the sliding mode position control algorithm based on the GBCP is applied. Three different desired dynamics for the mechanical system were chosen ($c_1 = 1$ and $c_2 = 0.04\,, 0.06\,, 0.08$).

In Figure 5.8 step responses of the angular position θ for the control that is based on fast torque and flux control is illustrated. Again, three different desired dynamics are assigned. They are chosen by the parameters in (5.48). Chattering is higher than in Figure 5.7. The stationary accuracy one receives is a relative deviating from the target position by

maximally $\pm 0.6\,^{\circ}$. If the desired dynamics is a fast response, the experimental results are supporting the usage of the strategy. However when a slower dynamics is desired, it is obvious that this method is not a viable control option. There exists noise in the system. The cascaded control approach proved to be very robust. For control unit design only a rough estimate of the load is required in order to assign sufficiently good observers. If a direct vector control decoupling controller is implemented in the inner control loop accuracy is getting worse, but noise is reduced.

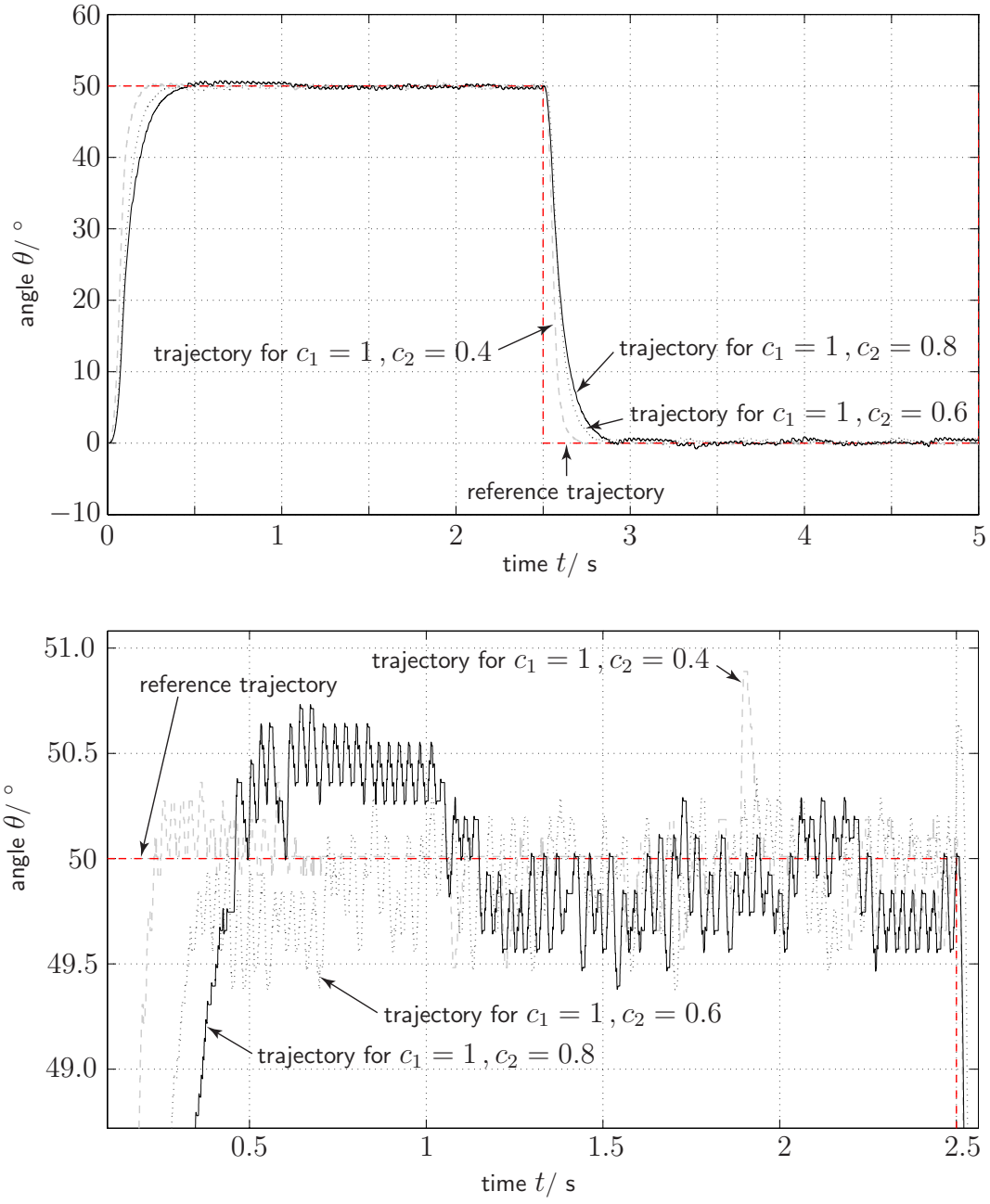

Figure 5.8: Experimental results: Position trajectories if the sliding mode position control algorithm based on fast flux and torque controllers is applied. Three different desired dynamics for the mechanical system were chosen ($c_1 = 1$ and $c_2 = 0.04\,, 0.06\,, 0.08$).

5.2.4 Discussion

The result presented prove, that the position control of an induction machine based on sliding mode techniques is possible. Both proposed control algorithms offer high dynamics. Their performances are quite similar. In the experimental setup accuracies of about 0.5° are achieved and the chatter effects are reduced to not hearable noise.

As expected, the cascaded control scheme is very robust, Contrary to expectations, the control algorithm based on the GBCP is quite robust as well. Nevertheless, due to a limited switching frequency and a given machine inductance for both control strategies chattering effects remain. The required hardware for both control approaches is simple. The design of the control algorithm base on the GBCP is simpler. It uses phase voltages are directly. The cascaded sliding mode control algorithm suffers from more chattering effects.

For both proposed controls besides measurement of the angular position and the current the implementation requires measurement or estimation of the angular speed and the acceleration signal. The application of other more appropriate observer concepts may increase the shown results.

5.3 Performance using Multiphase Inverter

In both proposed control algorithms the control action is the switching commands $\boldsymbol{g}$ entering the inverter. However, only four out of the seven stator voltages shown in Figure 5.3 are applied, as specified in [70]. The reason for this is equation (5.53), which makes the control inputs $u_\alpha = 0$ or $u_\beta = 0$ impossible, excluding three of the seven possible stator voltages. Furthermore, the controllers are not applicable to multilevel inverters, as the inverse model of the inverter is a linear transformation, providing against the handling of the appearing switching redundancies (multiple switch positions that lead to the same stator voltage vector $\boldsymbol{g}$).

Following the motor model (5.2), the stator voltages act on the derivative of the stator currents. The stator currents then act on the derivative of the rotor flux. Both stator currents and rotor flux act on the torque. Therefore the smoothness of the current is directly related to the chattering in the torque and the rotor flux. It is also affected by the quantization of the stator voltages.

Therefore, this section investigates, how performance of sliding mode controllers can be improved by using multiphase converters. Exemplary, the controller based on fast flux and torque control of section 5.2.2 will be extended in order to generate a continuous control output $\boldsymbol{u}_{\alpha\beta}$. This will allow the application of methods that use all possible stator voltages for either two-level or multilevel inverters, in order to improve quantization of the control input.

5.3.1 Control Unit Design

In order to achieve the goal of designing a controller allowing the usage of all stator voltages, the discontinuous control law (5.53) is replaced by a new control law delivering a

continuous stator voltage vector $\boldsymbol{u}_{\alpha\beta}$ that can then be applied as reference voltage to the inverter and then be converted to appropriate switching actions $\boldsymbol{g}$.

Based on the sliding manifolds (5.51) and (5.52) two new sliding manifolds are defined

$$\breve{\mathbf{s}} = \begin{pmatrix} \breve{s}_1 \\ \breve{s}_2 \end{pmatrix} = \mathbf{C}^T \boldsymbol{s} \tag{5.68}$$

$$= \begin{pmatrix} d_1\lambda_{\beta r} & -d_2\dfrac{\lambda_{\alpha r}}{|\boldsymbol{\lambda}_r|} \\ -d_1\lambda_{\alpha r} & -d_2\dfrac{\lambda_{\beta r}}{|\boldsymbol{\lambda}_r|} \end{pmatrix} \begin{pmatrix} s_1 \\ s_2 \end{pmatrix} \tag{5.69}$$

$$= -\frac{1}{|\boldsymbol{\lambda}_r|} \begin{pmatrix} \lambda_{r\alpha} & -\lambda_{r\beta} \\ \lambda_{r\beta} & \lambda_{r\alpha} \end{pmatrix} \begin{pmatrix} d_2 s_2 \\ |\boldsymbol{\lambda}_r|\, d_1 s_1 \end{pmatrix} \tag{5.70}$$

$$= -A_{\alpha,\beta}^{d,q} \begin{pmatrix} d_2 s_2 \\ |\boldsymbol{\lambda}_r|\, d_1 s_1 \end{pmatrix} \tag{5.71}$$

$$d_1 = \frac{3L_h N_r}{2(L_r L_s - L_h^2)}\,, \quad d_2 = \frac{L_h R_r}{L_r L_s - L_h^2}\,. \tag{5.72}$$

Vector $\left(\begin{smallmatrix} d_2 s_2 \\ \|\boldsymbol{\lambda}\| d_1 s_1 \end{smallmatrix}\right)$ is a vector in the (d,q) coordinate system aligned along the rotor flux. More specifically, it is related to the desired stator flux change in (d,q) coordinates. As $\mathbf{A}_{\alpha,\beta}^{d,q}$ is a rotation matrix from (d,q) coordinates to (α,β) coordinates, vector components of $\breve{\mathbf{s}}$ represent the desired stator flux change in the stator fixed coordinate system (α,β). Therefore control law (5.53) compensates the desired stator flux change $\breve{\mathbf{s}}$. This also shows that it makes sense to relate the stator voltage $\boldsymbol{u}_{\alpha\beta}$ to the offset from the sliding manifold $\breve{\mathbf{s}} = \mathbf{0}$.

Computation of a desired stator flux change in stator coordinates is the general procedure for vector control of the induction machine. For sliding mode control, this can be accomplished explicitly as in [61] where the desired stator flux is used for the sliding manifold. This implies that switching is performed in (d,q)-coordinates, and the switching results must then be transformed into (α,β)-coordinates. Or this can be realized implicitly, as when Lyapunov design is applied, so that switching is done directly in (α,β)-coordinates. Latter is chosen for the new control law. Therefore, matrix $\mathbf{C}$ and vector $\breve{\mathbf{s}}$ are both kept. Only control law (5.53) is replaced by a continuous function.

A simple continuous approximation of the control law as presented in section 2.2.2 may be effective for special applications but does not reach sliding mode $\breve{\mathbf{s}} = \mathbf{0}$. Consequently, an integrator is added as in the super-twisting algorithm described in section 2.2.3. The new control law is defined as

$$\boldsymbol{u}_{\alpha\beta} = -U_0\,\mathrm{sat}\Big(\frac{\breve{\mathbf{s}}}{\varepsilon_M} + \frac{1}{\kappa_M}\int \frac{\breve{\mathbf{s}}}{\varepsilon_M}\mathrm{d}t\Big) \tag{5.73}$$

Parameter ε_M regards the connection between the controller output $\boldsymbol{u}_{\alpha\beta}$ and the offset from the sliding manifold $\breve{\mathbf{s}} = \mathbf{0}$. Parameter $\frac{1}{\kappa_M}$ is the parameter defining the rise rate of the integrator signal. The integrator signal is responsible for reaching sliding mode $\breve{\mathbf{s}} = \mathbf{0}$. It should be set slightly higher than the sampling rate. Since if it is close to the sampling rate, chattering can not be reduced. When chatter is too high, accuracy is affected.

Theorem 5.2 The ε_M-vicinity around $\boldsymbol{s} = \mathbf{0}$ is reached in finite time when control law (5.73) is applied.

Proof: The continuously differentiable Lyapunov function

$$V = \frac{1}{2}\boldsymbol{s}^T\boldsymbol{s}\,, \qquad \boldsymbol{s} = \begin{pmatrix} s_1 \\ s_2 \end{pmatrix} \tag{5.74}$$

with

$$V \geq 0 \tag{5.75}$$
$$V = 0 \quad \text{for} \quad \boldsymbol{s} = \mathbf{0} \tag{5.76}$$
$$\lim_{\boldsymbol{s}\to\infty} V = \infty\,. \tag{5.77}$$

is considered. When the derivative of V is taken with respect to time

$$\dot{V} = \boldsymbol{s}^T\underline{\dot{s}} \tag{5.78}$$
$$= \boldsymbol{s}^T(\boldsymbol{e} + \mathbf{C}\boldsymbol{u}_{\alpha\beta})\,, \tag{5.79}$$

where $\boldsymbol{e}$ is independent of the control input $\boldsymbol{u}_{\alpha\beta}$ and matrix $\mathbf{C}$, is dependent on it. Vector $\boldsymbol{e}$ and matrix $\mathbf{C}$ can be directly derived from the motor model (5.2) and (5.1).

$$\dot{V} = ((\mathbf{C}^T)^{-1}\breve{\mathbf{s}}^T)^T(\boldsymbol{e} + \mathbf{C}\boldsymbol{u}_{\alpha\beta}) \tag{5.80}$$
$$= \breve{\mathbf{s}}^T((\mathbf{C}^T)^{-1})^T(\boldsymbol{e} + \mathbf{C}\boldsymbol{u}_{\alpha\beta}) \tag{5.81}$$
$$= \breve{\mathbf{s}}^T\mathbf{C}^{-1}(\boldsymbol{e} + \mathbf{C}\boldsymbol{u}_{\alpha\beta}) \tag{5.82}$$
$$= \breve{\mathbf{s}}^T\mathbf{C}^{-1}\boldsymbol{e} + \breve{\mathbf{s}}^T\boldsymbol{u}_{\alpha\beta} \tag{5.83}$$
$$\leq \breve{\mathbf{s}}^T\mathbf{C}^{-1}\boldsymbol{e} - U_0\breve{\mathbf{s}}^T\operatorname{sign}(\breve{\mathbf{s}}) \tag{5.84}$$
$$\leq \breve{\mathbf{s}}^T\mathbf{C}^{-1}\boldsymbol{e} - U_0\,|\breve{\mathbf{s}}| \tag{5.85}$$

This equation is now simplified. The second right hand term is splitted

$$|\breve{\mathbf{s}}| = \breve{\mathbf{s}}^T\operatorname{sign}(\breve{\mathbf{s}}) \leq |\breve{s}_1| + |\breve{s}_2| \tag{5.86}$$

and the first right hand term is simplified

$$\boldsymbol{e}' = \mathbf{C}^{-1}\boldsymbol{e} = \begin{pmatrix} e_1' \\ e_2' \end{pmatrix} \tag{5.87}$$

Inequation (5.85) is then

$$\dot{V} \leq \breve{s}_1 e_1' + s_2^* e_2' - U_0\,|\tilde{\boldsymbol{s}}| \tag{5.88}$$
$$\leq \breve{s}_1 e_1' + s_2^* e_2' - U_0\,|\breve{s}_1| - U_0\,|\breve{s}_2| \tag{5.89}$$

With the knowledge that vector $\binom{e_1'}{e_2'}$ is bounded, which can be shown by calculation of (5.87), and

$$U_0 > |e_i{}^*| \quad i = 1, 2 \tag{5.90}$$

condition

$$\dot{V} < 0 \tag{5.91}$$

is fulfilled. Therefore, when the supply voltage U_0 is high enough, the system is converging to ε-vicinity around $\boldsymbol{s} = \mathbf{0}$ in finite time.

Outside of the ε-vicinity around $\boldsymbol{s} = \mathbf{0}$, the control law (5.73) can be designed as

$$\boldsymbol{u}_{\alpha\beta} \leq -U_0 \operatorname{sign}(\tilde{\boldsymbol{s}}) \tag{5.92}$$

This approximation is only valid for

$$|\underline{s^*}| \geq \begin{pmatrix} \varepsilon \\ \varepsilon \end{pmatrix}. \tag{5.93}$$

■

5.3.2 Implementation of Multiphase Inverter Control Algorithms

For the implementation of the proposed multilevel flux and torque control two possibilities exist. An inverse inverter model can be applied to the control input $\boldsymbol{u}_{\alpha\beta}$ in order to quantize this stator voltage and generate the matching switch command vector $\boldsymbol{g}$. An alternative to this is to apply the continuous voltage as reference to a pulse width modulated inverter.

Implementation by Using the Inverse Model of the Inverter

The controller delivers a stator voltage $\boldsymbol{u}_{\alpha\beta}$ as control input. To find the right switch command vector $\boldsymbol{g}$ an inverse model of the inverter is required.

Unfortunately, equation (5.10) cannot just be inverted due to the many redundancies of this transformation. Choosing the right switch command when redundancies are available is important for the thermal balance of the inverter electronics. Therefore, for the inverse model of the inverter, the following algorithm is proposed.

As can be seen in Figure 5.9, all possible voltages are aligned on parallel lines orthogonal to the vectors p_1 and p_2. Those two vectors can be calculated by the forward model (5.10) and are given by:

$$p_1 = \frac{1}{2}\begin{pmatrix} \sqrt{3} \\ 1 \end{pmatrix} \tag{5.94}$$

$$p_2 = \frac{1}{2}\begin{pmatrix} -\sqrt{3} \\ 1 \end{pmatrix} \tag{5.95}$$

A linear transformation is applied in order to find out a projection of $\boldsymbol{u}_{\alpha\,\beta}$ to those two vectors, introducing the coordinates $\binom{a_1}{a_2}$

$$\begin{pmatrix} a_1 \\ a_2 \end{pmatrix} = \frac{1}{U_0}\begin{pmatrix} \boldsymbol{q}_1^T \\ \boldsymbol{q}_2^T \end{pmatrix} \boldsymbol{u}_{\alpha\,\beta} = \frac{1}{2U_0}\begin{pmatrix} \sqrt{3} & 1 \\ -\sqrt{3} & 1 \end{pmatrix}\begin{pmatrix} u_\alpha \\ u_\beta \end{pmatrix}. \tag{5.96}$$

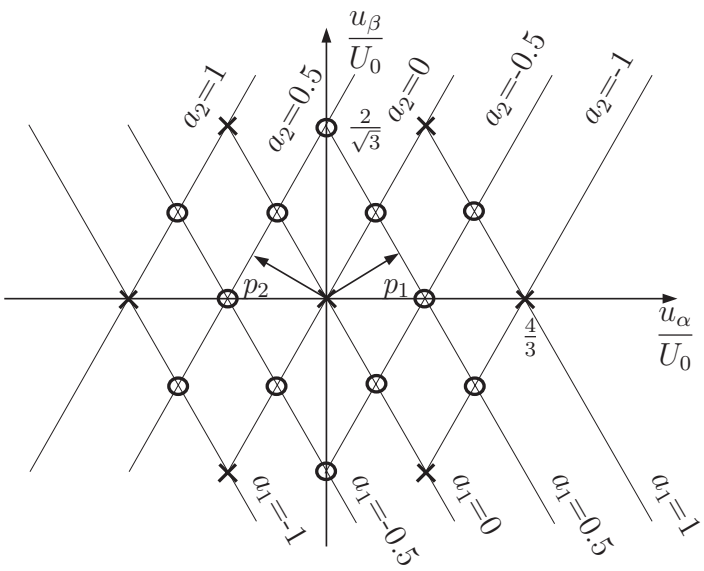

Figure 5.9: Stator voltages for the two- and three-level inverter.

The coordinates $\binom{a_1}{a_2}$ are then quantized. For the two-level inverter, they are quantized to take values from $\{-1, 0, 1\}$. For the three-level inverter, they are quantized to take values from $\{-1, -0.5, 0, 0.5, 1\}$. Those quantized coordinates all match exactly one possible stator voltage as shown in Figure 5.9. Consequently, $\binom{a_1}{a_2}$ are the indices for the lookup-tables, Table 5.1 is prepared for the two-level inverter, and Table 5.2 for the three level inverter. The output of these lookup-tables is the desired switch command vector $\boldsymbol{g}$.

The redundancies (multiple switch positions that lead to the same stator voltage vector) can be used to maintain a good thermal balance of the inverter as follows: All applicable switch command vectors $\boldsymbol{g}$ are read out of the lookup-table, after which an additional algorithm decides which one to take. Decision parameters can be that those switches that have been used excessively in the past are avoided.

The method can be extended to control any other multilevel inverter, only the quantization of $\binom{a_1}{a_2}$ and the lookup-table have to be adapted. Furthermore, when using the quantization algorithm, it should be noted that the values do not exceed their ranges. So the stator voltages have to be limited to their maximum values

$$-\frac{4U_0}{3} \leq u_\alpha \leq \frac{4U_0}{3} \tag{5.97}$$

$$-\frac{2U_0}{\sqrt{3}} \leq u_\beta \leq \frac{2U_0}{\sqrt{3}} \tag{5.98}$$

as follows from the forward model (5.10). This will avoid that the algorithm wants to look up empty positions in the lookup-table, as for example $\binom{a_1}{a_2} = \binom{1}{1}$. The coordinates $\binom{a_1}{a_2}$ have to be limited to

$$-1 \leq a_1 \leq 1 \tag{5.99}$$

$$-1 \leq a_2 \leq 1 \tag{5.100}$$

$a_1 \ddots a_2$	-1	0	1
1	(1,-1,-1)	(1,1,-1)	
0	(1,-1,1)	(1,1,1);(-1,-1,-1)	(-1,1,-1)
-1		(-1,-1,1)	(-1,1,1)

Table 5.1: Lookup-table for the 2-level inverter.

$a_1 \ddots a_2$	-1	-0.5	0	0.5	1
1	(1,-1,-1)	(1,0,-1)	(1,1,-1)		
0.5	(1,-1,0)	(1,0,0),(0,-1,-1)	(1,1,0),(0,0,-1)	(0,1,-1)	
0	(1,-1,1)	(1,0,1),(0,-1,0)	(1,1,1),(0,0,0),(-1,-1,-1)	(0,1,0),(-1,0,-1)	(-1,1,-1)
-0.5		(0,-1,1)	(0,0,1),(-1,-1,0)	(0,1,1),(-1,0,0)	(-1,1,0)
-1			(-1,-1,1)	(-1,0,1)	(-1,1,1)

Table 5.2: Lookup-table for the 3-level inverter.

Implementation by Using PWM Operation of a Three-Phase Inverter

An alternative to the inverse inverter model is the pulse width modulation. A three-phase inverter can be controlled by three independent pulse width modulators, one for each phase.

From the desired stator voltage vector $\boldsymbol{u}_{\alpha\beta}$, the three desired phase voltages $\boldsymbol{u}_{abc}$ are calculated. As in [79], the pseudo inverse of matrix $A_{\alpha\beta}^{abc}$ from equation (5.9) is applied:

$$\begin{pmatrix} u_a \\ u_b \\ u_c \end{pmatrix} = (A_{\alpha,\beta}^{a,b,c})^{+} \begin{pmatrix} u_\alpha \\ u_\beta \end{pmatrix} = A_{a,b,c}^{\alpha,\beta} \begin{pmatrix} u_\alpha \\ u_\beta \end{pmatrix} = \begin{pmatrix} 1 & 0 \\ -\frac{1}{2} & \frac{\sqrt{3}}{2} \\ -\frac{1}{2} & -\frac{\sqrt{3}}{2} \end{pmatrix} \begin{pmatrix} u_\alpha \\ u_\beta \end{pmatrix} . \tag{5.101}$$

Out of the desired phase voltage u_i, the switch command for the respective phase g_i must be calculated. This is carried out by the pulse width modulation, where the pulse width is set by the duty cycle α. The duty cycle α is defined as the ratio of "on" time to "off" time

$$\alpha = \frac{T_{on}}{T_{on} + T_{off}} \, , T_{on} + T_{off} = T \, , T_{on} = \alpha T \tag{5.102}$$

Here, T corresponds to the sampling interval of the control system that generates the desired stator voltage vector $\boldsymbol{u}_{\alpha\beta}$.

For the two-level inverter, generation of the switch command is easy, as the duty cycle is directly proportional to the phase voltage u_i. The duty cycle is calculated by

$$\alpha_i = \frac{u_i + U_0}{2U_0} \, , \quad i = a, b, c \tag{5.103}$$

and the switch command is generated by

$$\begin{cases} g_i = +1 & 0 \leq t < \alpha_i T \\ g_i = -1 & \alpha_i T \leq t < T \end{cases} \, , \quad i = a, b, c \tag{5.104}$$

For a three-level inverter, this is moderately complicated as each element of the switch command vector can take three different values out of the set $\{-1, 0, 1\}$. The advantage is that the voltage resolution is higher, so for a positive output voltage, switch commands $\{1, 0\}$ are applied, whereas for negative voltages, switch commands $\{-1, 0\}$ are applied. As a result, three cases can be distinguished, based on a constant $U_m > 0$, which is specified later:

1. $u_i \geq U_m$

$$\alpha_i = \frac{u_i}{U_0}, \quad i = a, b, c \tag{5.105}$$

then

$$\begin{cases} g_i = +1 & 0 \leq t < \alpha_i T \\ g_i = 0 & \alpha_i T \leq t < T \end{cases}, \quad i = a, b, c \tag{5.106}$$

2. $u_i \leq -U_m$

$$\alpha_i = \frac{-u_i}{U_0}, \quad i = a, b, c \tag{5.107}$$

then

$$\begin{cases} g_i = -1 & 0 \leq t < \alpha_i T \\ g_i = 0 & \alpha_i T \leq t < T \end{cases}, \quad i = a, b, c \tag{5.108}$$

3. $-U_m < u_i < U_m$

$$\alpha_i = \frac{u_i + U_0}{2U_0}, \quad i = a, b, c \tag{5.109}$$

then

$$\begin{cases} g_i = +1 & 0 \leq t < \alpha_i T \\ g_i = -1 & \alpha_i T \leq t < T \end{cases}, \quad i = a, b, c \tag{5.110}$$

An arising problem is that minimum delay times must be kept in the switching range of a power switch. Because of this, the full range of the duty cycle $0 \leq \alpha \leq 1$ is not available. When the minimum delay time is T_{min}, the duty cycle is limited to

$$\frac{T_{min}}{T} \leq \alpha \leq (1 - \frac{T_{min}}{T}) \tag{5.111}$$

This will also limit the maximum phase voltage applied to the induction motor. For a two-level inverter, the phase voltage u_i cannot vary between $-U_0$ and U_0, but will be kept in the range

$$-U_0(1 - \frac{2T_{min}}{T}) \leq u_i \leq U_0(1 - \frac{2T_{min}}{T}) \tag{5.112}$$

For a three-level inverter, this range is

$$-U_0(1 - \frac{T_{min}}{T}) \leq u_i \leq U_0(1 - \frac{T_{min}}{T}) \tag{5.113}$$

The value for U_m for the three level inverter follows from the same problem and is therefore given as

$$U_m = \frac{T_{min}}{T} U_0 \tag{5.114}$$

The redundancies (multiple switch positions that lead to the same stator voltage vector) can again be used to maintain a good thermal balance of the inverter: The stator voltages $\boldsymbol{u}_{\alpha\beta}$ are related to the difference between the phase voltages $\boldsymbol{u}_{abc}$. Hence, setting the phase voltages to $\boldsymbol{u}^*_{abc} = \boldsymbol{u}_{abc} + \boldsymbol{u}_x$, where $\boldsymbol{u}_x = \begin{pmatrix} u_x \\ u_x \\ u_x \end{pmatrix}$ is any voltage generated by an additional algorithm, will lead to the same stator voltages but loading the switches in a different way.

5.3.3 Simulation Results

The sliding mode position controller presented in the previous section is evaluated in terms of simulation. Both the inverse inverter model and pulse-width modulation are tested for the control method presented in Section 5.2.2. The simulations are executed for a two- and three-level inverter and for an inverter delivering continuous output voltage in order to see the performance of the multilevel converter solution. The simulation details and results are presented in Section C.

Results show that the control algorithm with inverse inverter model does not show improvement. Control algorithm implemented with pulse width modulation is a great improvement when compared to the existing controllers and the implementation with inverse inverter model. It can also be seen that the three-level inverter is not such a great improvement when compared with the two-level inverter. For the implementation of the multiphase inverter control algorithm with pulse width modulation, the error as well as the high-frequency deviation are reduced on all three sliding manifolds, implying that chattering is reduced while control performance is improved.

5.3.4 Discussion

The new control law including the inverse inverter model does not improve control performance significantly. The results show that the new controller with inverse inverter model is worse that the existing controllers. However, one advantage is that it requires less electrical power than the other controllers. When a three-level inverter is applied, control performance is acceptable.

The new controller with a continuous voltage inverter was simulated in order to see the maximal performance of the new control law derived in the previous section. The results show that the new controller combined with pulse width modulation is a great improvement to the controller and the new controller with inverse inverter model. It can also be seen that the three-level inverter is not such a that great improvement compared to the two-level inverter. The new controller, that is applied together with a pulse-width modulated inverter, comes very close to that maximal performance and therefore is a great improvement at only low additional cost. The chattering problem can be considered as solved.

The three-level inverter is a slight improvement, however, it is a very small improvement at a very high cost.

The advantage of the inverse inverter model is that it is possible to benefit from the full voltage U_0 for each phase. However, the phase voltage will only change when an important deviation from $\check{\mathbf{s}} = \mathbf{0}$ appears. For pulse width modulated operation, only a part of the full voltage U_0 is available for each phase, but the phase voltage will be adapted continuously to the control input without the neccesity of a deviation from $\check{\mathbf{s}} = \mathbf{0}$ is necessary. Therefore, to access chattering reduction, pulse width modulation seems to be more promising.

5.4 Conlusion

In this chapter two position control algorithms for a mechanical system driven by an induction machine were developed. The control unit design for the complex systems was done based on the sliding mode control theory as well as the GBCP, which was introduced in Chapter 3 in this thesis.

The consequent inclusion of the actuator dynamics into the control design proved to be very efficient for the application example. In experiments the proposed control schemes show high dynamics. Chattering effects are low while robustness and disturbance rejection, the main benefits of sliding mode control, are retained. Accuracies of $0.5\,^\circ$ and $0.5\,^\circ$ were achieved. The GBCP allows to handle the control unit design process for thee complex system models that include the actuator dynamics. The implementation of the control law is very simple since the voltages impressed on the actuator are the actual discontinuous control input vector.

Unfortunately, in simulations the use of multiphase converters could not improve the performance of sliding mode controllers.

The experimental results, which were given in this chapter, show that the integration of inexpensive, robust and compact induction machines in control units for robotic systems by using sliding mode control concepts for electromechanical systems is possible. High robustness and high dynamics can be achieved. Induction machine are efficient electric sctuators and have small mass inertias. Therefore, in many cases their use in robotic systems would not require a gear box like other electric actuators. Then, improved performance in robotic systems, e.g. in telepresence applications, could be achieved.

6 Conclusion and Future Directions

6.1 Concluding Remarks

In this work sliding mode control strategies for mechanical systems driven by different types of electric motors were investigated.

The developed closed methodology for systematic sliding mode control design, the GBCP, simplifies the application of sliding mode control to arbitrary electromechanical systems. The number of nonlinear system transformations needed to design a control law was reduced e.g. from five transformations with the BCP to two transformations with the GBCP for the induction machine which drives an inverted pendulum system. The advantages of the GBCP over the BCP will scale with the complexity of the system considered.

The GBCP is applicable to a wider system class than the BCP. The sliding mode control of a flexible shaft was presented as an example of a system with infinite dimension.

Two implementation problems of the control design based on the BCP/GBCP were solved for the first time. The solutions have been verified in simulations. A method to reject disturbances with known structure as well as the necessary observer design was presented.

A sliding mode control concept for mechanical systems driven by electric motors that reduces chattering while preserving robustness was developed. It takes actuator dynamics into account and uses the voltages impressed on the actuator as the actual discontinuous control input vector. The efficiency of the control concept was proved for three applications by numerical simulations as well as experiments: the position control of an inverted pendulum system driven by a DC motor, a synchronous motor, and an induction machine. In addition, a benchmark control system was developed for the DC setup.

Theoretical stability in the presence of bounded parameter uncertainties or bounded disturbances was proved for all three application examples.

The examined systems were found to be very robust against parameter variations. Load changes applied to the three systems did not effect the performance of any of the setups considerably as long as the maximal force/torque provided by the actuators was not exceeded. In contrast, load changes applied to the benchmark controlled system generated a steady state error.

Compared to sliding mode control ignoring actuator dynamics, the application of the new control concept reduced chattering and increased the control accuracy. There was no steady state error in any of the experiments. For the induction machine a position accuracy of $\pm 0.5\,^{\circ}$ was achieved.

The new control scheme allows fast control tasks, because the control bandwidth is limited only by the characteristics of the electric actuator. The transient response time was found to decrease by 25% compared to the benchmark controlled system.

The implementation of the proposed sliding mode control is simple and the stability analysis can be made without problems using the sliding mode conditions. Nevertheless, fast hardware is required: A control unit offering at least 1 kHz sampling rate is necessary to get acceptable results regarding current and angle ripple. A special innovation of this thesis is the development of a position control for an induction machine providing high robustness and high control accuracy. This application example highlights the advantages of the proposed control concept. Even though the parameters of the used induction machine were not known exactly, the control performance was excellent and showed strong robustness.

The control approach developed in this thesis significantly improves and expands the applicability of sliding mode control to electromechanical systems. It addresses e.g. the requirements of human-interactive robotic devices. These applications require the devices to be fast in response to human contact while maintaining accurate position and force tracking. The performance of these systems is commonly limited by the underlying controller and amplifier architecture and the proposed control scheme is able to overcome these limitations.

6.2 Future Work

Further investigations of the sliding mode control concept, which is presented in this thesis, may build on the promising experimental results. They prove the applicability of sliding mode control algorithms to electromechanical systems without significant design efforts and underline their advantage of high robustness. The remaining chattering effects, which decrease the control accuracy, may be reduced by using faster hardware or sophisticated observers and disturbance estimators. Therefore, a challenging research direction is the investigation of an adaptive disturbance estimator for the flexible shaft system, which does not require information about the structure of a disturbance or the the frequency of periodical perturbations. The performance of the presented position control of an induction machine may be improved by implementing better observers for flux as well as for the angular velocity. Additionally, an estimator that provides information about the unknown load may lead to a more accurate control performance.

The given experimental results motivate to more experimental investigation in order to find the limits of the proposed control strategy for high-dimensional non-linear systems with unknown loads, e.g. multi-link robots or human-machine interfaces.

An rewarding future research direction is the evaluation of the power consumption of the proposed sliding mode control concept compared to other control algorithms. This analysis should include power losses due to switching processes of electronic devices in the power amplifier.

A Models and Experimental Setups

A.1 Inverted Pendulum System

The dynamics of the inverted pendulum system shown in Figure A.1 is given by

$$J\ddot{\theta} = mgl\sin(\theta) - \mu\omega + \tau \tag{A.1}$$

where m is the pendulum mass, g the gravitational constant, l the pendulum length and θ the angle of the pendulum with the upright position being zero. Parameter μ is a frictional constant $\left[\frac{\text{Nms}}{\text{rad}}\right]$). The moment of inertia of the pendulum system is given by $J = ml^2$.

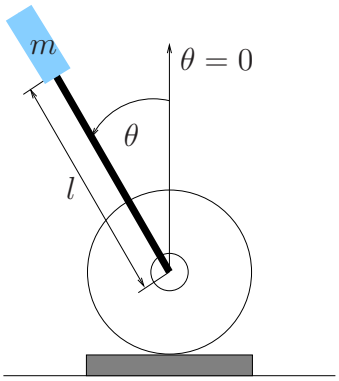

Figure A.1: Schematic diagram of the considered mechanical sample system, an inverted pendulum.

m	$= 0.01\,\text{kg}$	(pendulum mass)
g	$= 9.81\,\frac{\text{m}}{\text{s}^2}$	(gravitation constant)
l	$= 0.5\,\text{m}$	(pendulum length)

Table A.1: Parameters of the inverted pendulum system used for control design and in numerical simulations.

A.2 DC Motor

The proposed control algorithm is applied to the sample system (Figure A.1). The actuator is a 150 W Maxon DC motor with gear (1:90) as described in Section A.2. The mass and length of the pendulum can be modified and so different loads can be realized. An H-Bridge provides the required discontinuous control input for the sliding mode control. In the linear control system the DC motor is powered by a Copley PWM-amplifier. As framework for the control system Matlab/ Simulink Real Time Workshop is used. The controller runs under RT-Linux with a sampling time of 0.1 ms.

R_a	$= 0.316\,\Omega$	(resistance)
L	$= 0.00008\,\mathrm{H}$	(inductance)
K_m	$= 0.0302\,\frac{\mathrm{Nm}}{\mathrm{A}}$	(torque constant)
K_n	$= 60/317\,\mathrm{Vs}$	(induction constant)
J_m	$= 1.3400e-005\,\mathrm{kg\,m^2}$	(mass moment of inertia of the motor)
u_A	$= 24\,\mathrm{V}$	(supplied voltage)

Table A.2: DC motor setup- parameters.

A.3 Synchronous Motor

The experimental setup shown in Figure A.2 consists of a synchronous motor Maxon EC45, a three phase electronic inverter ST L6234, a Megatron MCP05 potentiometer for absolute measurement of the shaft position angle θ and a PC. Communication from the PC to the inverter is done via the PC's parallel port (maximal sampling frequency 400 Hz). The potentiometer is connected to an analog digital converter card Advantech PCI-1714. The

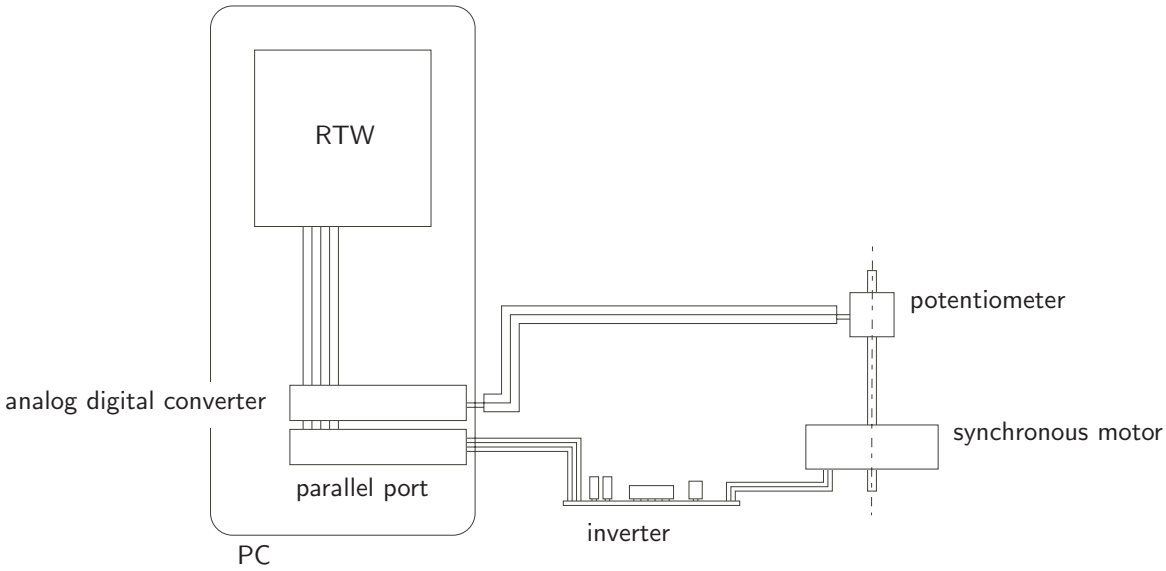

Figure A.2: Experimental setup (synchronous motor).

control algorithm is implemented in Matlab/ Simulink running on a Linux Real Time operating system. An executable target is generated using Matlab Real Time Workshop.

A.4 Induction Machine

The derived control schemes are tested on an experimental setup with a $1,1\,\mathrm{kW}$ three phase squirrel cage induction machine as shown in Figure A.5. The control algorithm is implemented using Matlab/ Real Time Workshop based on the real time operation system Linux RTAI on a PC. As illustrated in Figure A.4 the PC communicates via the parallel port with the inverter, which drives the induction machine. The maximal sampling frequency of the parallel port is 400 Hz, the maximal switching frequency of the IGBTs

R	$= 0.6\,\Omega$	(resistance)
L	$= 0.000205\,\mathrm{H}$	(inductance)
p	$= 8$	(number of permanent pole pairs)
k	$= 0.0255\,\mathrm{Vs}$	(motor constant)
J_m	$= 9.25 \cdot 10^{-6}\,\mathrm{kg\,m^2}$	
u	$= 12\,\mathrm{V}$	(supplied voltage)
$i_d^2 + i_q^2$	$\leq 2.3\,\mathrm{A}$	(quadratic voltage)
μ	$=5.033 \cdot 10^{-6}\,\mathrm{Nms}$	(frictional coefficient- estimated)
r	$=0.3\,\Omega$	(internal resistance of the switching devices)

Table A.3: Synchronous motor setup- parameters.

Figure A.3: Synchronous motor.

$L_{lr} =$	$15.7 \cdot 10^{-3}$ H	(rotor inductance)
$L_{ls} =$	$18.9 \cdot 10^{-3}$ H	(stator inductance)
$L_h =$	$439 \cdot 10^{-3}$ H	(mutual inductance)
$R_r =$	$6.8\,\Omega$	(rotor resistance)
$R_s =$	$10\,\Omega$	(stator resistance)
$N_r =$	2	(number of pole pairs)
$J_m =$	$3.5 \cdot 10^{-3}\,\mathrm{kgm^2}$	(mass moment of inertia of the machine)
$c_m =$	$5.752 \cdot 10^{-3}\,\mathrm{Nms}$	(friction coefficient of the machine)
$\lambda_0 =$	$2.95\,\mathrm{mVs}$	(nominal rotor flux)

Table A.4: Induction machine setup- parameters.

is approximately 70 kHz. Control signals are sent via optical fibers. Thus, problems like noise and electromagnetic disturbances are avoided. The inverter controls the three phase currents of the induction machine, which are measured by Hall sensors and sent back to the PC via an analog digital converter (PCI-1714, clock signal 60 MHz). An encoder possessing the accuracy of 0.018°, which is fixed at the motor shaft, sends the angular position of the motor shaft via an other analog digital converter (Sensoray 626) to the PC. Sampling rates for all experiments are $T_a = 20\,\mathrm{kHz}$. Table A.4 summarizes the parameters of the used induction machine.

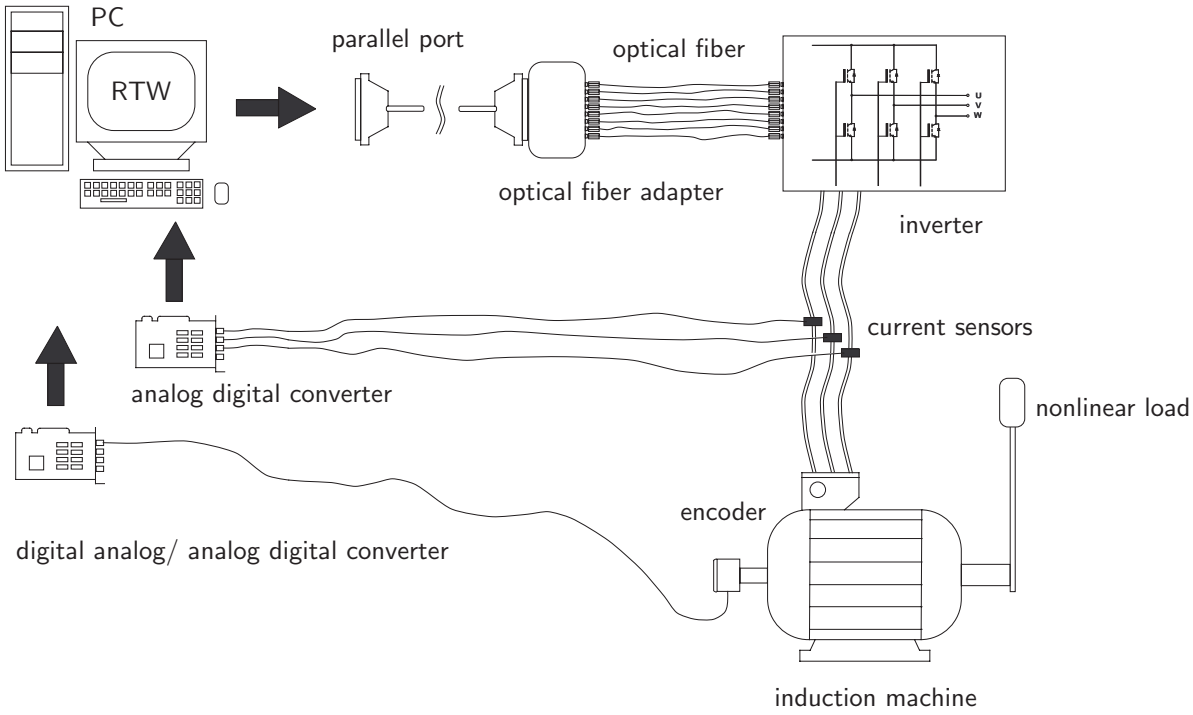

Figure A.4: Experimental setup (induction machine).

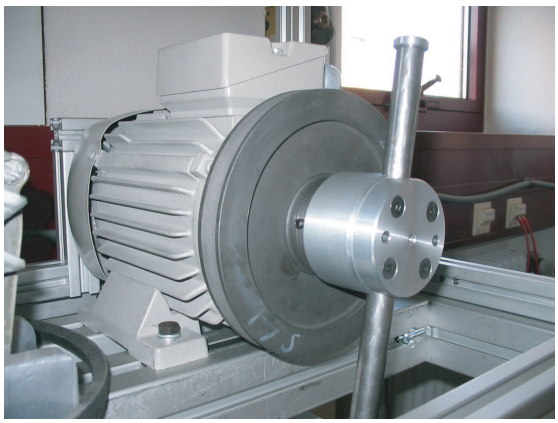

Figure A.5: Induction machine.

B Cost Functional Minimizing Sliding Mode Control Design for a Synchronous Motor

Desired dynamics of the mechanical system is chosen in such a way that the dissipative power loss Π of the synchronous machine

$$\Pi = \frac{3}{2}(R+r)(i_d^2 + i_q^2) + \mu\omega^2 \tag{B.1}$$

is minimized during operation. Parameter r represents the internal resistance of the switching devices connected in series to the winding resistance R for each phase of the three-phase system.[1] Transient time T, initial position θ_0 and target position θ_T are taken into account for the optimization problem.

In order to be able to carry out the optimization analytically, a simplified motor model is used. This model is derived from the original motor model equations (4.28) and (4.29) by neglecting electrical time constants, which are very small compared to the mechanical ones. This simplification, based on the theory of singular perturbation is done by setting

$$\dot{i}_d = 0 \tag{B.2}$$

$$\dot{i}_q = 0\,. \tag{B.3}$$

Furthermore, equation (4.29) shows that the direct current i_d does not contribute to the motor torque ki_q. The optimization task can therefore be further simplified by fixing i_d to an optimal value i_d^* using control input u_d. Considering the cost function (B.1), the optimal value of i_d is

$$i_d^* = 0\,. \tag{B.4}$$

With (B.3) and (B.4) the reduced state space model of the synchronous motor

$$\begin{aligned} \dot{\boldsymbol{x}} &= \begin{bmatrix} \dot{\theta} \\ \dot{\omega} \end{bmatrix} \\ &= \begin{bmatrix} \omega \\ -\frac{\mu}{J}\omega + \frac{k}{RJ}\left(u_q - \frac{2}{3}k\omega\right) - \frac{1}{J}\tau_L \end{bmatrix} \\ &= \begin{bmatrix} f_1(\boldsymbol{x}) \\ f_2(\boldsymbol{x}, \tau_L, u_q) \end{bmatrix} = \boldsymbol{f}(\boldsymbol{x}, \tau_L, u_q) \end{aligned} \tag{B.5}$$

is obtained. For optimization the value of the disturbance τ_L is set to be zero

$$\bar{\tau}_L = 0\,. \tag{B.6}$$

[1] The resistance factor r is equal to $\frac{3}{2}$ as a result of the transformation of the three dependent phase currents i_a, i_b and i_c into the two independent currents i_d and i_q.

The angles θ_0 and θ_T being initial and target angular positions respectively and T being the selectable transition time from initial to target position, the optimization problem turns into a problem of finding

$$\underset{u_q(t)}{\operatorname{argmin}} J(\boldsymbol{x}, \bar{\tau}_L, u_q, T) = \underset{u_q(t)}{\operatorname{argmin}} \int_0^T \Pi(\boldsymbol{x}, \bar{\tau}_L, u_q)\mathrm{d}t \tag{B.7}$$

taking into account the equality constraint

$$\dot{\boldsymbol{x}} - \boldsymbol{f}(\boldsymbol{x}, \bar{\tau}_L, u_q) = \mathbf{0} \tag{B.8}$$

and the boundary conditions

$$\boldsymbol{x}(0) = \begin{bmatrix}\theta_0 \\ 0\end{bmatrix} \text{ and } \boldsymbol{x}(T) = \begin{bmatrix}\theta_T \\ 0\end{bmatrix} . \tag{B.9}$$

The solution is the optimal feedback control law

$$\theta^*(t) = \theta_0 + K\left[\sinh(Qt) - \frac{D}{S}[\cosh(Qt) - 1] - qt\right] \tag{B.10}$$

$$\omega^*(t) = KQD\left[1 - \frac{1}{S}\sinh(Qt)\right] \tag{B.11}$$

where

$$\begin{aligned} Q &= \sqrt{\frac{f^2}{J^2} + \frac{2\mu k^2}{3(R+r)J^2}}\,, \\ S &= \sinh(QT)\,, \\ K &= \frac{S(\theta_T - \theta_0)}{2D - QTS} \text{ and} \\ D &= \cosh(QT) - 1\,. \end{aligned} \tag{B.12}$$

Remark B.1 To find the optimal continuous control $u_q^*(\boldsymbol{x})$ or directly the optimally controlled trajectory $\boldsymbol{x}^* = \binom{\theta^*}{\omega^*}$, the constrained continuous dynamic optimization theory is applied. That means Hamilton equations are set up and solved.

The necessary conditions for minimizing Π are

$$\frac{\partial H}{\partial \boldsymbol{x}} = -\dot{\boldsymbol{\lambda}}^T \tag{B.13}$$

$$\frac{\partial H}{\partial \boldsymbol{\lambda}} = \dot{\boldsymbol{x}}^T \tag{B.14}$$

$$\frac{\partial H}{\partial \boldsymbol{u}} = \mathbf{0}^T\,. \tag{B.15}$$

When the necessary conditions are substituted in (B.5) - where state vector $\boldsymbol{x} = [\theta\, \omega]^T$, co-state vector $\boldsymbol{\lambda} = [\lambda_\theta\, \lambda_\omega]^T$, control input $u = u_q$, nominal disturbance values (B.6) and loss function (B.1) the Hamiltonian system

$$\frac{\partial H}{\partial \lambda_\theta} = \omega = \dot{\theta} \tag{B.16}$$

$$\frac{\partial H}{\partial \lambda_\omega} = -\frac{f}{J}\omega + \frac{k}{RJ}\breve{u} - \frac{Lk}{RJ}\dot{i}_q - \frac{1}{J}M = \dot{\omega} \tag{B.17}$$

$$\frac{\partial H}{\partial \theta} = 0 = -\dot{\lambda}_\theta \rightarrow = \lambda_\theta = \text{constant} \tag{B.18}$$

$$\frac{\partial H}{\partial \omega} = \frac{3(R+r)}{R^2}\tilde{u}\frac{2}{3}k\omega + 2f\omega - \left(\frac{f}{J} + \frac{2k^2}{3RJ}\right)\lambda_\omega = -\dot{\lambda}_\omega \tag{B.19}$$

$$\frac{\partial H}{\partial u_q} = \frac{3(R+r)}{R^2}\breve{u} + \frac{k}{RJ}\lambda_\omega = 0 \rightarrow \tilde{u} = \frac{Rk}{3(R+r)J}\lambda_\omega \tag{B.20}$$

where $\breve{u}$ represents

$$\breve{u} := u_q - \frac{2}{3}k\omega \tag{B.21}$$

is obtained. The Hamilton function takes the form

$$H(\boldsymbol{x}, u_q, \boldsymbol{\lambda}) = \Pi(\boldsymbol{x}, u_q) + \boldsymbol{\lambda}^T \boldsymbol{f}(\boldsymbol{x}, \bar{\boldsymbol{z}}, u_q)\,. \tag{B.22}$$

Substitution of $\tilde{u}$ leads to the following four dimensional Hamiltonian system

$$\dot{\theta} = \omega \tag{B.23}$$

$$\dot{\omega} = -\frac{\mu}{J}\omega - \frac{k^2}{3J^2(R+r)}\lambda_\omega \tag{B.24}$$

$$\lambda_\theta = \text{constant} \tag{B.25}$$

$$\dot{\lambda}_\omega = -2\mu\omega + \frac{\mu}{J}\lambda_\omega - \lambda_\theta\,. \tag{B.26}$$

Since λ_θ is constant and (B.25) and (B.26) do not depend on θ, only the reduced system

$$\dot{\tilde{\boldsymbol{x}}} = \mathbf{A}\tilde{\boldsymbol{x}} + \tilde{\boldsymbol{u}} \tag{B.27}$$

where

$$\tilde{\boldsymbol{x}} = [\omega\ \lambda_\omega]^T \tag{B.28}$$

$$\mathbf{A} = \begin{bmatrix} -\frac{\mu}{J} & -\frac{k^2}{3J^2(R+r)} \\ -2\mu & \frac{\mu}{J} \end{bmatrix} \tag{B.29}$$

$$\tilde{\boldsymbol{u}} = [0\ -\lambda_\theta]^T \tag{B.30}$$

has to be solved. ■

C Performance using Multiphase Converter: Simulation Results

The multiphase converter control scheme introduced in Section 5.3 is tested based on the sliding mode position control algorithm that is presented in Section 5.2.2 Table C.1 summarizes the parameters of the machine and the control parameters which are used in the numerical simulations.

The load consists of the inertia of the machine and a pendulum, which is a point mass of 0.1 kg at a distance of 0.5 m from the motor axis. Angle θ is the angle from the top vertical position. Initially, the position is $\theta = \pi$ rad, meaning that the mass of the pendulum is at the lower vertical. Three sliding manifolds are to be evaluated, $s_1 = 0$ for the torque, $s_2 = 0$ for the rotor flux and $s_3 = 0$ for the position. Initially, the position is $\theta = \pi$ rad, meaning that the mass of the pendulum is at the lower vertical position. The control objective is to reach the position $\theta = \frac{\pi}{2}$ rad. The simulation time is $t_s = 1$ s. All evaluation factors are computed after $t = 0.1$ s to allow the machine and controller to initialize and reach sliding mode. For the controllers applying pulse-width modulation, the sampling rate is set to 2 kHz, for all other controllers the sampling rate is set to 10 kHz.. Those settings sound reasonable for an example switching device requiring $T_{min} = 50\,\mu$s delay between switching.

Results of the case, when seven instead of four control input signals are generated by switching commands, are shown in Figures C.1 to C.2. The results belonging to the case, when a 3-level inverter is used, are shown in Figures C.4 to C.4.

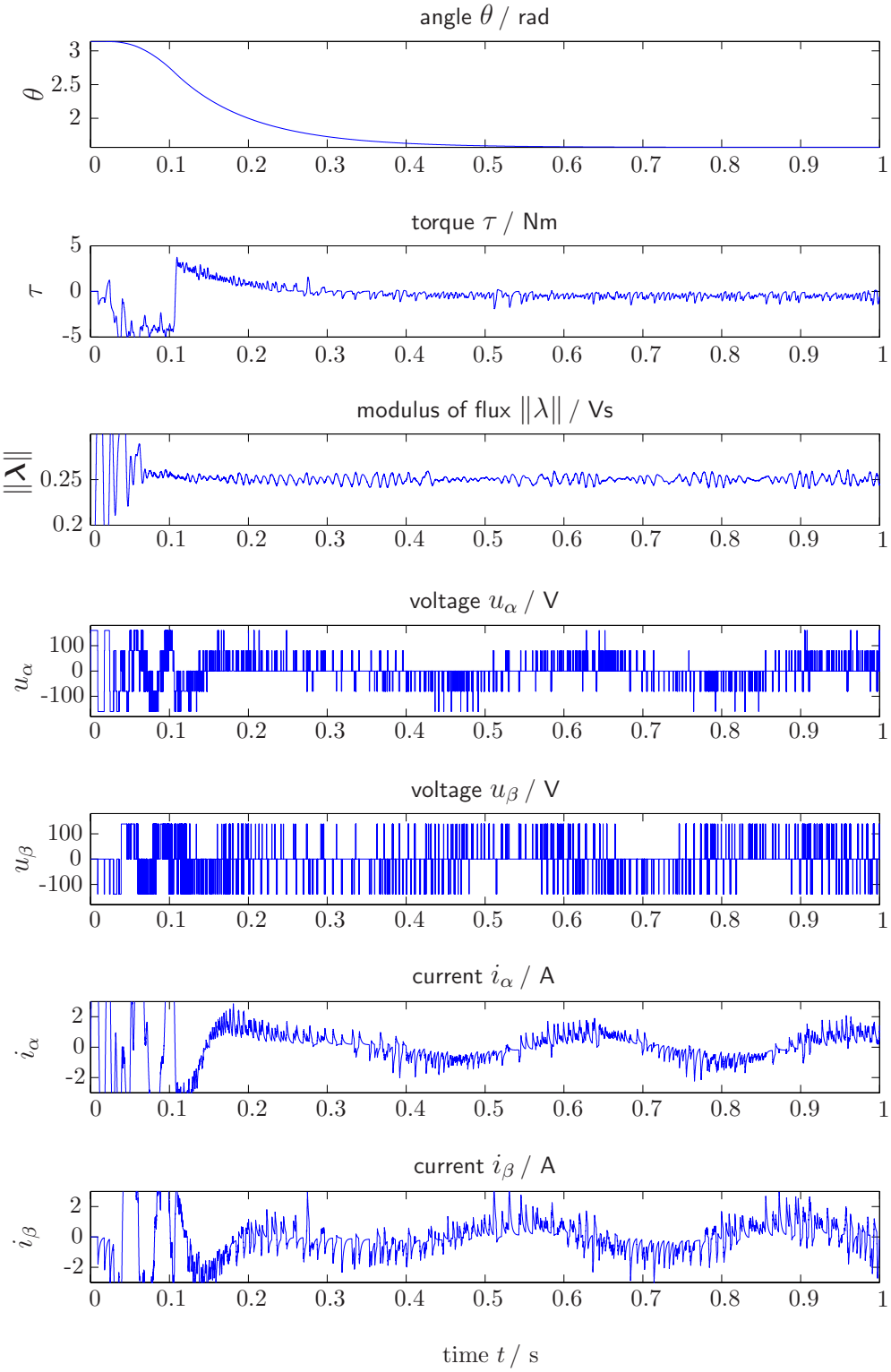

Figure C.1: Simulation results: Position control of an induction machine with inverse inverter model and a 2-level inverter.

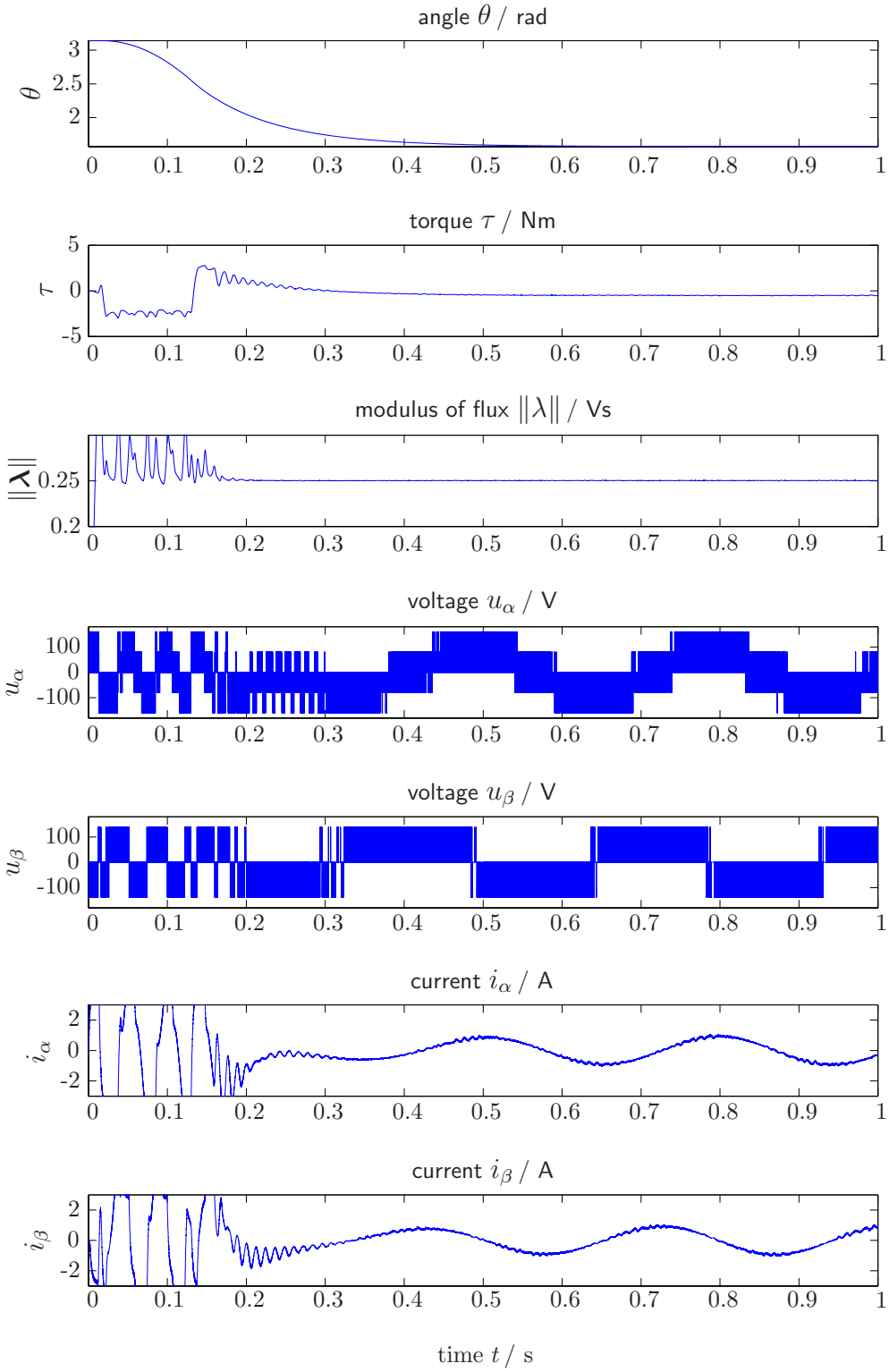

Figure C.2: Simulation results: Position control of an induction machine with PWM and a 2-level inverter.

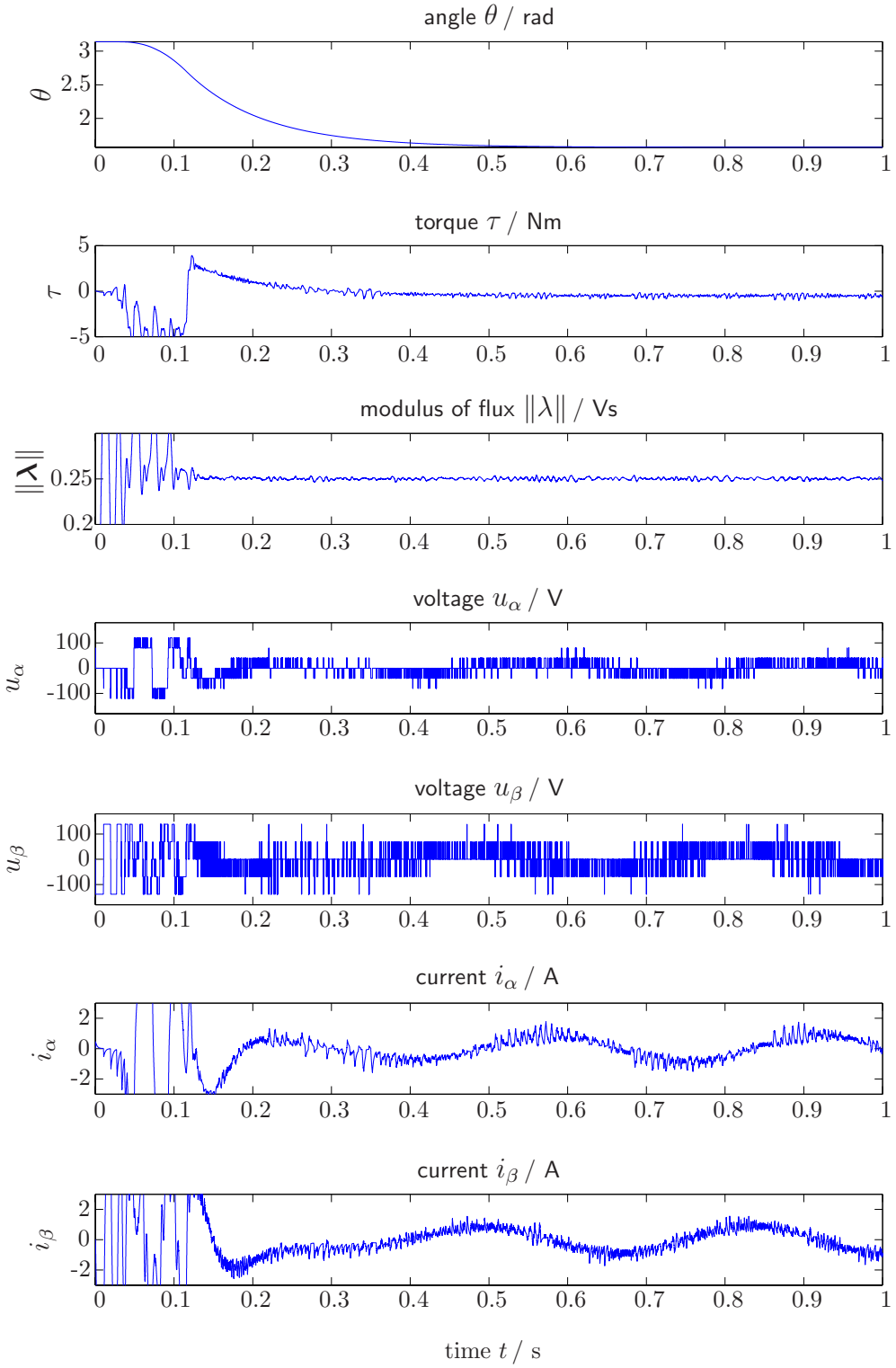

Figure C.3: Simulation results: Position control of an induction machine with inverse inverter model and a 3-level inverter.

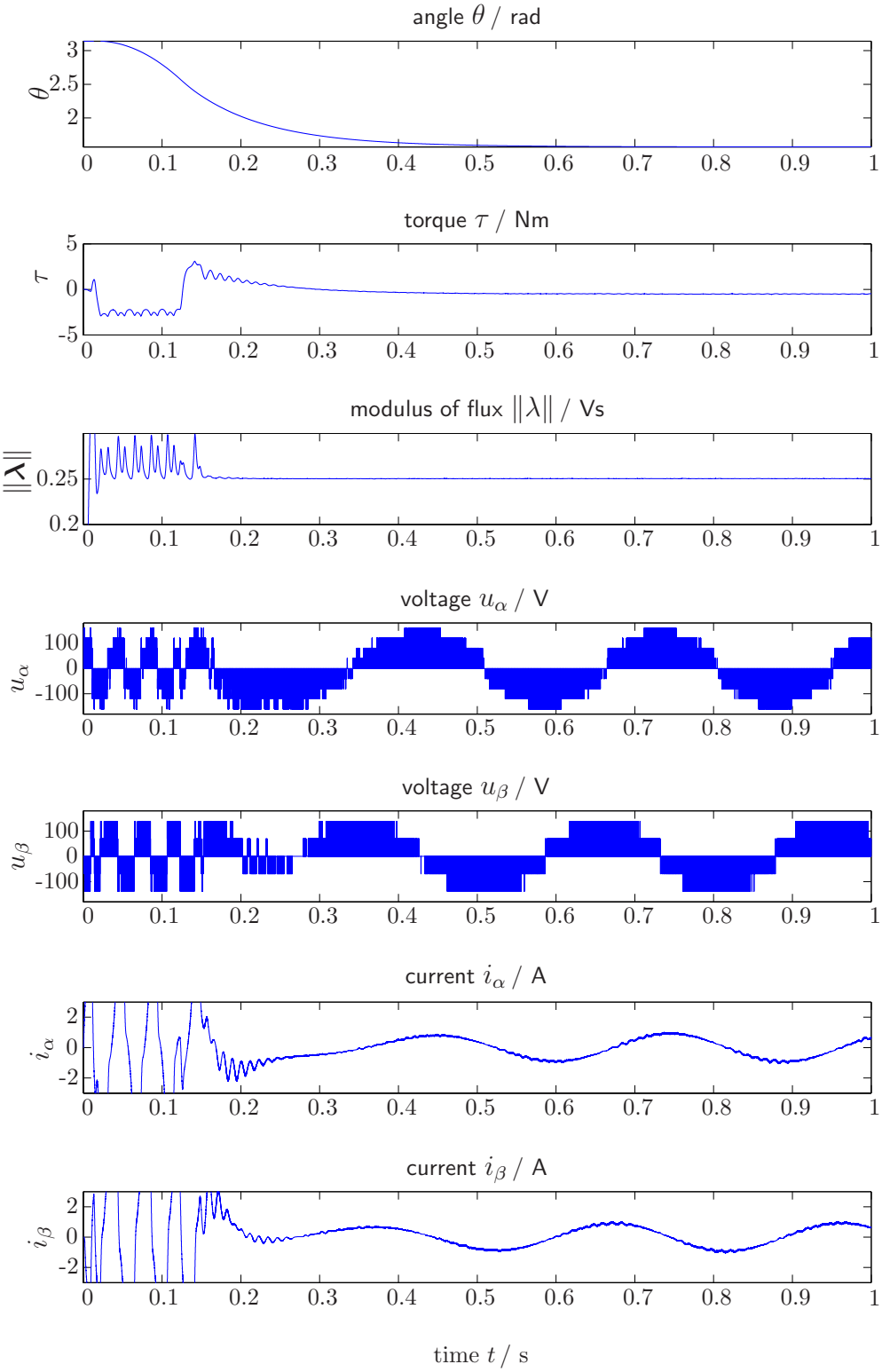

Figure C.4: Simulation results: Position control of an induction machine with PWM and a 3-level inverter.

$L_h =$	$454 \cdot 10^{-3}$ H	(mutual inductance)
$L_r =$	$458 \cdot 10^{-3}$ H	(rotor inductance)
$L_s =$	$439 \cdot 10^{-3}$ H	(stator inductance)
$R_r =$	6.8 Ohm	(rotor resistance)
$R_s =$	10 Ohm	(stator resistance)
$N_r =$	2	(number of pole pairs)
$c_m =$	$5.75 \cdot 10^{-3}$ Nms	(friction coefficient of the machine)
$J_m =$	$3.5\,10^{-3}\,\mathrm{kgm}^2$	(mass moment of inertia of the machine)
$\lambda_{r0} =$	0.2 Vs	(nominal rotor flux)
$\tau_{max} =$	4 N	(maximal torque)
$U_0 =$	120 V	(supply voltage)
$c_1 =$	42.5	(control parameter)
$c_2 =$	800	(control parameter)
$c_3 =$	0.1	(control parameter)
$c_{1_{STA}} =$	0.4	(control design parameter - super twisting algorithm)
$c_{2_{STA}} =$	57.3	(control design parameter - super twisting algorithm)
$\rho_{STA} =$	0.75	(control design parameter - super twisting algorithm)
$\kappa_M =$	2 ms	(control parameter)
$\varepsilon_M =$	5000	(control parameter)

Table C.1: Multiphase converter control of an induction machine- simulation parameters.

Bibliography

[1] M-R. Akbarzadeh–T, G. Faezian, H. Tabatabaei–Y, and N. Sargolzaei. A New Variable Structure Control Methodology for Electrical/ Mechanical Parameter Estimation of Induction Motor. In *Proceedings of the American Control Conference*, Denver, Colorado, June 2003.

[2] K. J. Astrom and B. Wittenmark. *Adaptive Control*. Prentice Hall, 1995.

[3] Eric P. Bailey and Aristotle Arapostathis. Contributions to the sliding mode control of robot manipulators. *24th IEEE Conference on Decision and Control*, 24:358–359, December 1985.

[4] O. Barambones, A.J. Garrido, and F.J. Maseda. A Robust Field Oriented Control of Induction Motor with Flux Observer and Speed Adaptation. In *IEEE Conference on Emerging Technologies and Factory Automation, ETFA'03*, volume 1, pages 245–252, Sept. 2003.

[5] G. Bartolini, A. Ferrara, and E. Usai. Chattering avoidance by second-order sliding mode control. In *IEEE Transactions on Automatic Control, Vol. 43, No. 2*, pages 241–246, 1998.

[6] G. Bastin, J.M. Coron, B. D'Andréa-Novel, and L. Moens. Boundary control for exact cancellation of boundary disturbances in hyperbolic systems of conservation laws (i). pages 1086–89, 2005.

[7] A. Benchaib, A. Rachid, E. Audrezet, and M. Tadjine. Real-Time Sliding-Mode Observer and Control of an Induction Motor. *IEEE Transactions on Industrial Electronics*, 46(1):128–138, February 1999.

[8] F. Blaschke. The principle of field orientation as applied to the new transvector closed-loop control system for rotating field machine. *Siemens Rev.*, (39):217–220, 1972.

[9] I. Boiko, L. Fridman, and R. Iriarte. Analysis of steady state behavior of second order sliding mode algorithms. In *Proceeding of the 2004 American Control Conference*, pages 632–638, Boston, MA, 2004.

[10] A. Cavallo and F. Vasca. DC Motor Control with Sliding Mode Switching Modulator. *International Conference on Industrial Electronics, Control and Instrumentation*, 3:1455–1459, September 1994.

[11] C.Edwards and S.K. Spurgeon. *Sliding Mode Control: Theory and Applications*. Taylor & Francis, London, 1998.

[12] S. Colombi, T. Raimondi, and G. Costi. Improvements of actuators in teleoperators. *ORIA 91: Telerobotics in Haptile Enviroments*, 1991.

[13] F. Cupertino, A. Lattanzi, and L. Salvatore. Sliding Mode Control of an Induction Motor. In *Power Electronics and Variable Speed Drives*, 2000.

[14] B. Curk and K. Jezernik. Sliding mode control with perturbation estimation:application on dd robot mechanism. volume 19, pages 641–648, 2001.

[15] M. Depenbrock. Direct self-control (dsc) of inverter-fed induction machine. *Power Electronics, IEEE Transactions on*, 3(4):420–429, October 1988.

[16] A. Derdiyok, M.K. Guven, N. Inanc, H.R., and L. Xu. A DSP-Based Indirect Field Oriented Induction Machine Control by Using Chattering-Free Sliding Mode. In *Proceedings of the IEEE 2000 National Aerospace and Electronics Conference, NAECON 2000*, pages 568–573, 2000.

[17] A. Derdiyok, Z. Yan, M. Guven, and V. Utkin. A Sliding Mode Speed and Rotor Time Constant Observer for Induction Machines. In *IECON'01: The 27th Annual Conference of the IEEE Industrial Electronics Society*, pages 1400–1405, 2001.

[18] L. Dong, Y. Li, and X. Liao. Novel speed sensorless vector control with adaptive rotor flux identification of induction motors. In *The 29th Annual Conference of the IEEE Industrial Electronics Society, IECON'03*, volume 2, pages 1691–1696, Nov. 2003.

[19] C.M. Dorling and A.S.I. Zinober. Two approaches to sliding mode design in multivariable variable structure control systems. *International Journal of Control*, 44(1):65–82, July 1986.

[20] S. Drakunov and V. Utkin. Sliding mode observers. tutorial. In *Prceedings of the 34th Conference on Decision and Control*, pages 3376–3378, New Orleans, LA, December 1995. IEEE.

[21] S.V. Drakunov, D.B. Izosimov, A.G. Luk'yanov, V.A. Utkin, and V.I. Utkin. The Block Control Principle. I. *Automation and Remote Control*, 51:601–609, 1990.

[22] S.V. Drakunov, D.B. Izosimov, A.G. Luk'yanov, V.A. Utkin, and V.I. Utkin. The Block Control Principle. II. *Automation and Remote Control*, 51(6):737–746, 1990.

[23] S.V. Drakunov and V.I. Utkin. Sliding mode control in dynamic systems. *International Journal of Control*, 55(4):1029–37, 1992.

[24] B. Drazenovic. The invariance conditions in variable structure systems. *Automatica*, 5:287–295, 1969.

[25] G.; Sira-Ramirez H. Enriquez-Zarate, J.; Silva-Navarro. Sliding mode control of a differentially flat vibrational mechanical system: experimental results. *Proceedings of the 39th IEEE Conference on Decision and Control*, 2:1679–1684 vol.2, 2000.

[26] A. Filippov. *Differential Equations with Discontinous Righthand Sides*. Kluver, Dordrecht, 1988.

[27] Chr. Fischer, **H. Brandtstädter**, and M. Buss. Cost Functional Minimizing Sliding Mode Control Design. In *Proceedings of the IEEE International Conference on Control Applications CCA'06*, Munich, Germany, 2006.

[28] M. Fliess, J. Levine, P. Martin, and P. Rouchon. On differentially flat nonlinear systems. In *Proc. IFAC Nonlinear Control Systems Design Symposium*, pages 408–412, Bordeaux, Frankreich.

[29] M. Fliess, J. Levine, P. Martin, and P. Rouchon. Flatness and defect of nonlinear systems: Introductory theory and examples. *Int. J. Control*, 61:1327–1361, 1995.

[30] K. Furuta. Vss type self-tuning control. *Industrial Electronics, IEEE Transactions on*, 40(1):37–44, Feb 1993.

[31] K.B. Goh, M.W. Dunnigan, and B.W. Williams. Sliding Mode Position Control of a Vector-Controlled Induction Machine with Non-linear Load Dynamics. In (Conf. Publ. No. 498), editor, *Second International Conference on Power Electronics, Machines and Drives*, volume 1, pages 87 – 92, 2004.

[32] Q.H.; Rye D.C.; Durrant-Whyte H.F. Ha, Q.P.; Nguyen. Fuzzy sliding-mode controllers with applications. *Industrial Electronics, IEEE Transactions on*, 48(1):38–46, Feb 2001.

[33] T.G. Habetler and D.D. Divan. Control Strategies for Direct Torque Control Using Discrete Pulse Modulation. *IEEE Transactions on Industry Applications*, 27(5):600–606, 1991.

[34] T.G. Habetler, F. Profumo, M. Pastorelli, and L.M. Tolbert. Direct Torque Control of Induction Motor Using Space Vector Modulation. *IEEE Transactions on Industy Applications*, 28(5):1045–1053, Sept./Oct. 1992.

[35] K. Hasse. Drehzahlregelverfahren für schnelle umkehrantriebe mit stromrichtergespeisten asynchron kurzschlusslaufmethoden. *Regelungstechnik*, 22:60–66, 1972.

[36] **H. Brandtstädter** and M. Buss. Control of Electromechanical Systems using Sliding Mode Techniques. In *Proceedings of the 44th IEEE Conference on Decision and Control, and the European Control Conference 2005*, pages 1947–1952, Seville, Spain, 2005.

[37] J. Holtz. Sensorless Control of Induction Motor Drives. *Proceedings of the IEEE*, 90(8):1359–1394, August 2002.

[38] K. Jezernik, B. Curk, and J Harnik. Observer Based Sliding Mode Control of Robotic Manipulator. volume 12, pages 433–448, 1994.

[39] P. Kokotovic, H.K. Khali, and J. O'Reilly. *Singular Perturbation Methods in Control-Analysis and Design*. SIAM, 1997.

[40] M. Krstic, I. Kanellakopoulos, and P. Kokotovic. *Nonlinear and Adaptive Control Design (Nonlinear and Adaptive Control Design (Adaptive and Learning Systems for Signal Processing, Communications and Control)*. Wiley, New York, 1995.

[41] C.M. Kwan, F.L. Lewis, and K.S. Young. Adaptive Control of Induction Motors Without Flux Measurements. *Automatica*, 32(6):903–908, 1996.

[42] A. Levant. Sliding order and sliding accuracy in sliding mode control. In *Int. J. Control, Vol. 58, No. 6*, pages 1247–1263, 1993.

[43] S.-K. Lin and C.-H. Fang. Sliding-Mode Direct Torque Control of an Induction Motor. *The 27th Annual Conference of the IEEE Industrial Electronics Society, IECON'01*, 3:2171–2177, 2001.

[44] A.G. Loukianov. A block method of synthesis of nonlinear systems at sliding modes. *Automation and Remote Control*, 42(4):413–420, 1998.

[45] A.G. Loukianov. Optimal Non-linear Block Control Method. *Proc. of the 2nd European Control Conference, ECC'93*, pages 1853–1855, June, 1993.

[46] A.G. Loukianov, J.M. Canedo, O. Serrano, V.I. Utkin, and S. Celikovsky. Adaptive Sliding Mode Block Control for Induction Motors. In *Proceedings of the American Control Conference*, Arlington, VA, June 2001.

[47] A.G. Loukianov and S.J. Dodds. Sliding mode block control of uncertain nonlinear plants. In *Proceedings of the 13th World Congress of the International Federation on Automatic Control (IFAC)*, San Francisco, CA, 1996.

[48] A.G. Loukianov and V.I. Utkin. Methods of Reducing Equations for Dynamic Systems to a Regular Form. *Automation and Remote Control*, 42(4):413–420, 1981.

[49] R. Marino, S. Peresada, and P. Tomei. Global Adaptive Output Feedback Control of Induction Motors With Uncertain Rotor Resistance. *IEEE Transactions on Automatic Control Engeneering*, 44:967–981, 1999.

[50] R. Marino and P. Tomei. A New Global Control Scheme for Sensorless Current-Fed Induction Motors. In *Proceedings of the 15th Triennial World Congress, IFAC 2002*, Barcelona, Spain, 2002.

[51] M. Montanari, S. Peresada, and A. Tilli. Sensorless Indirect Field Oriented Control of Induction Motor Via Adaptive Speed Observer. In *Proceedings of the American Control Conference*, Denver, Colorado, 2003.

[52] K. S. Narendra and A. M. Annaswamy. *Stable Adaptive Systems*. Dover Publications, 2005.

[53] F.S. Neves, R.P. Landim, T.G. Habetler, B.R. Menezes, and S.R. Silva. Induction Motor DTC Strategy Using Discrete-Time Sliding Mode Control. In *Conference Record of the 34th IAS Annual Meeting Industry Application Conference*, volume 1, pages 79–85, Oct. 1999.

[54] K. Erbatur O. Kaynak and M. Ertugrul. The fusion of computationally intelligent methodologies and sliding-mode control- a survey. *IEEE Trans. Ind. Electron*, 48(1):4–17, 2001.

[55] T. Ohtani, N. Takanda, and K. Tanaka. Vector Control of Induction Motor without Shaft Encoder. *IEEE Transactions on Industry Applications*, 28(1):157–165, 1992.

[56] T. Okuyama, N. Fujimoto, T. Matusi, and Y. Kubota. A High Performance Speed Control Scheme for Induction Motor Without Speed and Voltage Sensors. In *IEEE IAS Annual Meeting*, pages 106–111, Barcelona, Spain, 1986.

[57] B. Paden and S. Sastry. A calculus for computing filippov's differential inclusion with application to the variable structure control of robot manipulators. *IEEE Transactions on Circuits and Systems*, 34(1):73–82, January 1987.

[58] S. Rao, **H. Brandtstädter**, M.Buss, and V. Utkin. Sliding Mode Control in Mechanical Systems with Electric Actuators. In *Proceedings of the 8th International Workshop on Variable Structure Systems*, Vilanova i la Geltru, Spain, 2004.

[59] S. Rao, **H. Brandtstädter**, V. Utkin, and M. Buss. Generalized Block Control Principle. In *Proceedings of 16th IFAC World Congress*, Prague, Czech Republic, July 2005.

[60] H.U. Rehman, A. Derdiyok, M.K. Guven, and X. Longya. An MRAS Scheme for On-line Rotor Resistance Adaptation of an Induction Machine. In *IEEE 32nd Annual Power Electronics Specialists Conference, PESC 2001*, volume 2, pages 817–822, June 2001.

[61] M. Rodic and K. Jezernik. Speed-Sensorless Sliding-Mode Torque Control of an Induction Motor. *IEEE Transactions on Industrial Electronics*, 49(1):87–95, February 2002.

[62] W.J. Rugh. Analytical framework for gain scheduling. *IEEE Control Systems Magazine*, 11(1), 1991.

[63] E.P. Ryan and M. Corless. Ultimate boundedness and asymptotic stability of a class of uncertain dynamical systems via continuous and discontinuous feedback control. *IMA Journal of Mathematical Control and Information*, 1(3):223–242, 1984.

[64] A. Sabanovic and D.B. Izosimov. Applications of Sliding Modes to Induction Motor Control. *IEEE Transactions on Automation Control*, 17:41–49, 1981.

[65] C. Sahin, A. Sabanovic, and M. Gokasan. Robust Position Control Based on Chattering Free Sliding Modes for Induction Motors. In *Proceedings of the IEEE 21st International Conference on Industrial Electronics, Control, and Instrumentation, IECON 1995*, volume 1, pages 512–517, Nov. 1995.

[66] C. Schauder. Adaptive Speed Identification for Vector Control of Induction Motors without Rotational Transducers. *IEEE Transactions on Industry Applications*, 28(5):1054–1061, 1992.

[67] Nikolaus P. Schibli, Tung Nguyen, and Alfred C. Rufer. A three-phase multilevel converter for high-power induction motors. In *IEEE Transactions on Power Electronics, Vol. 13, No. 5*, pages 978–986, 1998.

[68] J-J. E. Slotine. Sliding controller design for non-linear systems. *Int. Journal of Control*, 40(2):421–434, 1984.

[69] J.J. Slotine and S.S. Sastry. Tracking control of non-linear systems using slidin surfaces, with application to robot manipulators. *Int. Journal of Control*, 38(2):465–492, 1983.

[70] R. Soto and K. S. Yeung. Sliding mode control of an induction motor without flux measurement. In *IEEE Transactions on Industry Applications, Vol. 31, No.4*, pages 744–751, 1995.

[71] I. Takahashi and T. Noguchi. A New Quick Response and High Efficiency Control Strategy of an Induction Motor. *IEEE Transactions on Industry Applications*, 22:820–827, Sept./Oct. 1986.

[72] I. Takahashi and Y. Ohmori. High Performance Direct Torque Control of an Induction Motor. *IEEE Transactions on Industry Applications*, 25(2):257–264, 1989.

[73] M. Tursini, R. Petrella, and F. Parasiliti. Adaptive Sliding Mode Observer for Speed-Sensorless Control of Induction Motors. *IEEE Transactions on Industry Applications*, 36(5):1380–1387, 2000.

[74] V. Utkin. Equations of Slipping Regimes in Discontinuous Systems I. *Automation and Remote Control*, 32(1897-1907), 1971.

[75] V. Utkin. Equations of Slipping Regimes in Discontinuous Systems II. *Automation and Remote Control*, 33(211-219), 1972.

[76] V. Utkin. Sliding mode control in discrete time and difference systems. In A. Zinober, editor, *Variable Structure and Lyapunov Control*. Springer Verlag, 1993.

[77] V. Utkin. Sliding Mode Control Design Principles and Applications to Electric Drives. *IEEE Transactions on Industrial Electronics*, 40(1), February 1993.

[78] V. Utkin, De-Shiou Chen, and Hao-Chi Chang. Block Control Principle for Mechanical Systems. *Journal of Dynamic Systems, Measurement, and Control*, 122(1):1–10, March 2000.

[79] V. Utkin, J. Guldner, and J. Shi. *Sliding Mode Control in Electromechanical Systems*. Taylor & Francis, London, 1999.

[80] V.I. Utkin. Variable Structure Systems with Sliding Modes. *IEEE Transactions on Automatic Control*, AC-22(2):212–222, April 1977.

[81] V.I. Utkin. *Sliding Modes in Control and Optimization*. Springer-Verlag, Berlin, 1992.

[82] V.I. Utkin and H.-C. Chang. Sliding mode control in electro-mechanical systems. *Mathematical Problems in Engeneering*, 8(4-5):451–473, 2002.

[83] V.I. Utkin, H.C. Chang, I. Kolmanovsky, and J.A. Cook. Sliding mode control for variable geometry turbocharged diesel engines. In *?ACC?*

[84] V.I. Utkin and H. Lee. Chattering problem in sliding mode control systems. In *Proceedings of the 2006 International Workshop on Variable Structure Systems*, pages 346–350, Alghero,Italy, 2006.

[85] V. Vasic, S.N. Vukosavic, and E. Levi. A Stator Resistance Estimation Scheme for Speed Sensorless Rotor Flux Oriented Induction Motor Drives. *IEEE Transactions on Energy Conversion*, 18(4):476–483, Dec. 2003.

[86] J. Vittek, S.J. Dodds, J. Altus, and R. Perryman. Sliding Mode Based Outer Control Loop for Induction Motor Drive With Forced Dynamics. In *IASTED conference on Control and Applications*, Cancun, Mexico, 2000.

[87] Y. Xia, X. Yu, and W. Oghanna. Adaptive Robust Fast Control for Induction Motors. *IEEE Transactions on Industrial Electronics*, 47(4):854–862, 2000.

[88] Tsuneo Yoshikawa. *Foundations of Robotics. Analysis and Control.* The MIT Press, 1990.

[89] K. D. Young, V. I. Utkin, and Ü. Özgüner. A Control Engineer's Guide to Sliding Mode Control. *IEEE Transactions in Control Systems Technology*, 7(3):1063–6536, May 1999.